THE UNIVERSITY OF ADELAIDE

COUPLED FLUID FLOW-GEOMECHANICS SIMULATIONS APPLIED TO COMPACTION AND SUBSIDENCE ESTIMATION IN STRESS SENSITIVE & HETEROGENEOUS RESERVOIRS

A THESIS SUBMITTED FOR THE DEGREE
OF DOCTOR OF PHILOSOPHY

by
Ta Quoc Dung

Australian School of Petroleum, South Australia

2007

Acknowledgements

First of all, I would like to express my deep sense of gratitude to Dr. Suzanne Hunt for her principle supervision and important support throughout the duration of this PhD research. I am grateful to her not only for encouragement and guidance during academic years, but also for patience and help with regard to my English as well as spending time to understand me personally.

I am also highly indebted to Prof. Peter Behrenbruch for his constant direction through petroleum courses in the Australian school of Petroleum (ASP) and giving me guidance. His industrial experience contributes to my professional development.

I would like to thank my supervisor Prof. Carlo Sansour for his exceptional guidance and inspiration. He led me into the fascinating world of theory of continuum mechanics. In addition, he introduced me to the other beauty in my life: Argentinean Tango.

I also would like to take this opportunity to express my gratitude to all colleagues and administrators. Particularly, I would like to thank Do Huu Minh Triet, Jacques Sayers, Dr. Hussam Goda, Dr. Mansoor Alharthy, Son Pham Ngoc, Pamela Eccles and Vanessa Ngoc who have always been warm-hearted and helpful during the most challenging times of PhD life. Thanks go to all friends in the ASP who shared many hours of exciting soccer after working hours.

Financial support for both academic and life expenses was provided by the

Vietnamese Government. The ASP scholarship committee is highly acknowledged for approval of additional six months scholarship. Special thanks go to my Geology and Petroleum faculty at Ho Chi Minh City University of Technology for special support through this research.

Last, but not least, I would like to thank my family who believe in me at all times with their unconditional love.

ABSTRACT

Recently, there has been considerable interest in the study of coupled fluid flow – geomechanics simulation, integrated into reservoir engineering. One of the most challenging problems in the petroleum industry is the understanding and predicting of subsidence at the surface due to formation compaction at depth, the result of withdrawal of fluid from a reservoir. In some oil fields, the compacting reservoir can support oil and gas production. However, the effects of compaction and subsidence may be linked to expenditures of millions of dollars in remedial work. The phenomena can also cause excessive stress at the well casing and within the completion zone where collapse of structural integrity could lead to loss of production. In addition, surface subsidence can result in problems at the wellhead or with pipeline systems and platform foundations.

Recorded practice reveals that although these problems can be observed and measured, the technical methods to do this involve time, expense, with consideration uncertainty in expected compaction and are often not carried out. Alternatively, prediction of compaction and subsidence can be done using numerical reservoir simulation to estimate the extent of damage and assess measurement procedures. With regard to reservoir simulation approaches, most of the previous research and investigations are based on deterministic coupled theory applied to continuum porous media. In this work, uncertainty of parameters in reservoir is also considered.

This thesis firstly investigates and reviews fully coupled fluid flow – geomechanics modeling theory as applied to reservoir engineering and geomechanics research. A finite element method is applied for solving the governing fully coupled equations. Also simplified analytical solutions that present more efficient methods for estimating compaction and subsidence are reviewed. These equations are used in uncertainty and stochastic simulations. Secondly, porosity and permeability variations can occur as a result of compaction. The research will explore changes of porosity and permeability in stress sensitive reservoirs. Thirdly, the content of this thesis incorporates the effects of large structures on stress variability and the impact of large

structural features on compaction. Finally, this thesis deals with affect of pore collapse on multiphase fluid and rock properties. A test case from Venezuelan field is considered in detail; investigating reservoir performance and resultant compaction and subsidence.

The research concludes that the application of coupled fluid flow – geomechanics modeling is paramount in estimating compaction and subsidence in oil fields. The governing equations that represent behaviour of fluid flow and deformation of the rock have been taken into account as well as the link between increasing effective stress and permeability/porosity. From both theory and experiment, this thesis shows that the influence of effective stress on the change in permeability is larger than the effect of reduction in porosity. In addition, the stochastic approach used has the advantage of covering the impact of uncertainty when predicting subsidence and compaction.

This thesis also demonstrates the influence of a large structure (i.e. a fault) on stress regimes. Mathematical models are derived for each fault model to estimate the perturbed stress. All models are based on Mohr–Coulomb's failure criteria in a faulted area. The analysis of different stress regimes due to nearby faults shows that effective stress regimes vary significantly compared to a conventional model. Subsequently, the selection of fault models, fault friction, internal friction angle and Poisson's ratio are most important to assess the influence of the discontinuity on the reservoir compaction and subsidence because it can cause a significant change in stress regimes.

To deal with multiphase flow in compacting reservoirs, this thesis presents a new method to generate the relative permeability curves in a compacting reservoir. The principle for calculating the new values of irreducible water saturation (S_{wir}) due to compaction is demonstrated in this research. Using coupled reservoir simulators, fluid production due to compaction is simulated more comprehensively. In the case example presented, water production is reduced by approximately 70% compared to conventional modeling which does not consider changes in relative permeability. This project can be extended by applying the theory and practical methodologies developed to other case studies, where compaction and stress sensitivity dominate the drive mechanism.

PUBLICATIONS

Ta, Q. D., S. P. Hunt and C. Sansour (2005). Applying fully coupled geomechanics and fluid flow model theory to petroleum wells. The 40th U.S. Symposium on Rock Mechanics-USRMS, Anchorage, Alaska.

Ta, Q. D. and S. P. Hunt (2005). Investigating the relationship between permeability and reservoir stress using a coupled geomechanics and fluid flow model. 9th Conference on Science and Technology, held in Ho Chi Minh City University of Technology, Viet Nam.

Ta, Q. D. and S. P. Hunt (2005). Consideration of the permeability and porosity relationship in a FEM coupled geomechanics and fluid flow model. Intergrated geoenginering for sustainable infracstructure develpomnet. Hanoi Geoengineering 2005, Ha Noi - Viet Nam, Vietnam National University Publishing House

Ta, Q. D. and S. P. Hunt (2006). Stress variability around large structural features and its impact on permeability for coupled modeling simulations. 4th Asian Rock Mechanics Symposium (ARMS), Singapore.

Ta, Q. D., M. Al-Harthy, S. Hunt and J. Sayers (2007). The impact of uncertainty on subsidence and compaction prediction. First Sri Lankan Geotechnical Society (SLGS) International Conference on Soil and Rock Engineering, Colombo, Sri Lanka.

STATEMENT OF ORIGINALITY

This work contains no material which has been accepted for the award of any other degree or diploma at any university or other tertiary intuition and, to the best of my knowledge and belief, this thesis contains no material previously published or written by another person, except where due reference has been made in the text.

I give consent to this copy of my thesis, when deposited in the University Library, being available for loan and photocopying.

Signed:……..Date……..

CONTENTS

LIST OF FIGURES

LIST OF TABLES

CHAPTER 1: LITERATURE REVIEW ON COUPLED SIMULATION AND COMPACTION RESEARCH

1.1 Problem statement

Recently, considerable interest has been generated in the study of coupled fluid flow-geomechanics simulations integrated into reservoir engineering due to its relevance to many issues in oil field development. One of the most serious problems which could potentially cost millions of dollars, is ground subsidence caused indirectly as a result of petroleum production and the resulting compaction (Geertma 1973; Merle et al. 1976; Gutierrez 1994). Principally, the pore pressure decreases in the reservoir when oil and gas is produced. This phenomenon results in an increase in effective stress acting on the solid skeleton and compaction of the reservoir takes place. Consequently, the ground surface or seafloor can subside. Although, in some oil fields, the compacting reservoir can be considered as a support for enhancing petroleum production (Merle et al. 1976), the phenomena can cause excessive stress at the well casing and within the completion zone where collapse of structural integrity could lead to failure and lost production. In addition, surface subsidence also results in problems at the wellhead, pipeline systems and platform foundations.

Although subsidence and compaction can be observed and measured by many technical methods it usually takes time, significant expense and hence is not often performed unless serious problems arise post-production. Alternative, prediction of compaction and subsidence can be done using reservoir simulation that using

numerical methods. With regard to reservoir simulation approaches, most of the previous research on this topic and prior investigations are based on coupled theory applied to continuum porous media in which coupled equations between fluid flow and rock behavior are solved simultaneously. However, dealing with uncertainty of input reservoir parameters, the influence of large structure and aspects of multiphase flow in prediction of subsidence and compaction are still areas for continued research.

The following section presents a concise description of the thesis content through literature review related to the development of the mathematical models related to coupled theory as applied to stress sensitive reservoir. The applications of stochastic methods as applied to compaction and subsidence are also discussed.

1.2 Summary of literature and thesis overview

1.2.1 Coupling of fluid flow and rock deformation.

In the last century, industry and academia have tried to build a fully coupled model for applications in reservoir simulation that applying to solve many problems such as ground subsidence, reservoir compaction, well-bore stability and hydraulic fracturing. Originally, coupled formulations of deformation and fluid flow were first analyzed by Terzaghi (1925; 1943) as a problem in material consolidation. Subsequent to this, Biot (1940) focused on extending Terzaghi's theory to three dimensions. Also, focusing on a linear stress-strain relationship and single-phase fluid flow, both Terzaghi's and Biot's analyses are linear, and solutions have not been extended to non-linear systems. Following their work, coupled models have existed not only in petroleum engineering but also in civil engineering, geotechnical engineering and rock mechanics. These include Sandhu and Wilson (1969), Ghaboussi and Wilson (1973), Gambolati and Freeze (1973), Noorishad et al. (1982)

which are some of the earliest coupled hydromechanical models. In recent years, Gutierrez (1994) presented the general equations and theory of a fully coupled analysis for hydrocarbon reservoir compaction and subsidence. Gutierrez showed that compaction drive could not be properly represented by simply adjusting the value of rock compressibility used in traditional reservoir simulation. Also Chen et al. (1995) extended Biot's two phase, isothermal and linear poroelastic theory for porous fluid-flow modeling. Their theory can be applied for coupled rock mechanics and fluid flow problems. McKinley (1998) investigated coupled consolidation for a radial coordinate system and he derived a new formulation for the plane strain axisymmetric consolidation problem. Although the work presents results for coupling effects, only the finite difference method was used for numerical computation. Bai et al. (1999) developed the dual porosity poroelastic model and applied it using cylindrical coordinate system. Their research shows good results for the simplified axisymmetric configuration. The numerical analysis attempted to replicate laboratory experiments, where both divergent flow through a centrally located borehole, and point injection and collection across a cylindrical rock specimen are incorporated. However, Bai's et al. research did not mention how to apply a new coupling porosity value at each time step. Chin et al. (2000) developed a fully coupled fluid flow – geomechanics model of wells with stress dependence. However, the limitation of the theory is that it is applicable only to two dimensions and only using Cartesian coordinates. In advancing research, Wan (2003) developed a new framework for coupled analyses, using a stabilized finite element method for the force balance equations. Although the studies were applied to fully coupled models, they were also restricted to two dimensions and the numerical method used was the control volume finite difference method, which solved the remaining component mass balance equations. Alternatively, Sansour

(2003) proposed a theory developed for biomedical research that is equally applicable to petroleum engineering and is described herein. In Sansour's coupled theory, the porosity values are updated at each calculation time step and integration point. The advantage allows for application to models with inhomogeneous porosity distribution.

1.2.2 Stress sensitive permeability and porosity

A clear understanding of rock stress and its effect on permeability and porosity is important in a coupled simulation where fluid production causes a significant increase in the effective stress within a reservoir. Changing the *in situ* rock stress state can alter reservoir properties. For example, porosity and permeability can be affected due to the rearrangement of rock particles and the redistribution of stress associated with sensitive pore structures.

In the past, a variety of laboratory based testing procedures to measure permeability under *in situ* stress conditions have been used. Some of the earliest work relating to sensitivity of permeability due to stress variation was presented analytically with permeability measurements conducted for gas well testing (Vairogs, Hearn et al. 1971). Skin values for the gas well tests were found to vary as permeability decreased during production, resulting from the permeability reduction near the well-bore; the inclusion of stress sensitive permeability effects altered the welltest analysis significantly. Most authors reached the conclusion that permeability is reduced from 10% to 30% when confining stress was increased in a range of 1000psi - 8000psi (Holt 1990; Warpinski and Teufel 1992). Further results showed that the reduction of permeability in a low permeability core is proportionally greater than the reduction of permeability in a high permeability core (Vairogs and Rhoades 1973). The above non-linear effect implies that only certain rock types will

demonstrate significant stress sensitive permeability. Consequently, reduction of permeability is dependent on lithology (John, David et al. 1998) and it will also be case-specific. Some work has been done in characterizing the stress sensitivity of various rock types, but no absolute method has been found to determine where a cut-off occurs. Certainly, it is generally considered important to incorporate stress sensitive permeability for tight gas reservoirs where the permeability value is a dominant factor for investigating the behaviors of fluid flow. A thorough review of hydro-mechanical testing procedures was carried out by Heiland (2003) where three laboratory procedures were described. In most cases a decrease in permeability occurred with increasing stress. One exception to this is, when under triaxial conditions, dilatancy leading to brittle failure occurs so that high shear stresses acted to give rise to increased permeability.

The influence of temperature on permeability was also investigated to understand the reduction of permeability in reservoir Gobran et al. (1987). This research showed the association of absolute permeability as a function of confining pressure, pore pressure and temperature. The conclusion reached was that permeability was independent of temperature but was a linear function of confining pressure.

Jelmert et al. (2000) investigated correlations between permeability and effective stress, reviewing power-law relationships and stating that straight-line correlations were inappropriate as opposed to polynomial fits to averaged core data. Warpinski and Teufel (1992) had previously fitted polynomial equations to experimental results. The reduction of permeability with effective stress increase is discussed further and mathematical relationships are summarized by Nathenson (1999).

A number of field studies relating to compaction and subsidence in the North Sea have also shown that permeability changes during production significantly influenced the stress path of the reservoir (Rhett and Teufel 1992; Economides, Buchsteiner et al. 1994). Consequently, there is no doubt that the constant permeability values assumed in a conventional reservoir simulation may result in considerable errors. Ambastha and Meng (1996) presented alternative one-parameter and two-parameter models to calculate a permeability modulus that can be applied to produce a more accurate transient analysis in conventional fluid equations. Although these models look promising, the authors do not discuss the correlation between the reduction of reservoir pressure and effective stress resulting in the reduction of permeability. The influence of the stress path under varying reservoir conditions was discussed by Mashiur and Teufel (1996). Importantly their results demonstrated that sensitivity of permeability to stress perturbation was not only dependent on effective stress but also on the size, geometry and other reservoir properties (i.e. reservoir boundary conditions). These experimental results on stress sensitivity demonstrated that the trend of maximum permeability is parallel to the maximum principal stress and the magnitude of permeability anisotropy also increases for lower stress paths. To deal numerically with the stress sensitive permeability problem, Mashiur and Teufel (1996) used the finite element method that is more rigorous in solving stress and fluid flow equations simultaneously. It is certain that permeability is a function of effective stress. In turn, production conditions will directly influence the reservoir condition where effective stress is one of the most important properties. In a detailed break-down of the numerical modeling methodology for permeability variation within a producing reservoir, Osorio et al. (1997) showed that the most sensitive stress permeability region is near the well-bore and within the production zone. The effect

of stress on permeability decreases far from the well-bore where the change in local effective stress is insignificant. Osorio et al. also incorporated the stress – permeability relationship into his model by incorporating generic relationships for shear modulus, bulk compressibility, and permeability against effective stress.

1.2.3 Numerical scheme – Finite element advancement

Conservation of mass and momentum as well as Darcy's law govern the behavior of fluid in a porous media. These physical laws are represented mathematically by a set of partial differential equations. The differential equations that explain the behavior of the system in general way are usually difficult to solve. With the advent of high performance computers, it is possible to solve such differential equations. Various numerical solution techniques have been developed and applied to deal with these differential equations in order to find their approximate solution. Each numerical method has both advantages and disadvantages in term of solving the governing equations. For example, the finite difference method that is commonly used in a simulator for solving the momentum governing equations (with corner point grid) does not contain any correction terms for non-orthogonal, skewed grids. Although the simulator can be faster in computation, it can lead to unacceptable errors if these types skewed corner-point grids are present in the simulation (Eclipse 2005a). Nowadays, the finite element method is one of the major numerical solution techniques. The Galerkin finite element method is chosen because of its ability to handle anisotropic and heterogeneous regions with complex boundaries (Young's and Hyochong 1996). Sansour (2003) applied the generic Galerkin finite element method to solve problems in both biomechanics and porous media related problems. In addition, the finite element method retains second order accuracy when the grid points

are skewed as discussed earlier. This is particularly important for modeling complex pore structure. In this research, the finite element method is chosen to solve the governing differential equations in coupled reservoir engineering.

1.2.4 Uncertainty in subsidence and compaction research

As mentioned, the need for a more reliable predicting approach in assessing the impact of subsidence and compaction on production management of the reservoir has led to a continuous improvement of numerical models employed. Such approaches use the continuum poroelastic theory. For example, the use of advanced models for accurate prediction of land subsidence were documented by Gambolati et al. (2001) and Ta et al. (2005). However, although sophisticated poroelastic constitutive models have been developed for a realistic description of the actual rock mass behavior (Biot 1940; Gutierrez 1994; Terry, Garfield et al. 2000), the geomechanical analysis of producing fields is usually performed deterministically, thus limiting breadth of solution and sensitivities involved. While geostatistical models have been extensively used over the last few decades for modeling fluid flow and transport in random porous media, only a limited number of studies have addressed the benefit of using stochastic – based approaches to assess the effect of rock properties on the geomechanical behavior of the reservoir (Diego, Marcio et al. 2004).

1.2.5 Multiphase continua in the coupled model

Unlike classical single-phase continua that have homogeneous bodies (ideal material); multi-phase continua incorporate homogeneous bodies with internal interaction. In general, multi-phase continua also consist of solid part and liquid or gas parts and sometimes of other chemical constituents. As is known, the multi-phase

continua can be found in several areas of engineering. The skeleton of such material has pores (porous) that can be filled with liquid or gas. There is no information about the geometry of the internal pore structure. The solid and liquid have different motions and due to these different motions and the different material properties, there is interaction between the constituents. This makes the description of the mechanical or thermodynamical behavior difficult. The classical continuum mechanics therefore normally do not fully answer the questions concerning the change in pore structure and the different motions of the constituents.

Until now, the change in multiphase fluid properties and rock properties due to compaction happening in the reservoir is not fully understood. Most current research focus on numerical methods and solvers to get the compaction and subsidence results (Eclipse 2005a, Wan 2003). The behavior of the reservoir when compaction happens is still simplified. As a result, the influence of pore collapse on multiphase fluid and rock properties is also ignored with reservoir simulation, subsequently leading overestimating of subsidence and compaction variation.

1.3 Research objectives

Based on the above thesis overview and literature, to gain insight into the objectives in coupled rock deformation and fluid flow research, it is evident that many tools can be used:

- ✓ Field measurement of subsidence and compaction data including wellbore failure, borehole instability and stress field over production time;
- ✓ Rock and fluid properties from experiment in the laboratory, and

- ✓ Mathematic models to deal with the interaction between rock deformation and behavior of fluid in the reservoir.

To date, although there are many existing fully coupled mathematics models used, few of the fully coupled mathematics models applied in radial coordinate system have been utilized to specifically study compaction and subsidence caused from fluid withdrawal. In addition, due to high cost, most subsidence and compaction measurements in both the field and laboratory are usually noted and performed in big fields. More advance use of multiphase continua theory has also not been comprehensively used in application of reservoir simulation. Moreover, taking into account uncertainty and using stochastic based simulation are also not commonly used in the area of compaction and subsidence estimation. On the other hand, some published papers have take into account the stress sensitive permeability and porosity effects on subsidence and compaction, but results are still in debating. Results seem case-specific and vary with different parameters. Thus, the main objective of this thesis is to provide a detail theory and show how to create and integrate all these above aspects applying in petroleum industry (Figure 1-1).

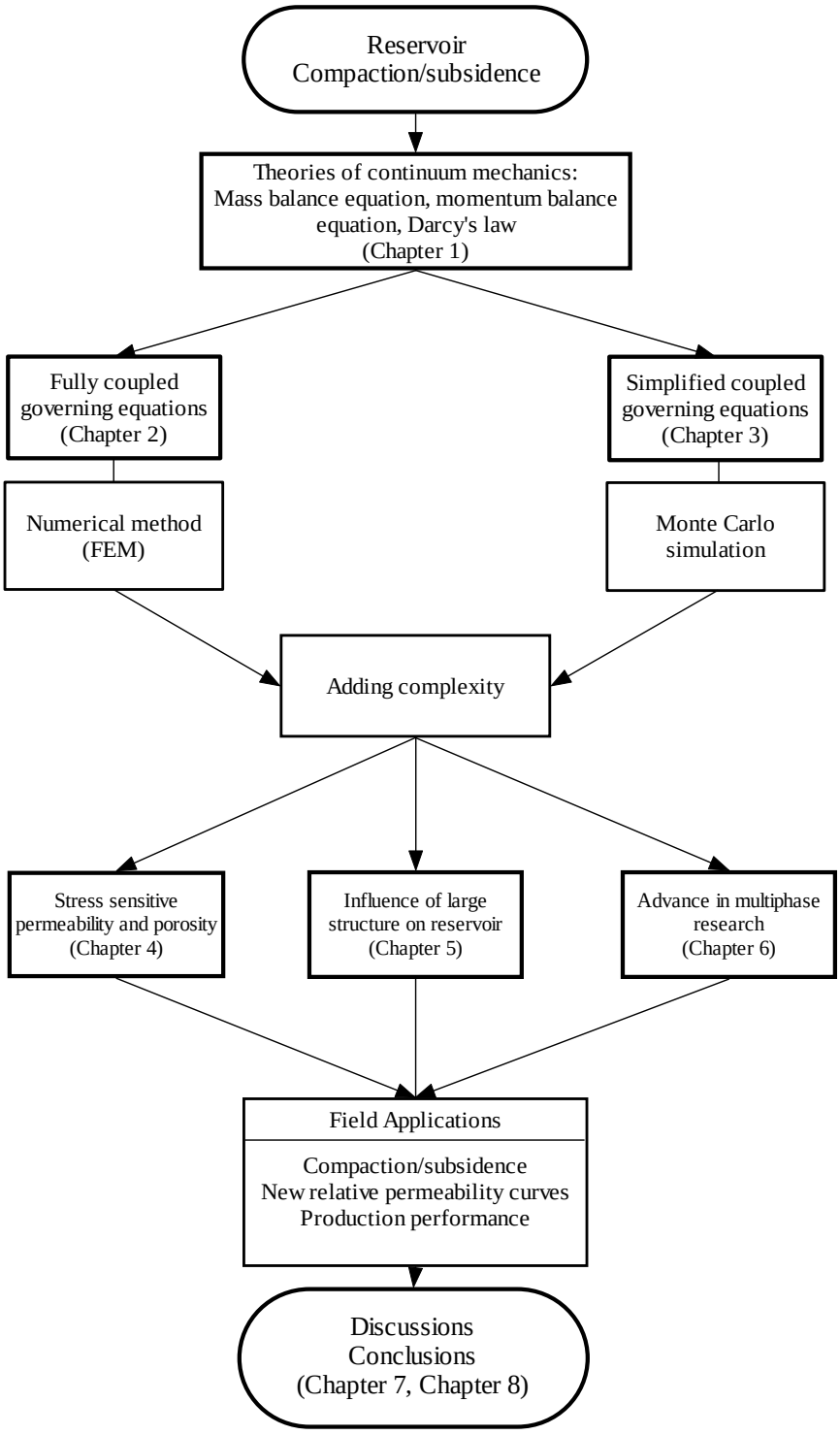

Figure 1-1: Flow chart showing objectives of the PhD research.

1.4 Outline of the thesis.

Chapter 1 has covered the general introduction relating to subsidence and compaction and defining the problems. A critical review of all aspects related to the research is also included.

Chapter 2 derives the equation for fully coupled fluid flow – geomechanics model theory as applied to reservoir engineering and rock mechanics research. The finite element method is applied for solving the governing fully coupled fluid flow – geomechanics model. Simplified solutions are presented that can be used quickly for estimating compaction and subsidence. These equations will be incorporated into uncertainty and stochastic – based simulations in the following chapters.

The impact of uncertainty and stochastic to subsidence and compaction is presented in Chapter 3. In this chapter, principal of statistics relating to Monte Carlo simulation are addressed as a potential tool for ascertaining uncertainty and model input variability.

Chapter 4 focuses more on porosity and permeability relationships in stress sensitive reservoir. This chapter presents the experimental equations suited for the relationship between permeability and porosity or the relationship between permeability and effective stress. Comparisons simulations using these relationships are implemented in the coupled reservoir simulation code. Core data from South Australia Petroleum fields are shown as a case example.

Chapter 5 shows the principle for the influence of a large structure (i.e fault) on compaction and subsidence and stress variability around large structural features. Also, sensitivity of permeability to stress perturbation and influence of a discontinuity on permeability is included and assessed.

Chapter 6 concentrates on change in multiphase fluid properties and rock properties due to compaction happening in the reservoir. The influence of pore collapse will be investigated in detail with coupled reservoir simulation, subsequently leading understanding of subsidence and compaction variation. A real field application in Venezuela is used where reservoir simulation provides estimation of compaction and subsidence as a result of pore collapse.

Discussions, conclusions and recommendations for future work are presented in chapter 7 and chapter 8.

CHAPTER 2: THE CONTINUUM MECHANICS THEORY APPLIED TO COUPLED RESERVOIR ENGINEERING PARTICULARLY IN SUBSIDENCE AND COMPACTION RESEARCH

2.1 Introduction

The previous chapter presented a general literature review on compaction and subsidence and all other relevant aspects of research. This chapter presents particular the theories of continuum porous mechanics applied for subsidence and compaction simulation. This chapter also reviews the relevant literature in accordance with the objectives of this chapter focusing on the radial coupled model. The study also shows the simplified-coupled model.

The objectives of the chapter:

- ✓ Overviewing equations for fully coupled fluid flow – geomechanics model theory.
- ✓ Deriving the equations for radial model based on the coupled fluid flow – geomechanics theory as applied to compaction and subsidence in reservoir engineering.
- ✓ Finite element method is applied for solving the governing fully coupled fluid flow – geomechanics model.

- ✓ Simplified solutions are also presented which can be used for quickly estimating compaction and subsidence. These equations will be put into uncertainty and stochastic simulations in chapter 3.

2.2 Fundamental theories

The first step before presenting the coupled theory applied in compaction and subsidence is to define some basics of continuum mechanics.

2.2.1 Liner elasticity definition

Force

Base on Newton's second law, force (**F**) is an influence that may cause a body with mass (m) to acceleration (**a**) defined as

$$\mathbf{F} = m\mathbf{a} \tag{2-1}$$

Stress

As general definition, stress is a measure of force intensity, which is also directional quantity measured by unit force (**F**) acting through the unit section (A)

$$\boldsymbol{\sigma} = \frac{\mathbf{F}}{A} \tag{2-2}$$

The orientation of the cross section relative to direction of force is important. A force can be divided in to two components

Normal stress $\boldsymbol{\sigma}_n$ is the stress normal to the cross section

$$\boldsymbol{\sigma}_n = \frac{\mathbf{F}_n}{A} \tag{2-3}$$

Shear stress $\boldsymbol{\sigma}_s$ is the stress parallel to the section

$$\boldsymbol{\sigma}_s = \frac{\mathbf{F}_p}{A} \qquad (2\text{-}4)$$

Stress & Pressure

According to Hillis (2005) both stress and pressure given by F/A, but stress is a tensor with normal stress and shear stress, whereas pressure (P) implies stresses in all directions are equal (e.g. hydrostatic)

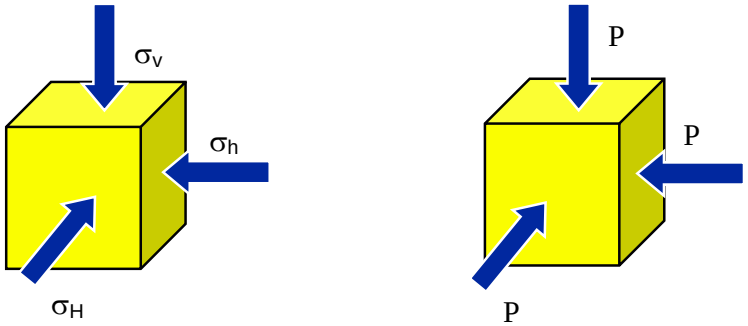

Stress & Strain

Strain is defined as fractional change in length (L) or volume (V)

$$\varepsilon = \partial L / L \text{ or } \varepsilon = \partial V / V \qquad (2\text{-}5)$$

The relationship between stress and strain in elastic theory is called the elastic modulus (E)

$$E = \frac{\sigma}{\varepsilon} \qquad (2\text{-}6)$$

Poisson's ratio (ν)

Poisson's ratio is the constant rate of lateral strain and longitudinal strain

$$\nu = -\frac{\varepsilon_x}{\varepsilon_y} \qquad (2\text{-}7)$$

2.2.2 Kinematics

Continuum mechanics deals with the mechanics of deformation and flow of materials under the assumption that all material bodies have continuous distribution of matter. It applies the laws of Newtonian mechanics to a deformable medium in suitable forms as well as developing constitutive laws, i.e. response of different categories of materials to external load in some idealized manner.

In mechanics of solids, the behavior of solids suggests that the material has memory; i.e. the past configurations of the body influence the state of stress at the current configuration. If the behavior of the body is purely elastic and the external load is withdrawn, the body will return to its original undeformed configuration (as if it remembers where it was initially). So reference configuration is a natural way for reference. In fluid dynamical problem in general, no such natural undeformed state exists. The fluid has no memory. After the fluid has undergone motion it doesn't come back to its original configuration after the forces causing the motion are withdrawn. The same is true for deformation of solids in the plastic zone. Reference state doesn't come naturally. Only the instantaneous values at the current configuration are important, although we can always refer to a configuration at a certain time, say, t_0, and study the motion of this configuration with time. In general the reference configuration need not be the undeformed state. It can be any configuration during the deformation process, say, at time t_0.

We define

$$\nabla(.) = \mathrm{Grad}(.) = \frac{\partial(.)}{\partial \mathrm{X}}$$

$$\nabla(.) = \mathrm{grad}(.) = \frac{\partial(.)}{\partial \mathrm{x}}$$

E = Green strain tensor

C = Right Cauchy-Green deformation tensor

g_i = Tangent vectors

dV = Referential volume element

dv = Current volume element

$\mathrm{x} = \varphi(\mathrm{X})$

u = Displacement

ρ_{ref} = Density at the reference configuration

ρ = Density at the current configuration

$\mathrm{F} = \text{Deformation gradient} = \frac{\partial \mathrm{x}}{\partial \mathrm{X}}$

J = Jacobian = det(F)

n = Normal vector

According to Sansour (2003), we have

$$J\rho = \rho_{ref} \qquad (2\text{-}8)$$

$$JdV = dv \qquad (2\text{-}9)$$

$$F = 1 + u \qquad (2\text{-}10)$$

$$\mathbf{C} = F^T F = 1 + \nabla u + (\nabla u)^T + (\nabla u)^T (\nabla u) \qquad (2\text{-}11)$$

$$\mathbf{E} = \frac{1}{2}(\mathbf{C} - 1) = \frac{1}{2}(\nabla u + (\nabla u)^T + (\nabla u)^T (\nabla u)) \qquad (2\text{-}12)$$

The velocity of the deformation gradient is given as:

$$\dot{F} = lF \Rightarrow l = \dot{F}\,F^{-1} \tag{2-13}$$

$$\dot{F} = \nabla \dot{u} = \frac{D}{Dt}(\nabla u) = \nabla v \tag{2-14}$$

$$F = \frac{\partial x}{\partial X} \Rightarrow F^{-1} = \frac{\partial X}{\partial x} \tag{2-15}$$

From (2-13), (2-14) and (2-15) follows

$$l = \nabla v \frac{\partial X}{\partial x} = \frac{\partial v}{\partial X}\frac{\partial X}{\partial x} = \frac{\partial v}{\partial x} = \mathrm{grad}(v) \tag{2-16}$$

$$g_i = FG_i \Rightarrow \dot{g}_i = \dot{F}\,G_i = lFG_i = lg_i \tag{2-17}$$

The decomposition holds:

$$l = d + w \tag{2-18}$$

with

$$d = \frac{1}{2}\left(l + l^T\right) \tag{2-19}$$

$$w = \frac{1}{2}\left(l - l^T\right) \tag{2-20}$$

$$\Rightarrow \dot{g}_i = (d + w)g_i \tag{2-21}$$

The deformation gradient F operates on a material line element dX giving dx at the current position. The deformation tensor C defines a metric on the deformed space, i.e., it gives a measure of the length of material line elements in the deformed

space. It also allows for the measurement of angles between two material line elements as well. C is a unit tensor at the reference configuration by definition. Strain tensor **E** gives the change in squired length of a material line element after deformation. **E** is a null tensor at reference configuration. The Jacobian J is the determinant of F and it physically shows the factor by which a material volume element dV is contracted or expanded after deformation and becomes dv. All the above quantities are to be understood in a local sense. In general they will vary from one material point to the next.

2.3 Principle laws

All material should follow with the conservation laws of physics where physical quantity is conserved; examples of such quantities are mass, electric charges and momentum. When we impose the fundamental laws of nature on the material body we can derive the basic equations of continuum mechanics valid for all types of materials, containing unknown variables of interest. This system of equations must be supplemented with constitutive laws to get specific solution for specific material behavior.

2.3.1 Conservation of mass

$$\int_B \rho_{ref}\, dV = const \Rightarrow \frac{D}{Dt}\int_B \rho_{ref}\, dV = 0 \qquad (2\text{-}22)$$

So

$$\dot{\rho}_{ref} = 0 \qquad (2\text{-}23)$$

The mass conservation law means at the rate of changing the mass is equal to zero.

$$\int_{B_t} \rho dv = const \Rightarrow \frac{D}{Dt}\int_{B} \rho J dV = \int_{B_t} \frac{D}{Dt}(\rho J)\frac{1}{J} dv = 0 \tag{2-24}$$

$$\Rightarrow \frac{(\dot{\rho J})}{J} = 0 \tag{2-25}$$

$$\Rightarrow (\dot{\rho J}) = 0 \tag{2-26}$$

$$\Rightarrow \dot{\rho} J + \rho \dot{J} = 0 \tag{2-27}$$

Now, we try to get an expression for $\dot{J}$

$$\frac{\partial(\det F)}{\partial F} = \det F F^{-T} \tag{2-28}$$

$$\Rightarrow \qquad \dot{J} = \frac{D}{Dt}(\det F) = \frac{\partial(\det F)}{\partial F} : \dot{F} = \frac{\partial(\det F)}{\partial F_{ij}} \dot{F}_{ij} \tag{2-29}$$

$$\begin{aligned} \dot{J} &= (\det F).F^{-T}\ \dot{F}^{T} : 1 \\ &= (\det F)trl^{T} \\ &= (\det F)trl \end{aligned} \tag{2-30}$$

So

$$\dot{J} = J\frac{\partial v_i}{\partial x_i} \tag{2-30}$$

From Equation 2-27

We have

$$\dot{\rho} + \rho \frac{\dot{J}}{J} = 0 \tag{2-31}$$

$$\Rightarrow \dot{\rho} + \rho \frac{\partial v_i}{\partial x_i} = 0 \tag{2-32}$$

So

$$\dot{\rho} + \rho \mathrm{div}(v) = 0 \tag{2-33}$$

2.3.2 Balance of momentum

For a continuum, conservation of momentum is expressed as follow: The rate of the change in linear momentum which instantaneously lies within a fixed region B is proportional to the resultant force applied to the material occupying B.

Definitions:

Force per volume: $\mathbf{b} = \lim_{\Delta V \to \delta V} \frac{\Delta F}{\Delta V}$

Force per surface: $\mathbf{t} = \lim_{\Delta a \to \delta a} \frac{\Delta F}{\Delta a}$

Where ΔV, Δa are of sufficiently small values

$$\int_{B_t} \mathbf{b} dv + \int_{\partial B_t} \mathbf{t} da = \frac{D}{Dt} \int_{B_t} \rho \dot{\mathbf{x}} dv \tag{2-34}$$

$$\frac{D}{Dt} \int_{B_t} \rho \dot{\mathbf{x}} dv = \frac{D}{Dt} \int_{B} \rho \dot{\mathbf{x}} (\mathbf{J} dV) \tag{2-35}$$

$$= \frac{D}{Dt} \int_{B} \rho_{ref} \dot{\mathbf{x}} dV \tag{2-36}$$

$$= \int_{B_t} \rho_{ref} \ddot{\mathbf{x}} dv \tag{2-37}$$

and, from Cauchy-Lemma $\mathbf{t}=\boldsymbol{\sigma}\mathbf{n}$ and we can convert the surface integral to a volume integral using Gauss's divergence theorem.

$$\int_{B_t} \mathbf{b}\,dv + \int_{\partial B_t} \mathbf{t}\,da = \int_{B_t} \rho \ddot{\mathbf{x}}\,dv \tag{2-38}$$

So

$$\mathbf{b} + \operatorname{div}(\boldsymbol{\sigma}) = \rho \ddot{\mathbf{x}} \tag{2-39}$$

$\Rightarrow$ Momentum balance equation!

2.3.3 The balance of angular momentum

Moment of momentum is the phrase used to designate the moment of the linear momentum with respect to some point. This vector quantity is also frequently called the angular momentum of the body. The principle of angular momentum states that the time rate of the change in the moment of momentum of a body with respect to a given point is equal to the moment of surface and body force with respect to that point.

$$\int_{B_t} x \times \mathbf{b}\,dv + \int_{\partial B_t} x \times \mathbf{t}\,da = \frac{D}{Dt}\int_{B_t} x \times \rho \dot{\mathbf{x}}\,dv \tag{2-40}$$

$$\int_{B_t} \varepsilon_{ijk} x_j b_k\,dv + \int_{\partial B_t} \varepsilon_{ijk} x_j t_k\,da = \frac{D}{Dt}\int_{B_t} \varepsilon_{ijk} x_j \rho \dot{x}_k\,dv \tag{2-41}$$

Taking the momentum equation into account, it follows

$$\int_{B_t} \varepsilon_{ijk} x_j b_k\,dv + \int_{\partial B_t} \left(\varepsilon_{ijk} x_j \sigma_{qk}\right)_{,q}\,da = \frac{D}{Dt}\int_{B_t} \varepsilon_{ijk} x_j \rho \dot{x}_k\,dv \tag{2-42}$$

$$\int_{B_t} \varepsilon_{ijk} \left[x_j \underbrace{\left(\rho \dot{v}_k - \sigma_{qk,q} - b_k \right)}_{=0} - \sigma_{jk} \right] dv = 0 \qquad (2\text{-}43)$$

This reduces to

$$\int_{B_t} \varepsilon_{ijk} \sigma_{jk} dv = 0 \qquad (2\text{-}44)$$

So

$$\sigma_{jk} = \sigma_{kj} \qquad (2\text{-}45)$$

or

$$\boldsymbol{\sigma} = \boldsymbol{\sigma}^T \qquad (2\text{-}46)$$

Thus, the law of conservation of angular momentum leads to the conclusion that the stress tensor is a symmetric tensor.

Stress Tensor

Tensor is symmetric with only six independent components (applies whether the point at rest or accelerating, but not if there is a torque)

$$\sigma_{12} = \sigma_{21}$$

$$\sigma_{13} = \sigma_{31}$$

$$\sigma_{23} = \sigma_{32}$$

Stress tensor in 2D written in matrix

$$\sigma_{ij} = \begin{bmatrix} \sigma_{11} & \sigma_{12} \\ \sigma_{21} & \sigma_{22} \end{bmatrix}$$

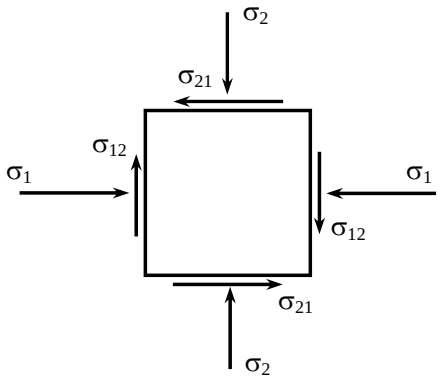

Stress tensor in 3D

In three dimensions, the stress is completely described by stress tensor which we have all together nine stress components related to one point in three dimensions as following:

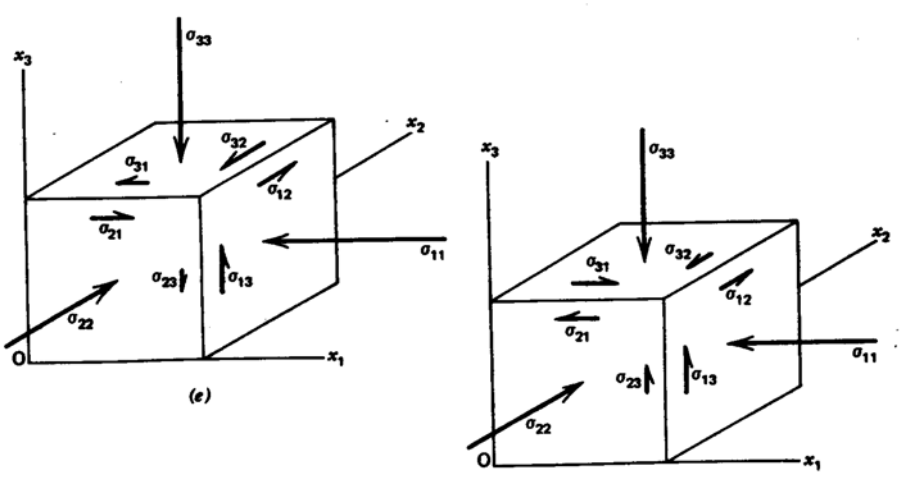

Written in matrix

$$\sigma_{ij} = \begin{bmatrix} \sigma_{11} & \sigma_{12} & \sigma_{13} \\ \sigma_{21} & \sigma_{22} & \sigma_{23} \\ \sigma_{31} & \sigma_{32} & \sigma_{33} \end{bmatrix}$$

In practice, stress tensor is usually redefined for convenience, where σ_{ij} denotes both types of stress (normal and shear). The subscripts i and j may be any of the number 1, 2, 3, which represent the x-, y-, z- axis, respectively. The first subscript (i) identifies the axis normal to the actual surface, while the second subscript (j) relates to the direction of the force.

Principal Stresses

At any point in homogeneous stress field can find three planes upon which shear stresses are zero. These planes are called principal planes of stress. Stresses normal to these planes are principal stresses: σ1, σ2 & σ3. In this case, stress tensor can be presented as

$$\begin{bmatrix} \sigma_1 & 0 & 0 \\ 0 & \sigma_2 & 0 \\ 0 & 0 & \sigma_3 \end{bmatrix}$$

So, state of stress can be characterized into: six independent stress components or magnitude and direction of σ1, σ2 & σ3

This study mainly deals with stress of reservoir and stress within the earth's crust in which vertical stress due to overburden rock can be considered as a principle stress. Hence, the two remaining stress are principle horizontal stresses. With such assumptions, stress tensor can be written as

$$\begin{bmatrix} \sigma_H & 0 & 0 \\ 0 & \sigma_h & 0 \\ 0 & 0 & \sigma_v \end{bmatrix}$$

where σ_v is the vertical principal stress, σ_h is the minimum horizontal principal stress and σ_H is the maximum horizontal principal stress (note that the positions of S_H, S_h and S_v on the diagonal are interchangeable depending on which is larger). Hence, if the vertical stress is assumed to be a principal stress, the stress tensor can be completely constrained by the orientation of one of the horizontal stresses and the magnitudes of the vertical and two principal stresses.

Anderson (1951) developed a classification of three different stress regimes: normal faulting, thrust (or reverse) faulting, and strike-slip faulting

- ✓ $\sigma_v > \sigma_H > \sigma_h$ normal fault
- ✓ $\sigma_H > \sigma_h > \sigma_v$ thrust fault

- ✓ $\sigma_H > \sigma_v > \sigma_h$ strike-slip fault

These three states of stress related to the three commonly seen modes of faulting in the earth's crust and are used throughout this thesis to describe relative stress magnitudes in the earth's crust.

2.4 Coupled fluid flow – geomechanics models

Many of the conservation laws of physics can be expressed in the form of statement that a physical quantity is conserved; examples of such quantities are mass conservation, momentum conservation, and an equation of state. When we impose the fundamental laws of nature on the material body we come up with the basic equations of continuum mechanics valid for all types of materials, containing unknown variables of interest. This system of equations must be supplemented with constitutive laws to get specific solution for specific material behavior.

Particularly in compaction and subsidence research, there are also three basic relationships of coupled fluid flow- geomechanics model: mass conservation, momentum conservation, and an equation of state. In general, reservoir deformation occurs very slowly compared to fluid flow. Hence, we can apply the fundamental assumptions with the small strain theory into these governing partial differential equations for the generalized coupled system in which the solid velocity is much smaller than the fluid velocity.

2.4.1 General form of coupled fluid flow – geomechanics models

Solid phase

Conservation of mass

$$\frac{\partial \rho}{\partial t} + \nabla.(\rho v) = 0 \qquad (2\text{-}47)$$

Applying Equation 2-47 to solid phase

$$\frac{\partial}{\partial t}\left((1-\phi).\rho_s\right) + \nabla.\left((1-\phi).\rho_s.v_s\right) = 0 \qquad (2\text{-}48)$$

Where v_s is the solid velocity, ϕ the formation porosity, and ρ_s the solid density. Assuming that deformation due to rearrangement of solid particles so ρ_s=const.

$$\frac{\partial}{\partial t}(1-\phi) + \nabla.\left((1-\phi).v_s\right) = 0 \qquad (2\text{-}49)$$

Because

$$\nabla.\left((1-\phi).v_s\right) = (1-\phi)\nabla.v_s + v_s.\nabla(1-\phi) \qquad (2\text{-}50)$$

So

$$\frac{\partial}{\partial t}(1-\phi) + (1-\phi)\nabla.v_s + v_s.\nabla(1-\phi) = 0 \qquad (2\text{-}51)$$

From the definition of the material derivative

$$\frac{dF}{dt} = \frac{\partial F}{\partial t} + v_s.\nabla F \qquad (2\text{-}52)$$

So Equation (2-51) become

$$\frac{d}{dt}(1-\phi) + (1-\phi)\nabla.v_s = 0 \qquad (2\text{-}53)$$

With volumetric strain definition we have

$$\varepsilon_{vol} = \nabla.u_s = \varepsilon_r + \varepsilon_\theta + \varepsilon_z \tag{2-54}$$

Substituting Equation (2-54) into Equation (2-53) yield:

$$\frac{d}{dt}(1-\phi) + (1-\phi)\frac{d\varepsilon_{vol}}{dt} = 0 \tag{2-55}$$

Rearrange Equation (2-55) we have

$$\frac{d(1-\phi)}{(1-\phi)} = -\frac{d\varepsilon_{vol}}{dt} \tag{2-56}$$

Integrating Equation (2-56) both sides with the initial condition, we have the variation of the porosity

$$\phi = 1-(1-\phi_0)e^{-\varepsilon_{vol}+\varepsilon_{vol,0}} \tag{2-57}$$

Where ϕ_0 is the initial porosity and $\varepsilon_{vol,0}$ is the initial volumetric strain which is the value at the previous time step. At t=0, the initial volumetric strain is equal to zero.

Conservation of momentum

Applying the conservation of momentum for solid phase, yield

$$\nabla.\sigma + f = 0 \tag{2-58}$$

Where: f is the body force per unit volume.

According to the theory developed by Fowler and Noon (1996), we have effective stress equation

$$\sigma' = \sigma - (1-\phi_0).I.P \tag{2-59}$$

Where σ and σ' are total stress and effective stress, respectively. I is the identity tensor and P is the pore pressure.

The effective solid is related to the solid strain with the following linear equation

$$\sigma' = D.\varepsilon \tag{2-60}$$

Fluid phase

Conservation of mass

$$\frac{\partial \rho}{\partial t} + \nabla.(\rho v) = 0 \tag{2-61}$$

Applying Equation 2-61 to fluid phase

$$\frac{\partial}{\partial t}(\phi.\rho_f) + \nabla.(\phi.\rho_f.v_f) = 0 \tag{2-62}$$

Conservation of momentum in fluid phase – Darcy's law

$$\phi(v_f - v_s) = -\beta \frac{K}{\mu} \nabla P \tag{2-63}$$

Equation of state (isothermal fluid compressibility)

$$C_f = \frac{1}{\rho} \frac{\partial \rho}{\partial P} \tag{2-64}$$

Both the fluid velocity v_f and the solid velocity v_s are local volume averaged values with respect to a stationary coordinate frame. The condition for a nondeformable (stationary) medium is v_s=0. Gravity effects are not considered. Fluid density and viscosity are assumed to be a function of fluid pressure only.

Substituting this Darcy's law into Equation 2-62 and rearranging this equation yields

$$\nabla.\left(\rho_f \frac{k}{\mu}\nabla P\right) = \frac{\partial(\phi\rho_f)}{\partial t} + \vec{v}_s.\nabla(\rho_f\phi) + \rho_f\phi\nabla.\vec{v}_s \tag{2-65}$$

By using the material derivative

$$\frac{d(\ )}{dt} = \frac{\partial(\ )}{\partial t} + \vec{v}_s.\nabla(\ ) \tag{2-66}$$

We have

$$\nabla.\left(\rho_f \frac{k}{\mu}\nabla P\right) = \phi\rho_f\left(\frac{1}{\rho_f}\frac{d\rho_f}{dP} + \frac{1}{\phi}\frac{d\phi}{dP} + \nabla.\vec{v}_s\right) \tag{2-67}$$

2.4.2 Coupled radial single-phase fluid flow – geomechanics model

The governing equations for radial single-phase flow model in a deforming porous media can be derived as following:

Solid phase

$$\frac{d}{dt}(1-\phi) + (1-\phi)\nabla.v_s = 0 \tag{2-68}$$

We also have the variation of the porosity

$$\phi = 1 - (1-\phi_0)e^{-\varepsilon_{vol}+\varepsilon_{vol,0}} \tag{2-69}$$

We have effective stress equation

$$\sigma' = \sigma - (1-\phi_0).I.P \tag{2-70}$$

In radial coordinates, σ', ε become

$$\sigma' = \left\{\sigma_r', \sigma_\theta', \sigma_z', \tau_{rz}'\right\}^T \tag{2-71}$$

$$\varepsilon = \left\{\varepsilon_r, \varepsilon_\theta, \varepsilon_z, \tau_{rz}\right\}^T \tag{2-72}$$

and

$$D = \frac{E}{(1+\nu)(1-2\nu)}\begin{bmatrix} 1-\nu & \nu & \nu & 0 \\ \nu & 1-\nu & \nu & 0 \\ \nu & \nu & 1-\nu & 0 \\ 0 & 0 & 0 & \frac{1-2\nu}{2} \end{bmatrix} \tag{2-73}$$

Where: E is elastic modulus and ν is Poisson' ratio.

Fluid phase

Conservation of mass

$$m_{in} - m_{out} = m_{acc} \tag{2-74}$$

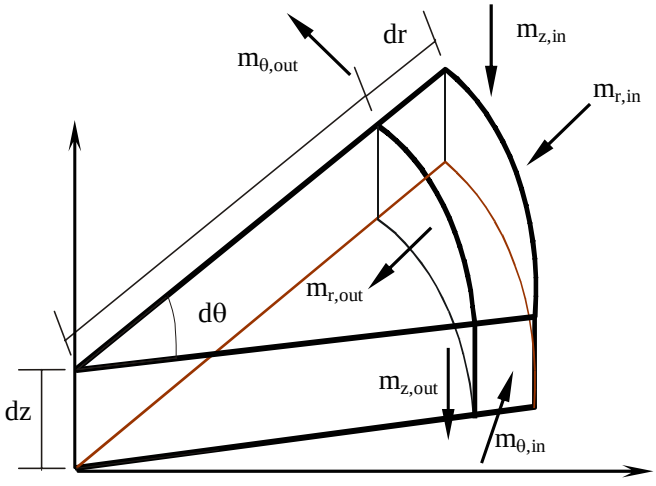

Figure 2-1: Schematic showing of fluid flow in a single element

We have

$$m_{acc} = (\rho.r.d\theta.dz.dr.\phi) \tag{2-75}$$

So, the variation of accumulated mass with time is

$$\frac{\partial m_{acc}}{\partial t} = \frac{\partial}{\partial t}(\rho.r.d\theta.dz.dr.\phi) \tag{2-76}$$

and

$$m_{in} = (\alpha.\rho.v_r.\phi.A_r) + (\alpha.\rho.v_z.\phi.A_z) + (\alpha.\rho.v_\theta.\phi.A_\theta) \tag{2-77}$$

With $A_r = r.d\theta.dz$, $A_z = r.d\theta.dr$ $A_\theta = dr.dz$

So

$$\begin{aligned} m_{out} &= \left((\alpha.\rho.v_r.\phi.A_r) + \frac{\partial(\alpha.\rho.v_r.\phi.A_r)}{\partial r} dr \right) \\ &+ \left((\alpha.\rho.v_Z.\phi.A_Z) + \frac{\partial(\alpha.\rho.v_Z.\phi.A_Z)}{\partial z} dz \right) \\ &+ \left((\alpha.\rho.v_\theta.\phi.A_\theta) + \frac{\partial(\alpha.\rho.v_\theta.\phi.A_\theta)}{\partial \theta} d\theta \right) \end{aligned} \tag{2-78}$$

Substituting Equation 2-76, 2-77 and 2-78 to Equation 2-74, yield

$$\begin{aligned} &\frac{\partial}{\partial t}(\rho.\phi) = \\ &-\left(\frac{1}{r} \frac{\partial(\alpha.\rho.v_r.\phi.r)}{\partial r} + \frac{\partial(\alpha.\rho.v_Z.\phi)}{\partial z} + \frac{1}{r} \frac{\partial(\alpha.\rho.v_\theta.\phi)}{\partial \theta} \right) \end{aligned} \tag{2-79}$$

Because the system is axisymmetric, Equation 2-79 becomes

$$\frac{\partial}{\partial t}(\rho.\phi) = -\left(\frac{1}{r} \frac{\partial(\alpha.\rho.v_r.\phi.r)}{\partial r} + \frac{\partial(\alpha.\rho.v_Z.\phi)}{\partial z} \right) \tag{2-80}$$

Conservation of momentum

Applying Darcy's law that can be derived from conservation of momentum we have

$$v_i = \phi\left(v_{if} - v_{is}\right) = -\beta\frac{K}{\mu}\nabla P \tag{2-81}$$

So

$$\phi v_{if} = v_i + \phi v_{is} \tag{2-82}$$

With i=r, z. Substituting this Darcy's law into Equation 2-80 yield

$$\begin{aligned}&\frac{1}{\alpha}\frac{\partial}{\partial t}\left(\rho.\phi\right)\\&= -\left(\frac{1}{r}\frac{\partial\left(\rho.\left(v_r + \phi v_{rs}\right).r\right)}{\partial r} + \frac{\partial\left(\rho.\left(v_z + \phi v_{zs}\right)\right)}{\partial z}\right)\end{aligned} \tag{2-83}$$

or

$$\begin{aligned}&\frac{1}{\alpha}\frac{\partial}{\partial t}\left(\rho.\phi\right)\\&= -\left(\frac{1}{r}\frac{\partial\left(\rho.\left(-\beta\frac{K}{\mu}\nabla P\right).r\right)}{\partial r} + \frac{\partial\left(\rho.\left(-\beta\frac{K}{\mu}\nabla P\right)\right)}{\partial z}\right)\\&-\left(\frac{1}{r}\frac{\partial\left(\rho.\left(\phi v_{rs}\right).r\right)}{\partial r} + \frac{\partial\left(\rho.\left(\phi v_{zs}\right)\right)}{\partial z}\right)\end{aligned} \tag{2-84}$$

Rearranging above equation, we have:

$$\begin{aligned}&\frac{1}{\alpha}\frac{1}{\rho\phi}\left(\phi\frac{\partial(\rho)}{\partial t}+\rho\frac{\partial(\phi)}{\partial t}\right)\\&=\frac{1}{\rho\phi}\left(\frac{K\beta}{\mu}\left(\begin{array}{l}\rho\dfrac{\partial(\nabla P)}{\partial r}+\dfrac{\rho}{r}\nabla P+\\ \nabla P\dfrac{\partial(\rho)}{\partial r}+\rho\dfrac{\partial(\nabla P)}{\partial z}+\nabla P\dfrac{\partial(\rho)}{\partial z}\end{array}\right)\right)\\&-\left(\frac{\partial v_{rs}}{\partial r}+\frac{\partial v_{zs}}{\partial z}\right)\end{aligned} \tag{2-85}$$

$$\begin{aligned}&\frac{\partial^2 P}{\partial r^2}+\frac{1}{r}\frac{\partial P}{\partial r}+C_f\left(\frac{\partial P}{\partial r}\right)^2+\frac{\partial^2 P}{\partial z^2}+C_f\left(\frac{\partial P}{\partial z}\right)^2\\&=\frac{1}{\alpha\beta}\frac{\mu\phi}{K}C_t\frac{\partial P}{\partial t}+\frac{1}{\beta}\frac{\mu\phi}{K}\left(\frac{\partial v_{rs}}{\partial r}+\frac{\partial v_{zs}}{\partial z}\right)\end{aligned} \tag{2-86}$$

$$\text{With } C_t=C_f+C_s=\frac{1}{\rho}\frac{\partial\rho}{\partial P}+\frac{1}{\phi}\frac{\partial\phi}{\partial P} \tag{2-87}$$

Where: C_t is the total compressibility. C_f and C_s are fluid and solid compressibility, respectively.

It is clear that

$\left(\frac{\partial P}{\partial r}\right)^2$ and $\left(\frac{\partial P}{\partial z}\right)^2$ are nonlinear and <<1

These terms are often neglected in the equations used for coupled reservoir simulation as follows:

$$\begin{aligned}&\frac{\partial^2 P}{\partial r^2}+\frac{1}{r}\frac{\partial P}{\partial r}+\frac{\partial^2 P}{\partial z^2}\\&=\frac{1}{\alpha\beta}\frac{\mu\phi}{K}C_t\frac{\partial P}{\partial t}+\frac{1}{\beta}\frac{\mu\phi}{K}\left(\frac{\partial v_{rs}}{\partial r}+\frac{\partial v_{zs}}{\partial z}\right)\end{aligned} \tag{2-88}$$

With

$$\left(\frac{\partial v_{rs}}{\partial r}+\frac{\partial v_{zs}}{\partial z}\right)=\left(\frac{\partial}{\partial t}\left(\frac{\partial u_{rs}}{\partial r}\right)+\frac{\partial}{\partial t}\left(\frac{\partial u_{zs}}{\partial z}\right)\right)$$
$$=\frac{\partial \varepsilon_r+\partial \varepsilon_z}{\partial t}=\frac{\partial \varepsilon_{vol}}{\partial t} \qquad (2\text{-}89)$$

So

$$\frac{\partial^2 P}{\partial r^2}+\frac{1}{r}\frac{\partial P}{\partial r}+\frac{\partial^2 P}{\partial z^2}=$$
$$\frac{1}{\alpha\beta}\frac{\mu\phi}{K}C_t\frac{\partial P}{\partial t}+\frac{1}{\beta}\frac{\mu\phi}{K}\frac{\partial \varepsilon_{vol}}{\partial t} \qquad (2\text{-}90)$$

The general case requires a numerical method to solve all of the above equations which have boundary and initial conditions

2.4.3 Coupled two phase fluid flow – geomechanics model

The governing equations for a coupled multiphase flow and geomechanics system can be similarly obtained using the same assumptions as in sections 2.4. For a coupled solid/oil/water system, water and oil are assumed immiscible. Consequently, the governing equations can be summarized (Eclipse 2005) as follows:

Oil/water mass balance equations

$$\nabla.\left[k\frac{k_{ro}}{B_o\mu_o}\left(\nabla p_o-\gamma_o\nabla D\right)\right]=\phi\frac{\partial}{\partial t}\left(\frac{S_o}{B_o}\right)+\alpha_p\frac{S_o}{B_o}\frac{\partial\left(\nabla.\vec{u}\right)}{\partial t}+q_o \qquad (2\text{-}91)$$

$$\nabla.\left[k\frac{k_{rw}}{B_w\mu_w}\left(\nabla p_w-\gamma_w\nabla D\right)\right]=\phi\frac{\partial}{\partial t}\left(\frac{S_w}{B_w}\right)+\alpha_p\frac{S_w}{B_w}\frac{\partial\left(\nabla.\vec{u}\right)}{\partial t}+q_w \qquad (2\text{-}92)$$

Solid force balance equations

$$G\nabla^2\vec{u} + (G+\lambda)\nabla(\nabla.\vec{u}) + \vec{f} = \alpha_p \nabla p_p \qquad (2\text{-}93)$$

Where

Porosity $\phi = 1-(1-\phi_o)e^{-\nabla.\vec{u}}$

Capillary pressure $p_c = p_w - p_o$

Pore pressure $p_p = S_w p_w + S_o p_o$

S_w and S_o are water saturation and oil saturation, respectively.

B_w and B_o are formulation volume factors of water and oil, respectively.

G and λ are the Lamé elastic parameters

u denotes the displacement of porous medium.

2.5 Numerical solution of the governing equations

The commonly used numerical methods in reservoir simulations are finite difference methods (FDM's), finite volume methods (FVM's), and finite element methods (FEM's). Each has its advantages and disadvantages in the implementation.

2.5.1 Finite Difference Method (FDM)

To achieve approximate solutions to partial difference equations (PDEs) in all aspects of engineering, the FDM is well-know numerical method used, especially in fluid dynamics, heat transfer and solid mechanics. The foundation of FDM is to replace the partial derivatives of the governing equations by differences defined over certain spatial intervals in the coordinate directions dx, dy, and dz; which generate a system of algebraic simultaneous equations of the governing equations at a mesh of

nodes over the domain of interest. Applying boundary conditions defined at boundary nodes, solution of the simultaneous algebraic system equations will yield the required values of the governing equation at all nodes, which meet with both the governing PDE's and special boundary conditions. The discretization schemes by finite difference (FD) are easy to construct but this method requires the use of a structured grid. In addition, FD code is memory and computational efficient, and can be easily parallelized. However, the requirement of a structured grid makes girding of complicated domains difficult. For example, it may be challenging to treat complicated geology structures such as faults, sills and fractures. If the grid needs to be aligned with these features, adaptive mesh refinement can sometimes alleviate grid geometry problems. Although there are still limitations, FDM is common used in petroleum industry (Eclipse 2005).

2.5.2 Finite Volume Method (FVM)

Another numerical method to obtain approximation of the PDE's is the Finite Volume Method (FVM). In an FVM, the integral form of an equation is discretized, which guarantees conversation. This method overcomes the limitation of FDM as FVM does not require a structured mesh. In addition, an FVM is preferable to other methods as a result of the fact that boundary conditions can be applied noninvasively because the values of the conserved variables are positioned within the volume element, and not at nodes or surfaces. FVM's are especially powerful on coarse nonuniform grids and in calculations where the mesh moves to track interface or shocks.

2.5.3 Finite Element Method (FEM)

The most useful numerical method is FEM. This method deals with an integral formulation of an equation by using a weak formulation. Because an FEM can be applied to problems of great complexity and unusual geometry, it is a powerful tool in the solution of complexity problems such as fracture in mechanics or fault within geology structure. An FEM is very flexible at representing complex geometries. Consequently, using this method the mesh can be refined near particular features. In addition, the mesh can also be reduced at the far field region. So that large volumes of free space can be included. But for a fine-grid system, the expense involved in solving this large system is usually prohibitive. Considering so many uncertain factors in reservoir parameters and the solving efficiency, this expense may be not justified.

2.5.4 Equation discretization

The formulations of coupled theories between fluid and solid applied to radial flow in reservoir engineering have been presented. Unfortunately, the general analytical solution for this equation has not been resolved except in simplified cases. Despite this, a numerical method can be applied to achieve the general solution. The Galerkin finite element method is chosen because of its ability to handle anisotropic and heterogeneous regions with complex boundaries (Young's and Hyochong 1996).

In the Galerkin method, the unknown variable pressure and displacements can be approximated by a trial solution in space using of the shape function N and nodal values (P, u)

$$P = \sum_{i=1}^{n} N_i P_i \qquad (2\text{-}94)$$

$$u_r = \sum_{i=1}^{n} N_i u_{ri} \tag{2-95}$$

$$u_z = \sum_{i=1}^{n} N_i u_{zi} \tag{2-96}$$

Therefore, in the coupled simulation, there are three principal degrees of freedoms at each node of the mesh.

We have the generally fully coupled equations as following

$$M_1 \dot{P} + K_1 P + M_2 \dot{u} = F_1 \tag{2-97}$$

$$K_2 d + C_2 P = F_2 \tag{2-98}$$

Applying the time integration technique with Crank-Nicholson method described we derived the coupled matrix system.

$$\begin{bmatrix} 2M_2 & 2M_1 + \Delta t K_1 \\ K_2 & C_2 \end{bmatrix} \cdot \begin{bmatrix} u^{t+\Delta t} \\ P^{t+\Delta} \end{bmatrix} = \begin{bmatrix} \Delta t\left(F_1^{\,t+\Delta t} + F_1^{\,t}\right) + \left(2M_1 - \Delta t K_1\right)P^t + 2M_2 u^t \\ \left(F_2^{\,t+\Delta t} + F_2^{t}\right) - \left(K_2 u^t + C_2 P^t\right) \end{bmatrix} \tag{2-99}$$

Where

$$M_1 = \int \frac{1}{\alpha\beta} \frac{\mu\phi}{K} C_t N_i N_j dR$$

$$K_1 = \int \frac{\partial N_i}{\partial r} \frac{\partial N_j}{\partial r} dR + \int \frac{\partial N_i}{\partial z} \frac{\partial N_j}{\partial z} dR$$

$$M_2 = \int \frac{1}{\beta} \frac{\mu\phi}{K} N_i \left(\frac{\partial N_j}{\partial r} + \frac{\partial N_j}{\partial z} \right) dR$$

$$F_1 = 2\pi r N_i \frac{\partial P}{\partial r} n_r \Big|_B + 2\pi r N_i \frac{\partial P}{\partial z} n_z \Big|_B$$

$$K_2 = \int \frac{\partial N_i}{\partial g}.D.\frac{\partial N_j}{\partial g} dR$$

$$C_2 = (1-\phi_0)\int N_j.\left(\frac{\partial N_i}{\partial r} + \frac{\partial N_i}{\partial z}\right) dR$$

in which

$$\dot{P} = \left\{\dot{P}_1, \dot{P}_2, \dot{P}_3, \dot{P}_4\right\}^T \quad \dot{u} = \left\{\dot{u}_1\ \dot{v}_1\ \dot{u}_2\ \dot{v}_2\ \dot{u}_3\ \dot{v}_3\ \dot{u}_4\ \dot{v}_4\right\}^T$$

$$u = \left\{u_1\ v_1\ u_2\ v_2\ u_3\ v_3\ u_4\ v_4\right\}^T$$

$$\sigma' = \left\{\sigma'_r, \sigma'_\theta, \sigma'_z, \tau'_{rz}\right\}^T$$

$$\varepsilon = \left\{\varepsilon_r, \varepsilon_\theta, \varepsilon_z, \tau_{rz}\right\}^T$$
$$= \left\{\frac{\partial u_r}{\partial r}, \frac{u_r}{r}, \frac{\partial u_z}{\partial z}, \frac{\partial u_r}{\partial z} + \frac{\partial u_z}{\partial r}\right\}^T$$

Noting that, porosity and permeability will be updated at each time step on each element. The influence of permeability and porosity on coupled simulation results can be found in Ta and Hunt (2005).

Boundary condition

There are 2 main types of boundary condition for each phase

Solid phase:

Dirichlet-type prescribed displacement

$$u(r,z,t) = \tilde{u} \text{ with } \forall r,z \in \Gamma_{s1} \tag{2-100}$$

Neumann-type prescribed surface traction.

$$\sigma.n = \tilde{h} \text{ with } \forall r,z \in \Gamma_{s2} \tag{2-101}$$

Where $\Gamma_{s1} \cup \Gamma_{s2} = \Gamma_s$

Fluid phase:

Dirichlet-type prescribed initial pressure

$$p(r, z, t) = \tilde{p} \quad \forall r, z \in \Gamma_{f1} \tag{2-102}$$

Neumann-type prescribed normal flux to boundary

$$\nabla p.n = 0 \ \forall r, z \in \Gamma_{f2} \tag{2-103}$$

Where $\Gamma_{f1} \cup \Gamma_{f2} = \Gamma_f$ and unit normal vector $n = \{n_r, n_z, n_\theta\}^T$. Subscript s and f refer to solid and fluid phase, respectively.

Initial condition (t=0)

$$u(r, z, 0) = u_0 \tag{2-104}$$

$$P(r, z, 0) = P_0 \tag{2-105}$$

Matrix Equation (2-99) must be completely constrained by initial and boundary conditions described by Equation (2-100) – (2-105) before a solution is obtained.

2.6 Analytical solutions for compaction and subsidence

Coupled mathematic models used in dealing with subsidence and compaction have been presented. Numerical methods are employed to solve total subsidence and compaction but complete study of subsidence including modeling and prediction is generally a difficult task and has to use advanced simulator which is costly. In this situation, the analytical method, using the Geertsma's equation (Geertsma 1973) based on nucleus-of strain equations from rock mechanics, is still quick and worthy tool in particularly evaluation of subsidence and compaction for disk shaped homogeneous reservoir which usually happens worldwide.

Geertsma's equation is described more detail by Holt (1990) from the 3D simplified coupled equations. The maximum vertical compaction (Δh) and subsidence (S) for a roughly disk-shaped oil and gas bearing reservoir formation can be estimated using the equations 2-106 and 2-107

$$\Delta h = \frac{1-\nu-2\nu^2}{(1-\nu)E}\Delta p_f h \qquad (2\text{-}106)$$

$$S = \frac{C_b}{2}\Delta p_f h A(\rho,\eta) \qquad (2\text{-}107)$$

Where C_b, ν, R, h, D, $A(\rho,\eta)$ are bulk coefficient, Poisson's ratio, average reservoir radius, average reservoir thickness, reservoir depth of burial and Bessel function, respectively.

2.7 Conclusions

The continuum mechanics theory as applied to a coupled fluid flow – geomechanics simulation has been presented in this chapter. Chapter 2 shows the importance of the fully coupled fluid flow – geomechanics model applying in compaction and subsidence calculation. Furthermore, governing equations for a radial model as applied to compaction and subsidence are derived. The finite element method is also used for solving the governing equation of fully coupled fluid flow – geomechanics model. Simplified solutions are also presented that can be employed for quickly estimating compaction and subsidence. These equations will be used in uncertainty evaluation and stochastic simulations in the following chapter.

CHAPTER 3: THE IMPACT OF UNCERTAINTY ON SUBSIDENCE AND COMPACTION

3.1 Introduction

Sub-surface compaction due to fluid withdrawal from a reservoir (oil, gas or water) has been well documented worldwide over the last few decades. Compaction of a reservoir can also lead to subsidence at the ground surface or the seafloor. Many methods are employed to calculate total subsidence and compaction. Among these methods, the deterministic method, using Geertsma' analytical equation (chapter 2), is particularly favorable for disk shaped homogeneous reservoir in compaction and subsidence calculations. Unfortunately, Geertsma's equation still ignores the uncertainty of the deterministic-based input parameters.

Objectives of this chapter are to present the stochastic approach using Monte Carlo simulation applied to compaction and subsidence estimation. The research addresses the impact of uncertainty on subsidence and compaction prediction when taking into account uncertainty of E, ν and Δp_f as applied to a deep-water petroleum field in the Gulf of Mexico. The reservoir model modeled stochastically is compared with the commercial numerical software-*Eclipse 300*. Finally, potential reservoirs where subsidence and compaction could happen are presented in term of describing the range of E and ν within a stochastic characterization of a large-scale regional reservoir model

3.2 Why do we need to investigate uncertainty on subsidence and compaction

Compaction of a reservoir can also lead to subsidence at the ground level or the seafloor. Examples of subsidence and compaction have been observed in many places such as Venezuela (Merle et al. 1976), the Gulf of Mexico and Gippsland Basin (Jim, Bailey et al. 2006). In the Cooper Basin – Australia, the compaction problem was first investigated by Ta and Hunt (2005).

The need for more sophisticated prediction approaches in assessing the impact of subsidence and compaction on production management of the reservoir has led to a continuous improvement of numerical models employed. Such approaches use the continuum poroelastic theory. For example, the use of advanced models for accurate prediction of land subsidence were documented by Gambolati (2001) and Ta et al. (2005). However, although sophisticated poroelastic constitutive models have been developed for a realistic description of the actual rock mass behavior (Biot 1940; Gutierrez 1994; Terry, Garfield et al. 2000), the geomechanical analysis of producing fields is usually performed deterministically, thus limiting breadth of solution and sensitivities involved. To overcome the limitation of the deterministic model which would require an extensive medium characterization, neither supported by the available data nor allowed by the available resources, the properties of rock heterogeneity at the field and regional scale can be incorporated stochastically into geostatistical models (Collin, Schroeder et al. 2005; Massimiliano, Giuseppe et al. 2006).

While stochastic models have been extensively used over the last few decades for modeling flow and transport into random porous media, only a limited number of studies have addressed the influence of using stochastic model to assess the effect of rock properties on the geomechanical behavior of the reservoir (Diego, Marcio et al. 2004). In particular, there are few studies that have been incorporated a stochastic-based simulation when analyzing rock heterogeneous media when applied to compaction and subsidence related problem. In addition, some of the most important parameters such as Young's modulus (E), Poisson's ratio (ν), and even reduction of pore fluid pressure (Δp_f) usually have ignored magnitude variation when modeling geomechanical parameters in compacting reservoir.

3.3 Statistics principle

There are two types of statistical approaches, classical statistics and spatial statistics. Geostatistics is the statistics of observations located in space or time. The data collected can be correlated spatially or temporally.

3.3.1 Histograms of data

Histograms are very useful data summaries which allow many characteristics of data to be presented in a single illustration. They are obtained simply by grouping data together into classes. For example, consider the Young's modulus data from core sample

227,108.9 195,165.2 165,745.9 140,259.7 105,730.6 76,290.8 64,396.0

64,768.9 50,221.0 50,967.9 50,136.3 48,843.4 190,634.0 145,776.8

117,687.3 100,144.2 89,398.9 82,897.2 75,410.7 70,696.1 68,170.3

70,404.2 74,087.6 78,870.5

We have a histogram as shown in Figure 3-1 which expresses the number of values in a class interval as a percentage of the total number of values.

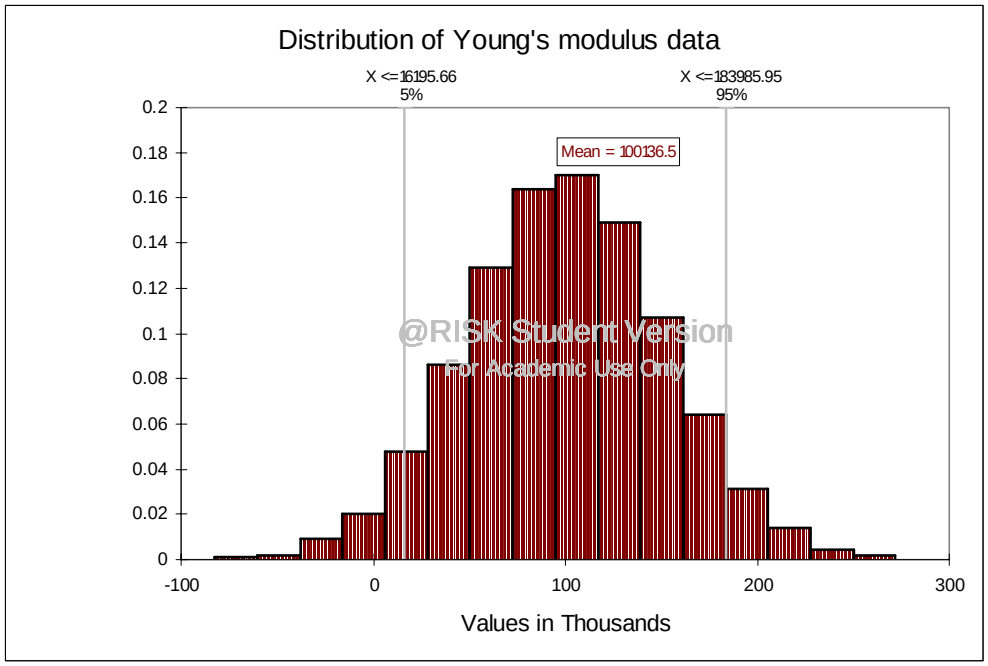

Figure 3-1: Histogram of Young's modulus data

3.3.2 The normal distribution

Suppose we have n sample values x_i, i=1,2..n. The first step in the analysis of these values consists in grouping them into classes and counting the number of samples within that class. The histogram is drawn from this data. If the histogram distribution is reasonably symmetrical and has density function as

$$f(x) = \frac{1}{\sqrt{2\pi}\sigma} e^{-\frac{1}{2}\left(\frac{x-\mu}{\sigma}\right)^2} \qquad (3\text{-}1)$$

Where: σ, μ are standard deviation and mean, respectively.

With

$$\mu = \frac{1}{n}\sum_{i=1}^{n} x_i \tag{3-2}$$

$$\sigma = \sqrt{\frac{1}{n-1}\sum_{i=1}^{n}(x_i - \mu)^2} \tag{3-3}$$

We have normal distribution as shown in Figure 3-1

In practice, the assumption of normal distribution of sample values is not often satisfied except when samples collected has a relative high grade. When taking samples from a new field, the number of samples might be insufficient to obtain a representative histogram. Judgment and past experience are then used to decide whether the assumption of normality can be accepted.

3.3.3 The lognormal distribution

In other situations, the distribution of sample values is not symmetrical, but has a positive skew. This distribution is well presented by a lognormal distribution using additional parameters. If log(x) is a variable with normal a distribution, then we have two-parameters lognormal. If log(x+β) is a variable with normal distribution, then we have three-parameters lognormal where β is constant.

So f(x), σ, and μ from 3-1, 3-2 and 3-3 become

$$f(x) = \frac{1}{x\sqrt{2\pi\sigma'}} e^{-\frac{1}{2}\left(\frac{\ln x - \mu'}{\sigma'}\right)^2} \tag{3-4}$$

$$\mu' = \ln\left(\frac{\mu^2}{\sqrt{\sigma^2 + \mu^2}}\right) \tag{3-5}$$

$$\sigma' = \sqrt{\ln\left[1+\left(\frac{\sigma}{\mu}\right)^2\right]} \qquad (3\text{-}6)$$

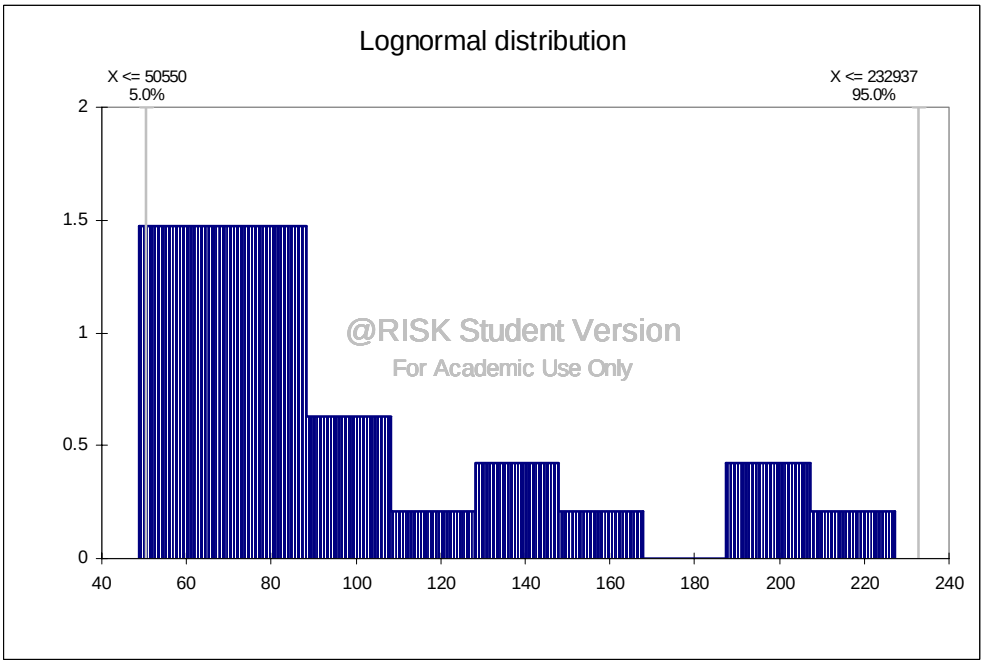

Figure 3-2: Example of lognormal distribution

3.4 Stochastic model - Monte Carlo simulation

In most engineering applications, deterministic models are more frequently used over stochastic models; in such case, a single output value is obtained for every input value, and for all variables (Figure 3-3). The assumption made is that the input variable is known precisely; in reality many input variables have uncertainty attached to them, hence the need for a stochastic approach (Al-Harthy, Khurana et al. 2006). Murtha (2000) defined risk as "Potential gains or losses associated with each particular outcomes" and uncertainty as "The range of possible outcomes". In such a

scenario risk and uncertainty estimate the input parameter as a range instead of a single point. For example, the price of a barrel of oil could be represented as a normal distribution with a mean of $20 per barrel and a standard deviation of $4 per barrel, instead of using a single value of $20 per barrel.

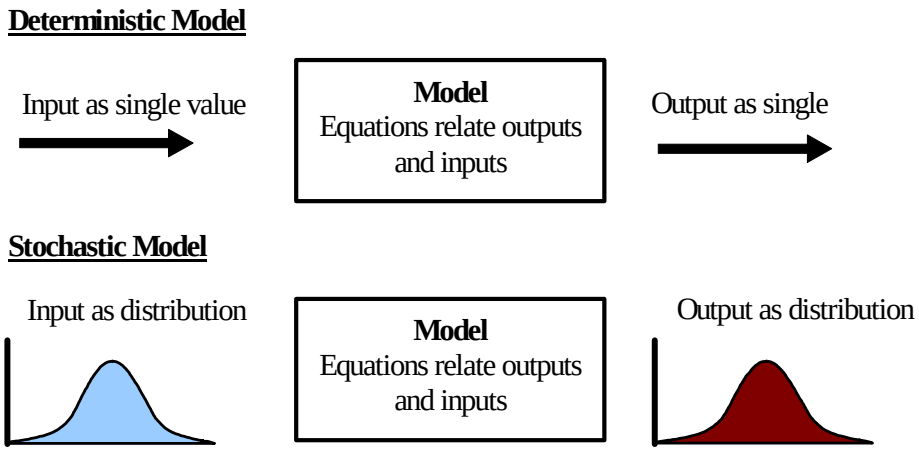

Figure 3-3: Stochastic vs. the deterministic model

Risk analysis is designed to handle the uncertainty of input variables through stochastic models using the Monte Carlo simulation method. The Monte Carlo simulation is a statistical method that uses a probability distribution for input and produces an output probability distribution (Figure 3-3). In this study, the Monte Carlo simulation is applied for the evaluation of the compacting reservoir based on the analytical geomechanical-fluid flow equation.

The Monte Carlo simulation method is applied to the calculation of compaction and subsidence. This accounts for the fact that the key input parameters E and ν have not been exactly presented or properly calculated at the field scale. Reduction of Δp_f related to fluid production has been taken into account. These input parameters, in the

sense of computer-based distributions of E, ν and Δp_f, are shown in terms of 26 sample data from two wells are presented in Figure 3-4.

The practice of describing the input parameters with range is actually more realistic because it captures our absence of information in estimating the true value of the input parameter.

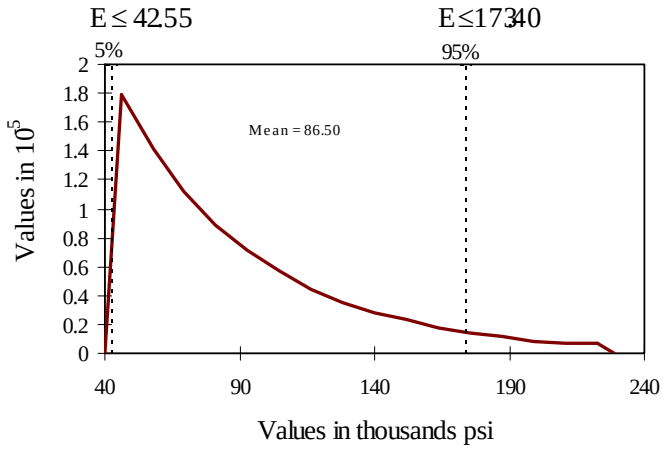

(a)

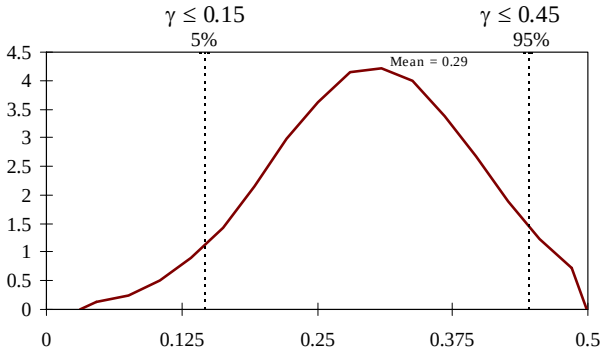

(b)

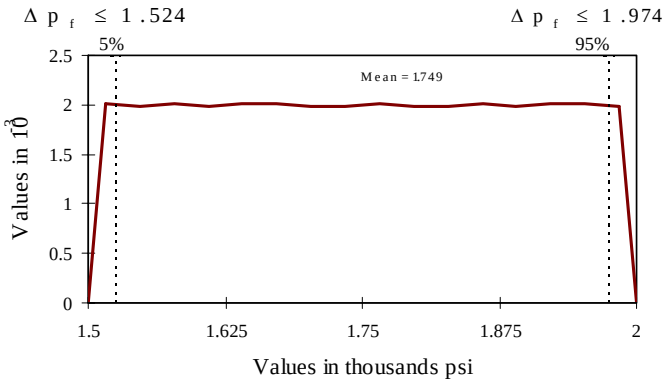

(c)

Figure 3-4: Distribution data for (a) Young's modulus (E) which fitted with the exponential distribution and truncated where a minimum value of 40,000psi and maximum value of 230,000psi. (b) Poisson's ratio (ν) distribution fitted with a normal distribution, Poisson's ratio distribution has a mean of 0.29 and a standard deviation of 0.09 and it is truncated leaving a range of 0.02 – 0.5. (c) Reduction of pore fluid pressure (Δp_f) which has uniform distribution with minimum value of 1500psi and maximum value of 2000psi.

Analytical geomechanics – fluid flow equations used here for stochastic-based simulations are based on nucleus-of strain equations from rock mechanics as described by Geertsma (1973) and further detailed by Holt (1990). The maximum vertical compaction (Δh) and subsidence (S) for a roughly disk-shaped oil and gas bearing reservoir with input parameters C_b, ν, R, h, D, and $A(\rho,\eta)$ (Table 3-1), can be estimated using equations 3-7 and 3-8

$$\Delta h = \frac{\left(1-\nu-2\nu^2\right)}{(1-\nu)E}\Delta p_f h \qquad (3\text{-}7)$$

$$S = \frac{C_b}{2}\Delta p_f h A(\rho,\eta) \qquad (3\text{-}8)$$

Table 3-1: Rock and model properties for the Gulf of Mexico

Variables	Symbol	Value	Unit
Distance from reservoir centre axis	a	10000	ft
Average reservoir radius	R	5000	ft
Reservoir depth of burial	D	10000	ft
Average reservoir thickness	h	160	ft
Dimensionless radial distance	$\rho=a/R$	2	--
Dimensionless depth	$\eta=D/R$	2	--
Bessel function	$A(\rho,\eta)$	--	--
Poisson's ratio	ν	--	--
Young's modulus	E	--	psi
Biot's constant	α	0.95	--
Reduction of pore fluid pressure	Δp_f	1500	psi
Bulk coefficient (base case)	C_b	2.56E-5	psi-1
Rock density	ρ_s	128	lb/ft^3

In the above equations it is assumed that the subsurface compaction is uniform across the area of interest and the overburden material deforms elastically and homogeneously. For example, considering a formation compacting a total of 32 ft even at a relatively shallow depth of 3200ft, the overburden material will deform a maximum of 32ft in the vertical direction over its 3200ft thickness, and generally much less, so that strains will be less than 1%. So, elastic material behavior assumptions are reasonable. Furthermore, for a greater depth of subsurface compaction, the resulting surface subsidence may be relatively insensitive to overburden material properties. It is evident that the analytical nucleus-of-strain equations actually provide very good compaction and subsidence approximations to even the most sophisticated geomechanical models, which account for inelastic and

heterogeneous overburden behavior. As a consequence, other situations using uncertainty input parameters should be also assumed to be valid, with the assumption that the overburden material deforms elastically and homogeneously when applying into stochastic based simulation.

3.5 Validation the results of stochastic based simulation with numerical reservoir based simulation

In this study, the coupled geomechanical–fluid flow model has been built using the *Eclipse 300* reservoir simulator software package as it has a 3D finite difference code for such modeling (Eclipse 2005).

A simplistic model using deterministic parameters is used here. The reservoir was discretised into eight layers. The model measures 10000 × 10000 × 160ft in the x, y and z directions, respectively. Grid size are 500 × 500 × 20ft. As a result, total number of cells is 3200. One production well is shown as Figure 3-5.

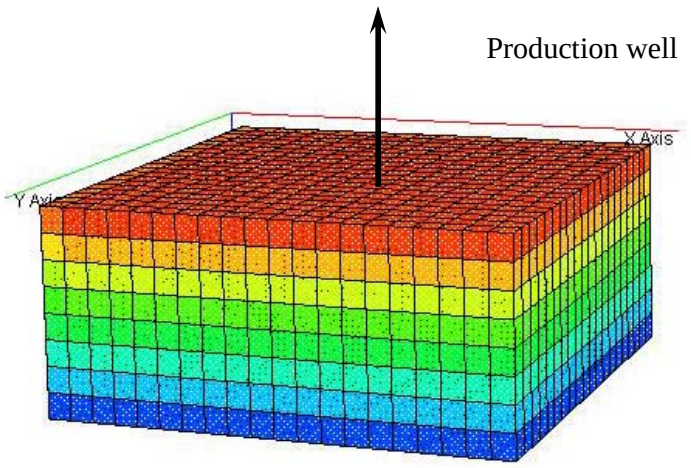

Figure 3-5: Eight layers reservoir model measuring 10000 × 10000 × 160ft, grid cell size 500 × 500 × 20ft in the x, y and z direction, respectively. Total number of cells is 3200.

Theories used in calculating of compaction problems are based on the mass balance equation, Darcy's law of fluid flow, and Terzaghi's principal of effective stress (Eclipse 2005). Rock and fluid property constants are from the Gulf of Mexico dataset. The coupled geomechanical-fluid flow equations are solved simultaneously. The simulation was run to ten years with a minimum time-step of one day and maximum of 500 days. Compaction calculations are made along a vertical cross-section that bisects the model's center position.

3.5.1 Reservoir rock properties

Geomechanical rock properties attached in each cell includes Young's modulus (E), Poisson' ratio (ν), Biot's constant (α), bulk coefficient (C_b) and density (ρ_s): these parameters describe a linearly elastic porous medium (Table 3-1). Here, the range of E and ν data, which come from two wells, are presented in statistic distribution (Figure 3-4). One restriction is that the coupled numerical model can only be simulated with the deterministic values of parameters extracted from the distribution of E and ν parameters in which the mean and medium values are considered.

3.5.2 Fluid properties

Fluid properties can have a strong influence on the depletion pattern within the reservoir (e.g. viscosity). Generally, fluid properties are a function of composition, temperature, saturation and pressure, and will vary spatially and temporally. Deterministic values of key fluid properties (Table 3-2) used in the simulation are order of magnitude estimates only and do not represent the detail of the Gulf of Mexico field. Both the fluid and rock properties, describing flow and geomechanical behavior, respectively, are then assigned within the coupled model.

Table 3-2: Fluid properties

Variables	Symbol	Initial value	Unit
Reservoir temperature	T_{res}	284	^0F
Reservoir pressure	P_{res}	6,000	psi
Oil viscosity at 6,000psi	μ_o	1.17	cp
Initial water saturation	S_{iw}	0.25	--
Oil gravity	ρ_o	128	lb/ft^3
Water gravity	ρ_w	63.02	lb/ft^3
Bubble point pressure at T_{res}	P_b	5,400	Psi

3.5.3 Computational methodology

In an attempt to verify the consistency from the Monte Carlo simulation, the simplest model was run (i.e. experiment-1) with all parameters required for the calculation fixed at the average, or most likely, value as presented in Table 3-1. For each of the next three experiments (i.e. 2-4), Monte Carlo simulations were used for compaction and subsidence calculations in which statistically generated values for each of the uncertain of E, ν and Δp_f input parameters were used. Experiment-2 takes E as uncertain. Experiment-3 has the addition of ν as uncertain. Experiment-4 takes the addition of pore fluid pressure reduction as uncertain.

Results of numerical model are then used to verify the results from the Monte Carlo simulation. So, the examination confirms that the most likely level of compaction and subsidence (i.e. that value of compaction arising from setting all parameters to their most likely value) is comparable to the 50-percentile result from the Monte Carlo simulation. In other words, the result of the deterministic model with

simulator should then be matched to the 50-percentile result for the Monte Carlo simulation of the same experiments.

3.5.4 Results and Discussions

Numerical simulation results

✓ Compaction over production period

As a result of numerical simulation, Figure 3-6 shows compaction versus production time over ten years. The model presented here has the constant production rate (Q) of 10,000 bbl/day. The value 1.3ft at May-90 could be considered the initial compaction at the beginning of the simulation. After ten years, the calculated compaction from the coupled model is approximately 2.4ft.

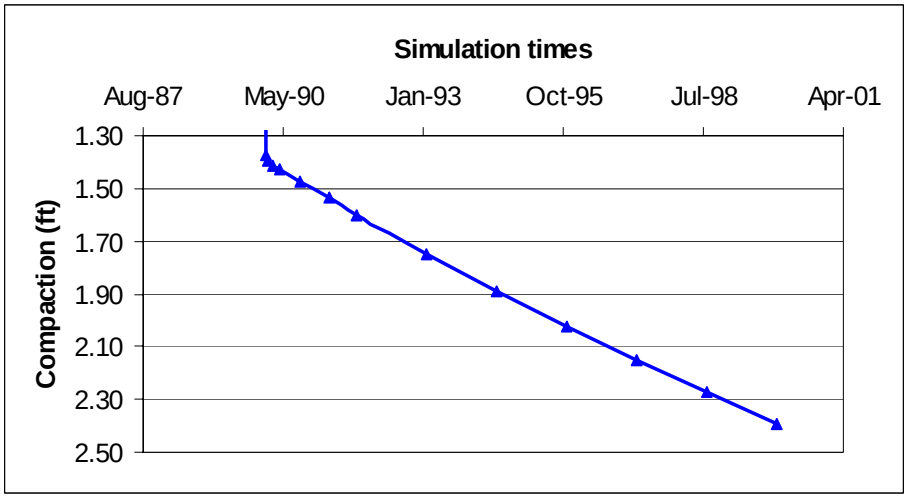

Figure 3-6: Compaction versus production period. Deterministic values of geomechanical rock properties used E=86500psi, ν=0.21

Thickness of reservoir is known to be about 165ft. The ratio of compaction to thickness is 0.66%. Such a ratio means that the reservoir could be considered to

deform elastically. Obviously, the compaction will increase moderately with longer production period and higher production rate with assumptions of elastic material.

Figure 3-7 presents the compaction profile at the end of numerical simulation measured in a vertical cross-section that bisects the well location. The minimum compaction of 2.21ft appears at the boundary of the reservoir tank whereas the maximum compaction of 2.39ft occurs at the center of the bowl, also coinciding with the production well location. Although compaction is supposed to be equal at the boundaries due to geometric symmetry, a small difference exists between left and right sides of the profile as the initial stress is applied to the left side.

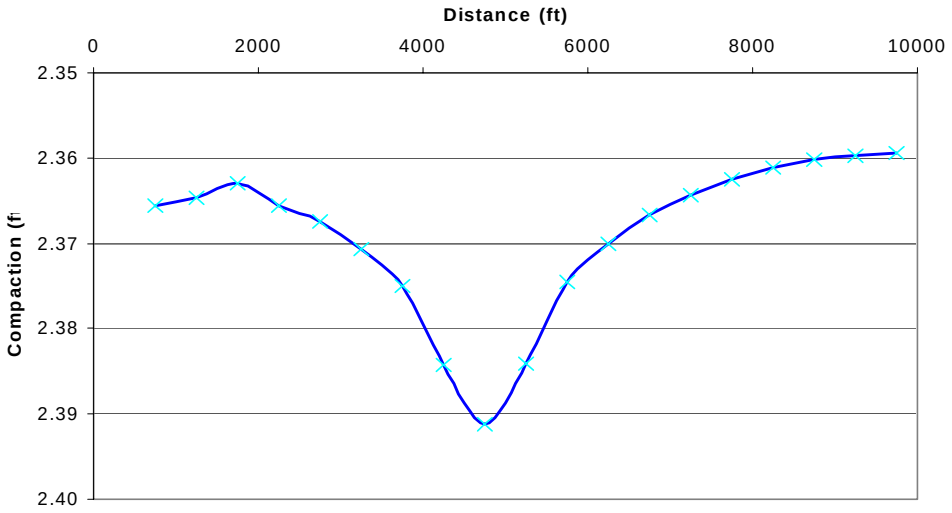

Figure 3-7: Compaction profile along at center of reservoir model at the end of numerical simulation. E=86,500psi, ν=0.21.

✓ Compaction versus Poisson's ratio

The fully coupled reservoir simulation shows that when fluid is withdrawn from the reservoir, the Δp_f will be reduced. In turn, effective stress will be increased (Wan

2003). Subsequently, the reservoir will deform causing compaction as shown in the previous section. However, the impact of rock properties was not taken into account. Figure 3-8 presents a case showing compaction estimation for two reservoir models with different Poisson's ratio but with the same Young's modulus (Table 3-3).

Table 3-3: Compaction with different values of Poisson's ratio

Young's modulus (psi)	Poisson's ratio	Max. compaction at well location (ft)	Min. compaction at the boundary (ft)
86500	0.21	2.74	2.58
86500	0.29	2.39	2.21

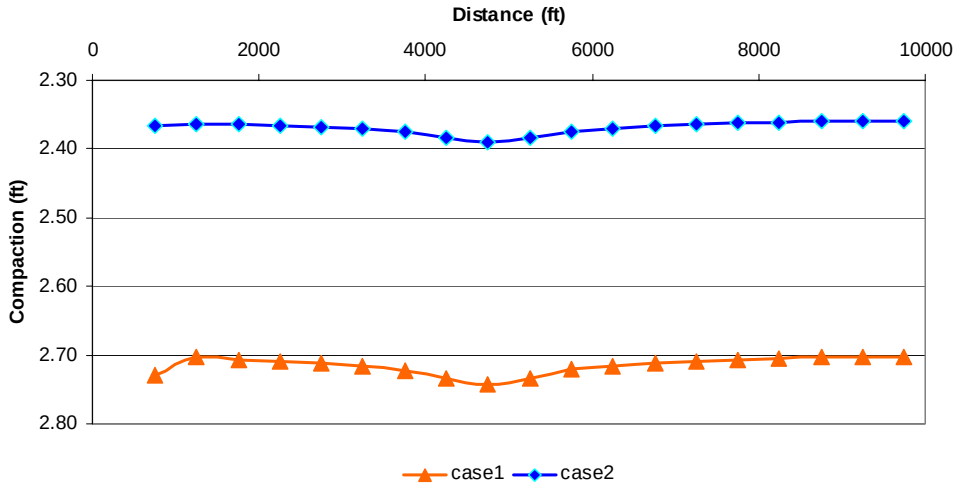

Figure 3-8: Compaction profile along at center of reservoir model at the end of numerical simulation taking into account influence of Poisson's ratio on compaction. (Case 1 with E=86,500psi, ν=0.21, Case 2 with E=86,500psi, ν=0.29).

When Poisson's ratio increases from 0.21 (case 1) to 0.29 (case 2) the compaction at the producer well location reduces from 2.74 to 2.39ft. Simultaneously,

the compaction at the boundary also reduces from 2.58 to 2.21ft. Therefore, higher Poisson's ratio causes a lower compaction. This result should be considered when planning infrastructure development (i.e. the production platform). A more sensitive test is investigated in the next section.

✓ Compaction versus various Poisson's ratio and Young's modulus

In this work, several numerical simulation tests are undertaken to investigate the influence of Young's modulus and Poisson's ratio on compaction. Table 3-4 shows the minimum and maximum compaction in each run for various E – ν combinations. As previously demonstrated, it is clear that compaction is lower where the reservoir has a higher Poisson's ratio. In addition, compaction also reduces moderately when Young's modulus increases. For example, when Young's modulus increase from 68000psi (base case) to 86500psi (mean value of Young's modulus), maximum compaction at the production well location falls from 3.27 to 2.74ft, where Poisson's ratio is held constant at 0.21. We have shown that an increase in Poisson's ratio and Young's modulus, therefore, decreases compaction.

Table 3-4: Numerical simulation results

Young's modulus (psi)	Poisson's ratio	Max compaction at the well location (ft)	Min compaction at the boundary (ft)
68000	0.21	3.27	3.18
68000	0.29	2.86	2.64
68000	0.4	1.99	1.82
86500	0.21	2.74	2.58
86500	0.29	2.39	2.21
100000	0.21	2.46	2.32
210000	0.3	1.21	1.13

210000	0.21	1.41	1.33
210000	0.4	0.79	0.72

Monte Carlo simulation results

The results of the Monte Carlo simulation are compared here with results from reservoir simulation. For experiment-1 (i.e. no uncertainty for E, ν and Δp_f), compaction is estimated at 3.27ft and subsidence at 0.91ft. The results of compaction lie exactly in accordance with results provided by the *Eclipse 300* simulation in the base case (first case in Table 3-4). This shows that Geertsma's analytical equations (Equations 3-7 & 3-8) can be used as a good approximation as complicated model such as fully coupled model using *Eclipse 300*.

In experiment-2, Young's modulus data collected from two wells of the deep-water field were fitted with a distribution. The results show that the exponential distribution is the best fit based on Chi-square measure (Figure 3-4a). The mean of Young's modulus is 86,508.81psi and a standard deviation is 41.17psi. The exponential distribution of Young's modulus was truncated where a minimum value of 40,000psi was taken for soft rock and maximum value of 230,000psi was taken for hard rock. Once the exponential distribution was determined, it replaced the Young's modulus single value. The Monte Carlo simulations were performed for 10,000 iterations. The results show that the uncertainty in Young's modulus results in a compaction distribution with a mean of 3.11ft and a standard deviation of 1.24ft (Figure 3-9) for both the probability and cumulative distribution functions. In addition, there is a 90% confidence interval where compaction falls between 1.28 –

5.24ft. The distribution also indicates that due to the existence of uncertainty in Young's modulus, there is a 50% chance that the compaction is greater than 3.11ft. As a result, this should help a decision maker to collect more data and try to reduce the range of uncertainty and the possibility of greater compaction during the field's life. These estimates should be accounted for during the field development.

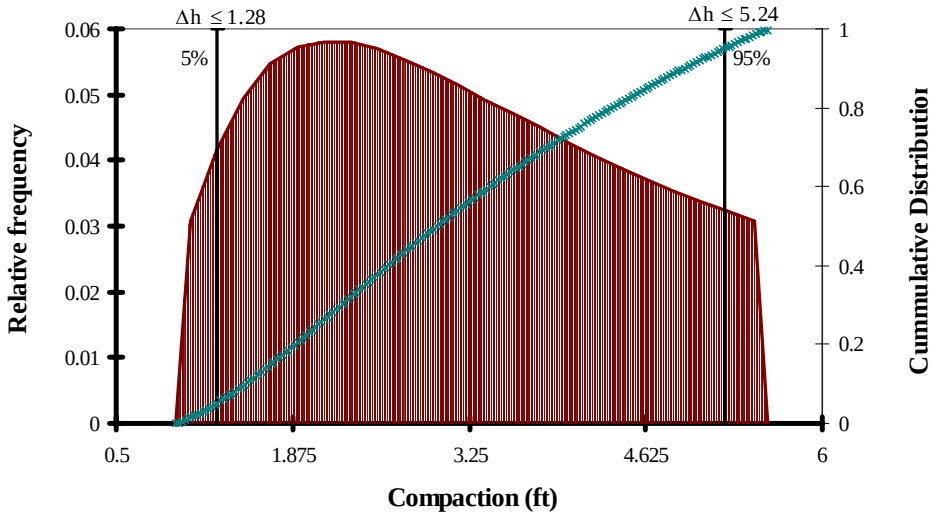

Figure 3-9: Compaction (Δh) distribution for experiment-2. The mean of Young's modulus used in the experiment-2 is 86,508.81psi and a standard deviation is 41.17psi. The constant value of Poisson's ratio is 0.21

Furthermore, Monte Carlo simulation results yield subsidence values with a mean of 0.87ft and a standard deviation of 0.34ft. These results show that because of the uncertainty in Young's modulus, the subsidence impact could range within a 90% confidence interval of 0.36 – 1.46ft (Figure 3-10). The results of Monte Carlo simulation provide the decision maker with the range of possible scenarios for preempting and appropriate decision-making.

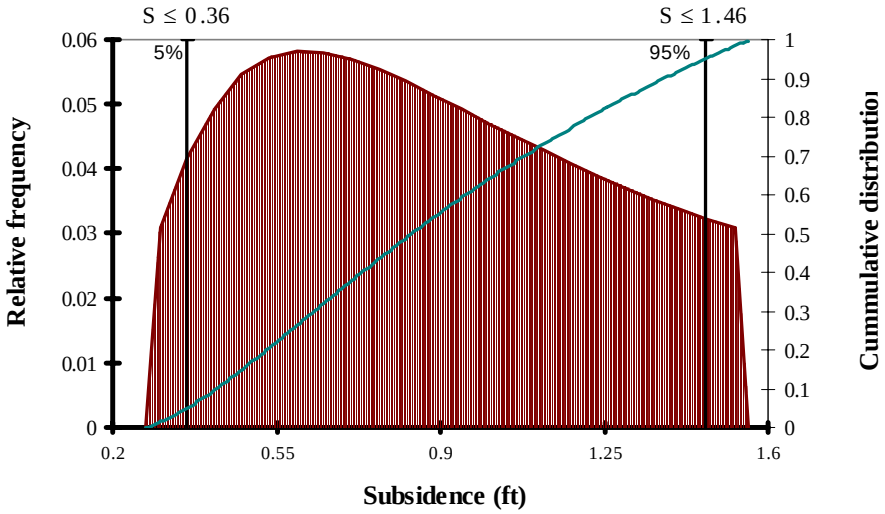

Figure 3-10: Subsidence (S) distribution for experiment-2. The mean of Young's modulus used in the experiment-2 is 86,508.81psi and a standard deviation is 41.17psi. The constant value of Poisson's ratio is 0.21Subsidence distribution for experiment-2

As shown in Figure 3-11, it is interesting to note that values of E ranging approximately from 40,000 to 140,000psi have more impact on compaction and subsidence than values of E lying beyond 140,000psi. This shows that uncertainty of Young's modulus beyond 140,000psi is insignificant.

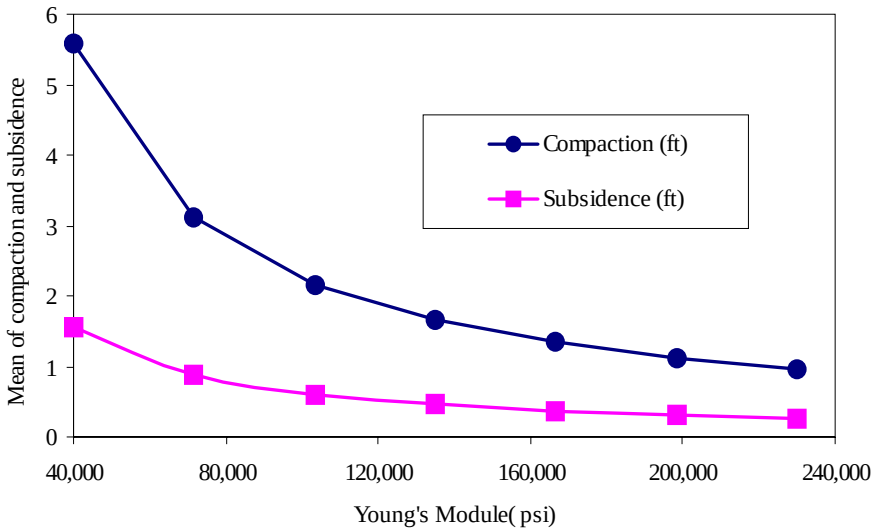

Figure 3-11: The impact of Young's module on compaction and subsidence

In experiment-3, data for Poisson's ratio from two wells were fitted with a normal distribution as the best fit based on the Chi-square measure. Here, Poisson's ratio distribution has a mean of 0.29 and a standard deviation of 0.09 and it is truncated leaving a range of 0.02 – 0.5 (Figure 3-4b). The impact of introducing uncertainty in both Young's modulus and Poisson's ratio has resulted in a compaction estimation having a mean of 2.43ft and standard deviation of 1.24ft, where the 90% confidence interval is 0.72 – 4.72ft (Figure 3-12).

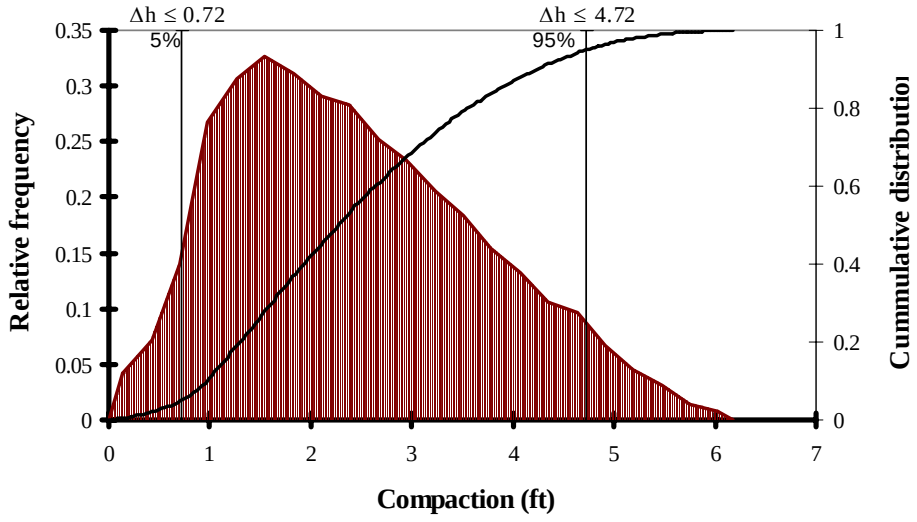

Figure 3-12: Compaction (Δh) distribution for experiment-3. The mean of Young's modulus used in the experiment-3 is 86,508.81psi and a standard deviation is 41.17psi. The mean of Poisson's ratio distribution used is 0.29 and a standard deviation is 0.09

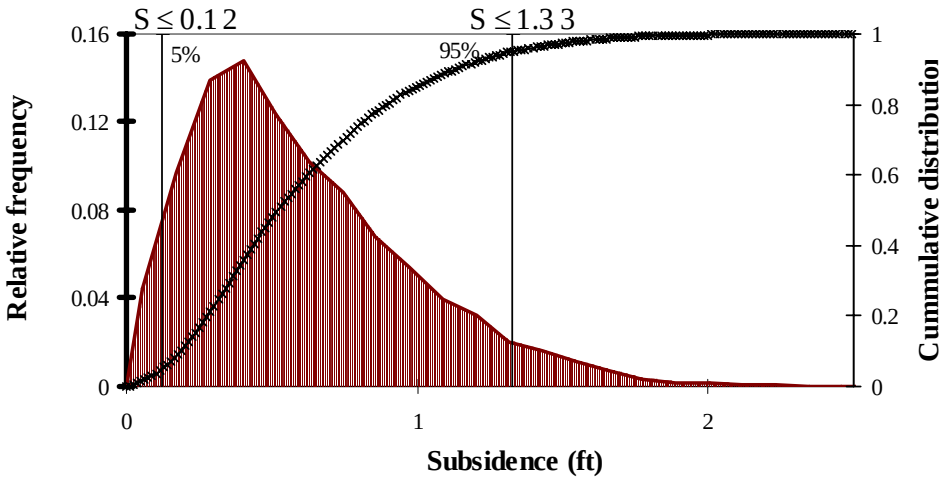

Figure 3-13: Subsidence (S) distribution for experiment-3. The mean of Young's modulus used in the experiment-3 is 86,508.81psi and a standard deviation is 41.17psi. The mean of Poisson's ratio distribution used is 0.29 and a standard deviation is 0.09.

The impact on subsidence as a result of allowing for both E and ν has resulted in a mean of 0.60ft and standard deviation of 0.37ft. A 90% confidence interval was estimated to range from 0.12 – 1.33ft (Figure 3-13).

It is important to emphasize that the difference between experiment-2 and experiment-3 is treating Poisson's ratio as uncertain. In the later case, compaction results with addition of Poisson's ratio as an uncertain variable has reduced the mean but the standard deviation is the same. Furthermore, the addition of Poisson's ratio in estimating subsidence has resulted in a decrease in the mean, with approximately the same value for standard deviation. The mean values are consistent with results found using numerical simulation methods. The advantage of the Monte Carlo simulation is in its allowance to investigate the impact of variation of both E and ν simultaneously, compared to numerical simulations where each variable is changed while others are held constant.

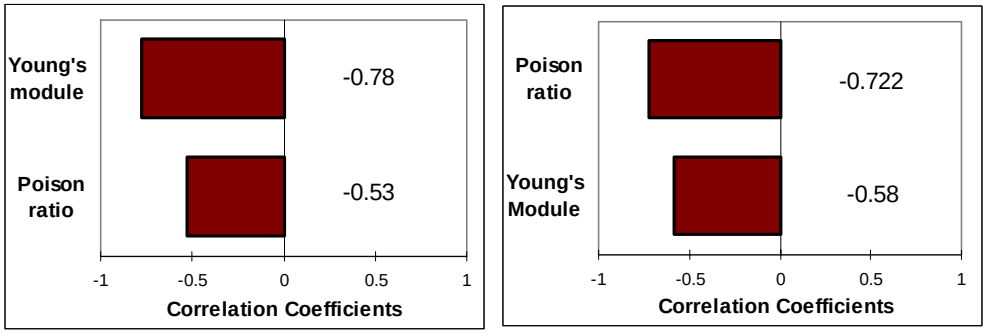

(a) (b)

Figure 3-14: Tornado plot for (a) compaction, (b) subsidence

A sensitivity analysis was performed to assess the impact of Young's modulus and Poisson's ratio on compaction. The Tornado plot for compaction (Figure 3-14a)

shows that Young's modulus has a greater impact than Poisson's ratio implying that more effort should be directed toward estimating Young's modulus than for estimating Poisson's ratio.

A similar sensitivity analysis was also done for subsidence (Figure 3-14b). Here we expected Young's modulus to have a bigger impact, however it was interesting to note that correlation coefficient for Poisson's ratio are larger than for Young's modulus indicating that more effort should be directed toward estimating Poisson's ratio when estimating subsidence.

Experiment-4 incorporated the addition of the uncertainty of Δp_f, here having a uniform distribution with minimum value of 1500psi and maximum value of 2000psi. The addition of Δp_f resulted in a small increase in compaction with a mean of 2.84ft and a standard deviation of 1.47ft. The 90% confidence interval ranges from 0.82 – 5.59ft. The subsidence mean after the addition of pore fluid pressure reduction is 0.60ft and a standard deviation of 0.37ft with a confidence interval between 0.14 – 1.58ft.

A sensitivity analysis was also conducted for compaction and the results show that the impact of pore fluid pressure reduction uncertainty is small compared to the impact of Young's modulus and Poisson's ratio (Figure 3-15). Simulation results are observed for subsidence, with Poisson's ratio having the biggest impact followed by Young's modulus and pore fluid pressure reduction.

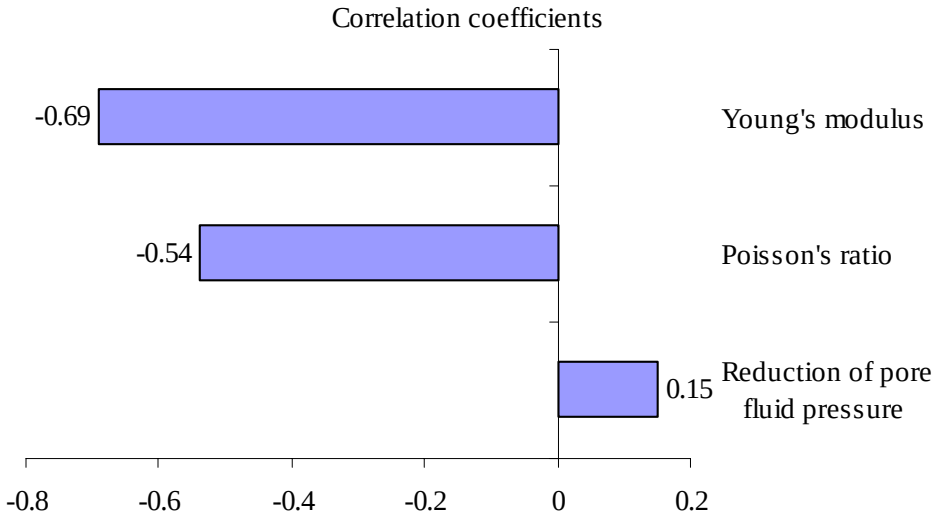

Figure 3-15: Tornado plot for compaction where with pore pressure reduction is added

When all the experiments were combined for the case of compaction (Figure 3-16), it is clear that as we add the uncertainty of Young's modulus, the compaction mean was reduced. In experiment-3 when the Poisson's ratio uncertainty was introduced, the mean compaction was reduced which is reflected in the left shift of the cumulative distribution function. As we add the uncertainty of pore fluid pressure reduction, compaction mean has increased again and the standard deviation has increased due to the addition of another uncertain parameter. This clearly shows that pore fluid pressure reduction increases the compaction mean, because it has positive impact on compaction while both Young's modulus and Poisson's ratio have negative impacts. The same trend was observed with subsidence.

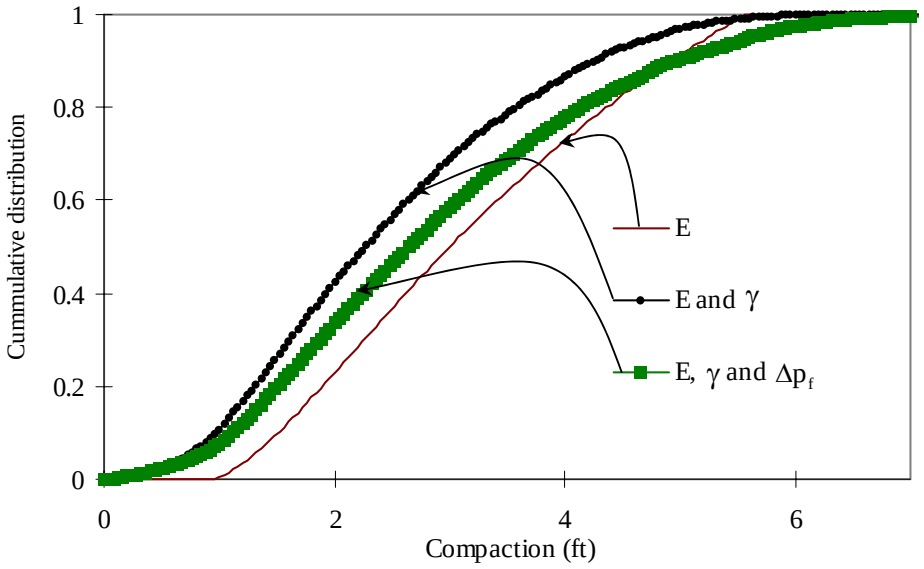

Figure 3-16: Compaction as uncertainty variables (E, ν and Δp_f) are added

The results of the Monte Carlo simulation are consistent with the results of numerical simulation method. Moreover, these results show the impact of uncertainty of Young's modulus, Poisson's ratio and reduction of pore fluid pressure on compaction and subsidence. In addition, the ability of identifying which variables among these has the greatest impact and the possibility of collecting more data to reduce uncertainty or develop better field development plans.

3.6 Conclusions

This chapter has discussed the impact of uncertainty on the calculation of subsidence and compaction. A stochastic model, incorporated within the Monte Carlo simulation, has been applied to analytical geomechanics – fluid flow equations to investigate the influence of uncertainties in a compacting reservoir. This method could extend to other fields with specific reservoir parameters.

The results reveal the impact of using probability distributions to estimate compaction and subsidence for a disk shaped-homogenous reservoir when taking into account uncertainties of Young's modulus, Poisson's ratio and the reduction of pore fluid pressure. The sensitivity analysis shows that Young's modulus has more impact on compaction than Poisson's ratio. The results also show that values of Young's modulus in this deep-water field lying beyond 140,000psi have an insignificant impact on compaction and subsidence. Based on estimates of compaction and subsidence with the stochastic model, large scale reservoirs that have potential for subsidence and compaction will be predicted quantitatively in advance. The additional numerical results also confirm that results obtained from numerical simulation with the coupled geomechanical – fluid flow model are within the range of acceptable distribution from the stochastic results.

CHAPTER 4: POROSITY AND PERMEABILITY IN STRESS SENSITIVE RESERVOIR

4.1 Introduction

The concept of stress-dependent permeability and porosity incorporated with coupled theory has attracted attention from reservoir engineering and production engineering. There are numerous researchers working on both the fully coupled mathematic model and petrophysical rock properties to assess more accurately the impact of subsidence and compaction. However, there is still a lack of research in investigation of the changes of permeability and porosity due to stress variation in reservoir caused by depletion. This chapter discusses in particular both theoretical and experimental work in which stress-dependent permeability and porosity relationship are reviewed and applied in coupled reservoir simulation.

The objectives of the chapter describes as following:

- ✓ The relationship between change in permeability and stress variation
- ✓ The relationship between the change in porosity and permeability reduction due to stress variation. Applying the advanced Carmen – Kozeny equation into coupled simulation.
- ✓ The reduction of permeability with in depleted reservoir.

4.2 The relationship between permeability and reservoir stress in coupled fluid flow – geomechanics model

During the last decade, there has been an increasing awareness within the petroleum industry that stress changes associated with reservoir depletion have an essential impact on field performance. Traditionally, pore pressure reduction has been thought to create compaction. Because the effect of rock compaction by itself does not affect the shape of the pressure trace, permeability change caused by stress change is the dominating factor that influences well responses in stress-sensitive reservoirs. It becomes clearly that the quantitative relationship between permeability and stress change must be known in order to estimate initial permeability from well-test data in stress-sensitive reservoirs. From a microscopic point of view, to establish a general relationship between permeability and stress change is difficult. Depending upon the characteristic of reservoir rock and reservoir conditions, many physical factors that relate to stress change may cause permeability to change. It is more pragmatic to experimentally determine rock permeability as a function of a macroscopic variable that is related to stress change and that can be measured in the laboratory.

From experimental work, Mattax et al. (1975) have shown that the average permeability decreased by almost 40% when the applied hydrostatic compaction pressure was increased from 65 to 3500psia. In general from an experimental point of view, Al Harthy et al.(1998) showed that the petrophysical properties such as permeability, capillarity, porosity, resistivity and relative permeability are influenced by the state of stress in the reservoir. This research is being further developed to enable a range of petrophysical and flow measurements under true triaxial stress and

elevated pore pressure conditions. Jelmert et al (2000) investigated correlations between permeability and effective stress, reviewing power-law relationships. They stated that straight-line correlations were inappropriate as opposed to polynomial fits to averaged core data. Warpinski and Teufel (1992) had previously fitted polynomial equations to experimental results. The reduction of permeability with effective stress increase is discussed further and mathematical relationships are presented by Nathenson (1999). The other experimental relationships between permeability and variation of stress that are common used in oil industry are summarized in Table 4 – 1.

Table 4-1: The summary relationships of stress sensitive permeability.

Stress sensitive permeability models	Main references	Note
$k = k_i e^{-\gamma \Delta P}$	(Wyble 1958)	$\Delta P = \sigma_{ei} - \sigma_e$ γ : Permeability modulus.
$k = k_i \left(1 - S \log \frac{\sigma_e}{\sigma_{ei}}\right)^{1/c}$	(Jones and Owens 1980)	S: the magnitude of negative slope. C=1/3
$k = k_i \left(1 - S \log \frac{\sigma_e}{\sigma_{ei}} + T\left(\log \frac{\sigma_e}{\sigma_{ei}}\right)^2\right)$	Extended from (Jones and Owens 1980)	T: temperature
$k = k_i \left(1 + a\Delta P + b(\Delta P)^2 + c(\Delta P)^3\right)$	(Warpinski and Teufel 1992)	a, b and c: constant parameters need to be determined by polynomial regression
$\frac{k}{k_i} = 1 - 2(\gamma_p + 1) c_{p\max} \Delta P$	(Roegiers 2007)	γ_p, c_p are the pore shape empirical coefficient and pore compressibility, respectively.

4.3 The relationship between porosity changing and permeability reduction due to stress variation. Carmen – Kozeny's equation

Although permeability is more sensitive to change in pore structure than porosity (Mattax, McKinley et al. 1975), we have recently stated the relationship between strain and porosity (Equation 2-57) and linear equation of effective stress and strain (Equation 2-60). So, we can use the experimental relationship of Carmen-Kozeny to model the influence of porosity changes on permeability integrated with stress field. According to Behrenbruch et al (2005), Carmen-Kozeny's equation can be arranged as

$$0.0314\sqrt{\frac{k}{\phi}} = \frac{\phi}{(1-\phi)}\left(\frac{1}{\sqrt{F_{ps}}\tau S_{vgr}}\right) \tag{4-1}$$

Permeability k is in mD, ϕ is effective porosity in fractional bulk volume, S_{vgr} is the specific surface area to grain volume ratio in μm^{-1}, F_{ps} is shape factor known as the Kozeny's constant (2 for a circular cylinder) and τ is tortuosity.

$$S_{vgr} = \frac{\text{area of spheres}}{\text{volume of sphere}} = \frac{\pi d_{gr}^2}{\frac{\pi}{6}d_{gr}^3} = \frac{6}{d_{gr}} \tag{4-2}$$

So

$$0.0314\sqrt{\frac{k}{\phi}} = \frac{\phi}{(1-\phi)}\left(\frac{d_{gr}}{6\sqrt{2}\tau}\right) \tag{4-3}$$

So, it is important to note again that

- ✓ Permeability increases dramatically with porosity which can be influenced by the stress state;

✓ Permeability also increases with grain radius d_{gr}; and

✓ Permeability reduces with tortuously τ;

In the simplest case, if we consider d_{gr} and τ keeping constant, we have the relationship between permeability and porosity

$$k = a.f(\phi) \tag{4-4}$$

In which the constant "a" can be calculated from the initial permeability and initial porosity;

$$f(\phi) = \frac{\phi^3}{(1-\phi)^2} \tag{4-5}$$

4.3.1 Case study using the advantage of modified Carmen – Kozeny's equation to predict subsidence and compaction.

For illustration purposes, the applications focusing on reservoir engineering are presented. The generally coupled formulation is summarized and is used to solve fluid flow and deformation problems for a radial flow model (chapter 2). The equations are based on the platforms of continuum theories of multiphase material. Results of this work can be specifically applied in studying compaction and subsidence in a reservoir simulation.

✓ Model description

This example simulates the subsidence and compaction of oil reservoir within radial model. The reservoir in this model is thick compared to the depth, perforated zone and a real field scale example as shown in Figure 4-1. 200 days of oil pumping

are simulated. The coupled model analysis is written within the Matlab programming environment and solves problems involving fluid flow through a saturated elastic porous medium under transient analysis.

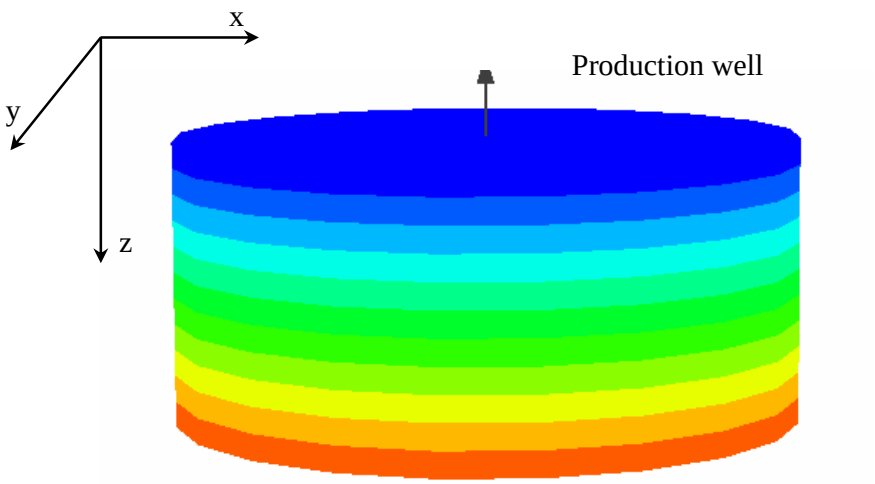

Figure 4-1: Production well model

In this model, a fully penetrating well of radius r_w is producing a single phase fluid at a constant rate q, from a saturated reservoir. The reservoir is assumed to be homogeneous and isotropic with a boundary being restrained from any radial displacement at the producing wellbore, but allowing free displacement in the vertical direction. A coarse mesh with isoparametric elements is selected for the illustrative purpose of this example. No mesh convergence study has been performed.

At t = 0, the reservoir pressure is equal to the initial reservoir pressure. Applying an axisymmetric model, we used isoparametric elements for the porous media in all

regions of the radial model which had 204 nodes meshed into 176 elements. Material properties of reservoir shows in Table 4-2

✓ Permeability data

At t=0, we have initial porosity and permeability from core analysis or logging data, so the constant can be calculated from Equation 4-5. From variation of porosity in simulation, the relationship between permeability and porosity presented in Figure 4-2

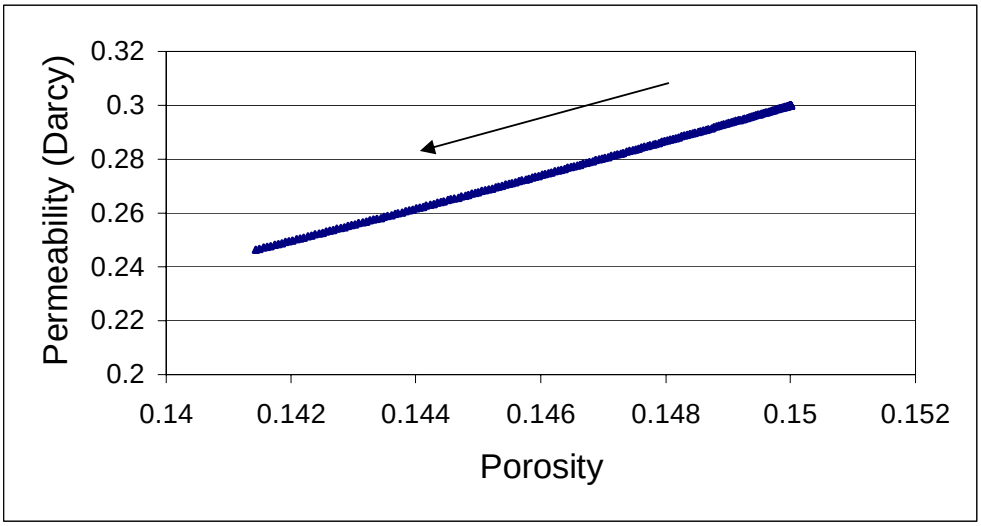

Figure 4-2: Variation of permeability and porosity with modified Carmen-Kozeny's relationship

Table 4-2: Material properties of reservoir in the simulation

Material properties	Symbol	Values	Field unit
Initial porosity	ϕ	0.15	-
Poisson' ratio	ν	0.25	-

Initial permeably	k	300	mD
Young's modulus	E	5.6 E6	psi
Fluid density	ρ_f	49.8	p/ft^3
Fluid compressibility	C_f	15.E-06	psi^{-1}
Solid compressibility	C_s	7.0E-06	psi^{-1}
Initial pressure at depth 4798 ft	P_i	5000	psi
Production rate	q	1200	STB/d
Well radius	r_w	0.5	ft
External boundary	R	7932	ft
Depth	z	4798	ft

4.3.2 Results and discussion

Effect on subsidence over time

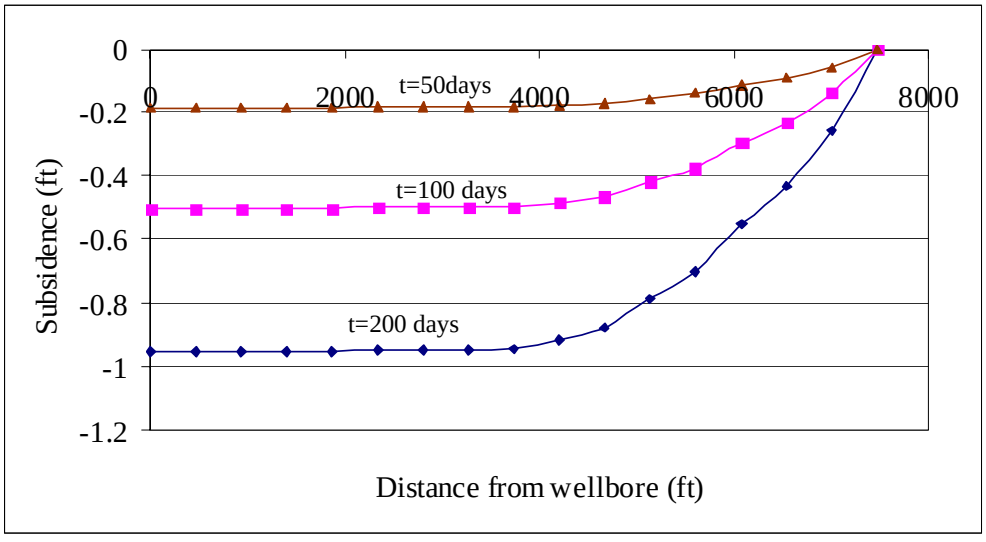

Figure 4-3: Sink subsidence with different production time.

The vertical deformation shown in the near wellbore environment can be calculated by solving the matrix of Equation 2-100 at each integration point. Figure 4-

3 shows subsidence (displacement in the z direction) of the reservoir during fluid production at different times, with an initial porosity of about 15%. With simplified soil properties that were applied for all layers, subsidence is about 0.2ft after 50days. Subsequently, the subsidence will reach about 0.5ft and nearly 1ft after 100days and 200days, respectively. Due to the boundary condition of the model that is being constrained from any vertical and horizontal displacement far from wellbore, the subsidence at the external boundary equals to zero.

Investigating subsidence with differently initial porosity.

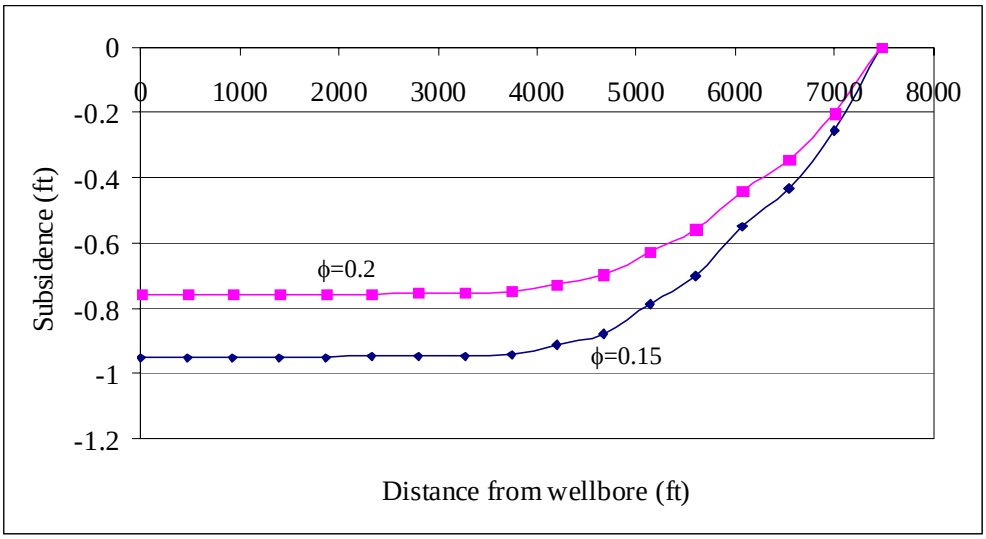

Figure 4-4: Subsidence of sink at differently initial porosity

Figure 4-4 presented the subsidence results in two models with differently initial porosity 0.15 and 0.2, respectively. It is evident that the initial porosity has a significantly effect on subsidence. An increase in the initial porosity parameter in the coupled simulation in which would produce a smaller change in effective stress and hence the subsidence would be smaller.

Pore pressure reduction

A simulation of reservoir depletion was also run for both different porosity models applying the same initial conditions for fluid production. Taking into account the rock deformation and its effect within the coupled model, the results in Figure 4-5 shows the gap between reductions in pore pressure between the two models. The results suggest that the pore pressure reduction in higher porosity model is less than the reduction in the lower porosity model. This result matches with previous conclusion about the influence of porosity parameter on subsidence simulation.

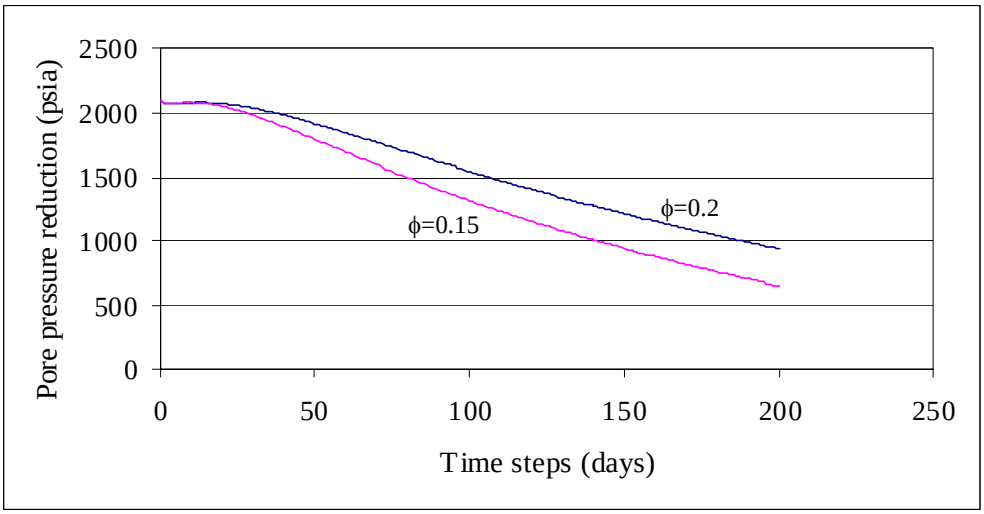

Figure 4-5: Pore pressure reduction with differently initial porosity models.

Investigating the influence of stress on both the permeability and porosity.

From previous experimental work, it was been shown that the permeability variation has a greater directly measurable effect on reservoir performance than porosity (Mattax et al. 1975). The results obtained in the modeling work are in

agreement with this finding, as shown plotted in Figure 4-6, where normalized porosity and permeability versus increasing effective stress are given. The results show a slight reduction in porosity when effective stress increases from 0 to nearly 1500psia. On the other hand, normalized permeability is heavily influenced by effective stress. Therefore, not only the porosity has an impact but also permeability changes considerably on stress sensitive reservoir.

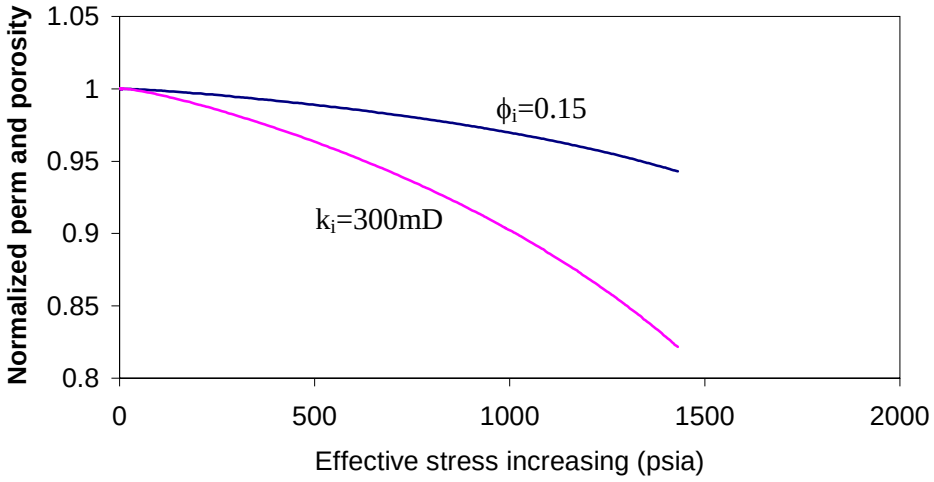

Figure 4-6: Normalized permeability and porosity (current by initial) plotted as function of effective stress. The initial porosity and permeability values are given.

The detail conclusions in the relationship between permeability and reservoir stress can be found in Ta and Hunt (2005).

Increase in effective stress.

The result of fully coupling the model for reservoir simulation shows that when fluid is withdrawn from the reservoir, the pore pressure will be reduced. In turn, effective stress will be increased. Subsequently, the reservoir will deform causing

changes in pore structure which closely relate to permeability changes in the reservoir.

Figure 4-7 clearly presents the increase in effective stress in the reservoir after nearly 200 days production. At the beginning of production, there is no sign of an increase in effective stress. However, after 30 days, the effective stress increases dramatically reaching about 1400psia after 200 days. This result should be considered for casing design and planning of reservoir development.

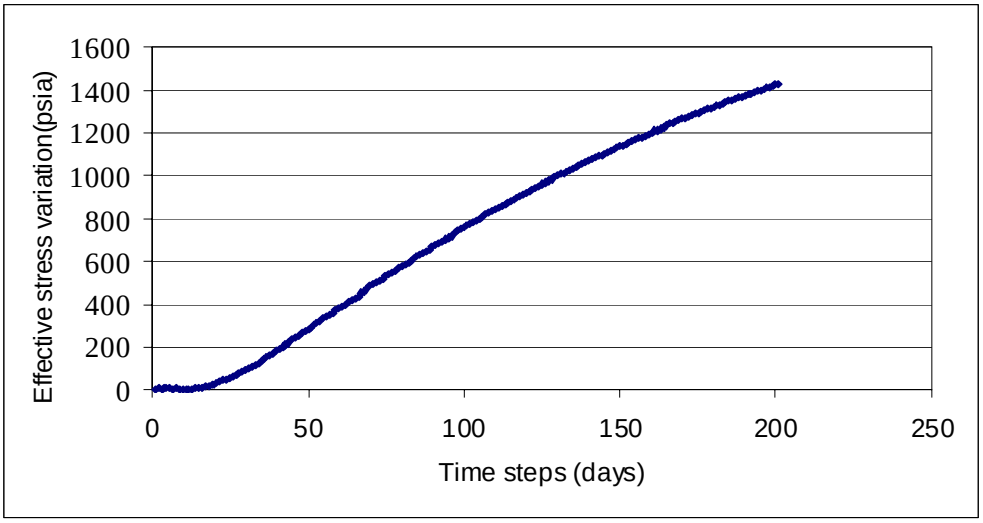

Figure 4-7: Effective stress increasing plotted with production times

4.4 Analytical equation of sensitive permeability with in depletion reservoir pressure.

It is well known that fluid pressure depletes during the oil production. As a result there is an increase in overburden stress. This stress in turn causes deformation of rock and consequentially permeability and porosity reduction as previously

presented. This section presents a mathematic model to estimate current permeability with radial oil flow toward wells in a deformable porous media which takes into account permeability change.

Assumptions

- ✓ Homogeneous reservoir
- ✓ 2D flow
- ✓ Steady state pressure condition
- ✓ Fluid in reservoir is compressible
- ✓ Low compressible of rock

4.4.1 Determination current permeability with production field data

Applying Darcy's law to the mass equation, we have a constant mass flux in a small well neighbor:

$$q_m = 2\pi rh\rho(P)k(P)\frac{k_{ro}}{\mu_o}\frac{dP}{dr} \tag{4-6}$$

Rearranging Equation 4-6 and integrating with conditions on the radius of contour ($r=R_c$) and the radius of well ($r=r_w$)

$$\frac{q_m\mu_o}{2\pi rhk_{ro}}\ln\left(\frac{R_c}{r_w}\right) = \int_{P_{we}}^{P_{res}}\rho(P)k(P)dP \tag{4-7}$$

Because fluid is compressible and permeability is sensitive with reduction of pore fluid pressure, we have (Wyble 1958)

$$\rho(P) = \rho_i e^{(\beta_\rho(P-P_i))} \tag{4-8}$$

$$k(P) = k_i e^{(\beta_k(P-P_i))} \tag{4-9}$$

To determine the value of β_k

Equation 4-6 becomes

$$\frac{q_m \mu_o}{2\pi r h \rho_i k_i k_{ro}} \ln\left(\frac{R_c}{r_w}\right) = \frac{1}{\beta_\rho + \beta_k} e^{(\beta(P_{res}-P_i))}\left[1 - e^{(\beta(P_w - P_{res}))}\right] \tag{4-10}$$

With $\beta = \beta_\rho + \beta_k$

Let us express mass flux in term of volumetric flux

$$q_m = q\rho(P_w) = q\rho_i e^{(\beta_\rho (P_w - P_i))} \tag{4-11}$$

Substitution of mass rate expression into Equation 4-10 for initial reservoir condition $P_{res}=P_i$ and for current reservoir condition P_{res}

$$\frac{q_i \rho_i e^{(\beta_\rho (P_{wi}-P_i))} \mu_o}{2\pi r h \rho_i k_i k_{ro}} \ln\left(\frac{R_c}{r_w}\right) = \frac{1}{\beta}\left[1 - e^{(\beta(P_{wi}-P_{res}))}\right] \tag{4-12}$$

and

$$\frac{q\rho_i e^{(\beta_\rho (P_w-P_i))} \mu_o}{2\pi r h \rho_i k_i k_{ro}} \ln\left(\frac{R_c}{r_w}\right) = \frac{1}{\beta} e^{(\beta(P_{res}-P_i))}\left[1 - e^{(\beta(P_w - P_{res}))}\right] \tag{4-13}$$

Dividing Equation 4-12 by Equation 4-13, we have

$$q = q_i e^{(\beta_\rho (\Delta P - \Delta P_i) + \beta_k (P_{res}-P_i))} \times \left[\frac{1 - e^{(-\beta \Delta P)}}{1 - e^{(-\beta \Delta P_i)}}\right] \tag{4-14}$$

Due to the assumption of steady state conditions, the difference between the reservoir pressure and well pressure is constant during reservoir depletion

$$\Delta P = P_i - P_{wi} = P_{res} - P_w \tag{4-15}$$

Equation 4-14 then becomes

$$\frac{q e^{(\beta_\rho (P_{res} - P_i))}}{q_i} = e^{(\beta (P_{res} - P_i))} \tag{4-16}$$

So, the rate between current flux and initial flux is

$$\frac{q}{q_i} = e^{(\beta_k (P_{res} - P_i))} \tag{4-17}$$

So

$$\beta_k = \frac{\ln\left(\frac{q}{q_i}\right)}{P_{res} - P_i} \tag{4-18}$$

Choosing region with constant drawdown in well history, we can have the value of β_k using for estimation current permeability.

4.4.2 Determination of current permeability from tested core data.

A formulation for permeability decline allows us to obtain an expression for determination of the permeability decrement β_k (Wyble 1958) from tested core.

$$\ln\left[\frac{k(P)}{k(P_i)}\right] = \beta_k (P - P_i) \tag{4-19}$$

The routine procedure to measure pressure sensitive permeability in the laboratory is described as following:

- ✓ Flow fluid through core with initial pressure;

- ✓ Permeability is calculated based on Darcy's law and measured flow rate;
- ✓ This routine is repeated with other reducing pressures; giving other values of permeability;
- ✓ Using the semi-logarithm graph, the value of β_k from flow test on core can be determined.

4.4.3 Planning for management in reservoir with the change in permeability.

- ✓ Conduct the test for determination of factor of permeability reduction (β_k) from core test.
- ✓ Analyse the well test data and production data to determine value of β_k.
- ✓ Compare and average two values β_k from field data and lab data.
- ✓ Model oil flow toward the producing well in a compaction reservoir model.
- ✓ Prediction of production rate for deformable reservoir.

4.4.4 Applications

In this example, production data from well test and core experiment are used to determine the value of β_k. Figure 4-8 shows the plot of log of the ratio q_i/q as function of reservoir depletion pressure. The solid straight line in Figure 4-8 is based on least square method. As a result, the permeability decrement β_k=0.0529 is obtained from slope of the straight line.

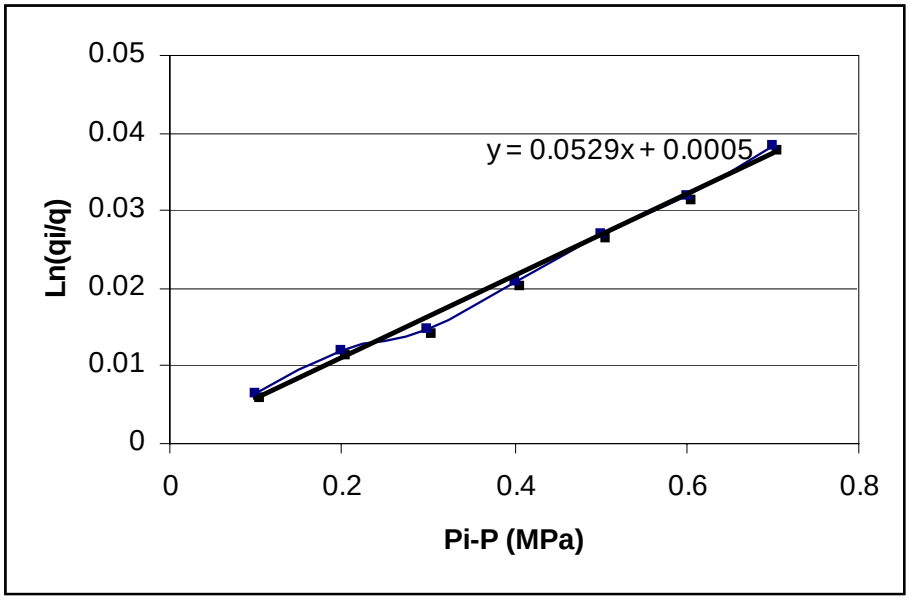

Figure 4-8: Plot of log of the ratio q_i/q as function of reservoir depletion pressure

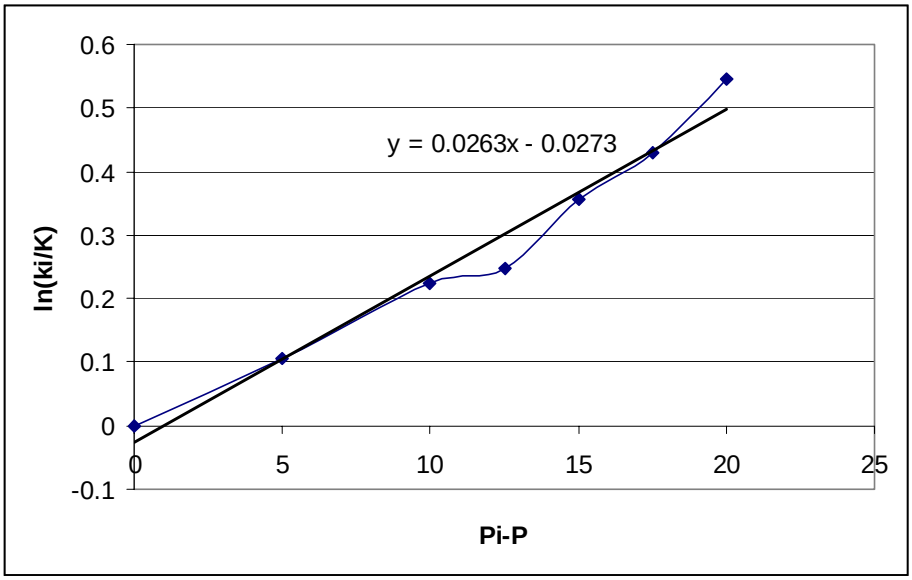

Figure 4-9: Plot of log of the ratio k_i/k as function of pressure decrease in laboratory

Figure 4-9 presents the plot of log of the ratio k_i/k as function of pressure decrease in laboratory. The line of best fit is the straight line in Figure 4-9 calculated from the least square method. The value of permeability decrement is 0.0263 1/Mpa. Interestingly, the permeability decrement obtained from welltest data in is nearly twice high than the permeability decrement from core testing in this example. The reason is due to differences between the scale of the reservoir and core scale. In the reservoir, fluid flows through the whole reservoir where quality of rock varies in a range from unconsolidated sand to consolidated sand. On the other hand, core sample is more consolidated when putting into Hassler sleeve holder. Consequently, the compressibility in reservoir scale is expected to be higher than the compressibility of the core sample. Under production and testing with overburden conditions, the rate of pore volume reduction in core sample is lower than the rate of pore volume reduction in reservoir. Therefore, based on the relationship between porosity and permeability in Carmen – Kozeny's equation, permeability reduction is also higher in reservoir condition compared to laboratory conditions.

4.5 Permeability and porosity core data in South Australia oil field

4.5.1 Apparatus and experimental procedure

The experiments to determine the stress sensitive reservoir properties were performed using a LP401 permeameter and helium porosimeter for measurement of porosity, permeability. Plug samples 1.48in (3.7cm) in diameter and 1.72in (4.3cm) in length were tested in Hassler sleeve holder capacity up to 6000psi confining pressure uniformly as overburden pressure. Permeability to fluid could be controlled with difference pressure between input and output up to 125psi and measured at low flow

rate to avoid turbulence. In this research, the effective maximum stress is difference between the external applied stress and average fluid pressure.

Figure 4-10: LP401 permeameter

4.5.2 Porosity, permeability properties at overburden stress condition

Only limited work was undertaken on the reservoir unit porosity–permeability trends in the Eromanga-Cooper basin. The most significant observation is that there is no simple relationship or adequate models for estimating the reservoir quality with depth in the Cooper-Eromanga basin (Table 4-3). Consequently, a simplified relationship was used in order to demonstrate the stress permeability effect in this compaction study (Jelmert, Torsceter et al. 2000). The absolute radial permeability

values ranged from about 0.2mD to 18mD and they decreased in virtually all samples as a function of increasing effective overburden stress.

Table 4-3: Porosity and permeability at ambient conditions (AC) and overburden condition (OC) in the Cooper basin

Formation	Depth (m)	Press (psi) AC	Porosity (%)AC	Perm (mD)AC	Press (psi)OC	Porosity (%)OC	Perm (mD)OC
Cuddapan	2663	1000	9.2	1.58	3861.35	8.74	1.054
Tinchoo	2497	1000	11.9	26.1	3620.65	11.305	18.459
Wimma	2157	1000	10	0.926	3127.65	9.5	0.471
Paning	2173	1000	11.6	1.98	3150.85	11.02	1.328
Callamurra	2465	1000	9.7	0.62	3574.25	9.215	0.252
Toolachee	2180	1000	12.4	3.363	3161	11.78	2.280
Daralingie	2424	1000	9.7	0.397	3514.8	9.215	0.125
Epsilon	2409	1000	9.1	0.68	3493.05	8.645	0.291
Patchawarra	2463	1000	10.5	0.933	3571.35	9.975	0.476
Tirrawarra	2643	1000	11.1	1.59	3832.35	10.545	1.061
Merrimelia	2990	1000	7.7	0.109	4335.5	7.315	0.017

Figure 4-11 shows a compilation of all permeability data for the Eromanga Basin, normalized with respect to the first permeability measurement at about 145psi effective vertical stress. The normalized permeability range shows a maximum permeability reduction for the Namur, Hutton and Murta formations of 30%. On the other hand, the normalized permeability for the Poolowanna and Birkhead formations decreased only 10%.

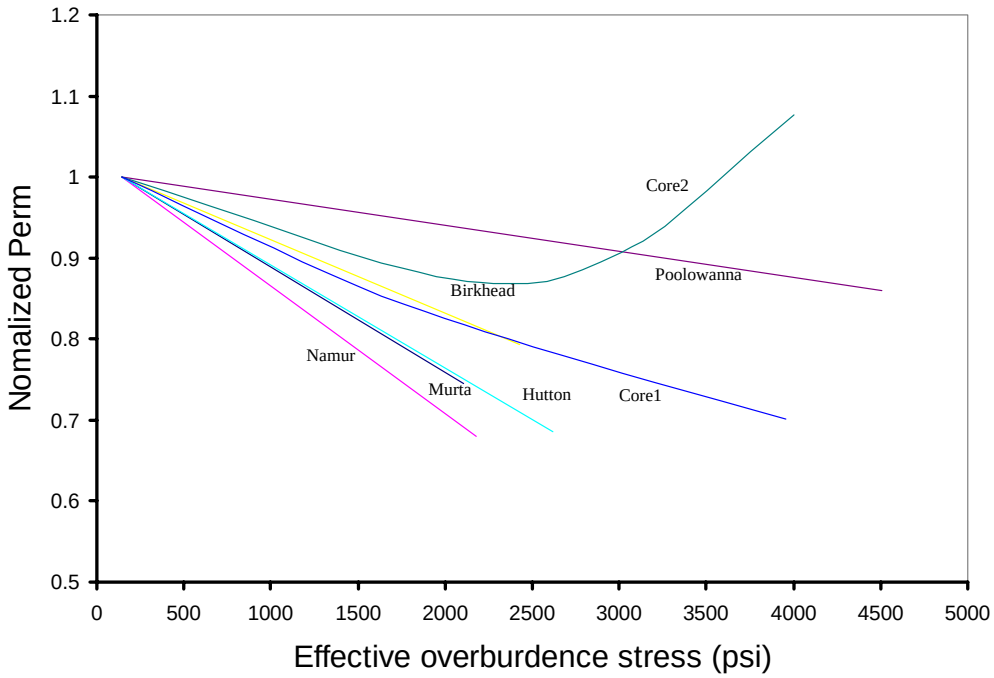

Figure 4-11: Normalized permeability as a function of effective overburden stress for Eromanga Basin. Core 1 and core 2 are the Berea Sandstone used for comparative purpose

4.6 Conclusions

This chapter illustrated the impact of stress sensitive reservoir to porosity and permeability. Firstly, this study presented both theoretical and experimental work in which stress-dependent permeability and porosity relationships are applied in a coupled reservoir simulation. Secondly, modified Carmen-Kozeny's equation is then used to generate the relationship between porosity and permeability. A modeled example study clearly describes the large impact of the change in permeability on the compaction results for a stress sensitive reservoir. Finally, the most important result of Chapter 4 shows principles for calculating reduction of permeability in a pressure

depletion scenario. Thus, the methodology can be applicable in determining current permeability in both field and laboratory – based data of stress sensitive reservoirs.

Experiment results from the Eromanga–Cooper basins show that permeability decreased by 5 to 10% of the initial permeability for every 1000 psi decrease in reservoir fluid pressure. Most experimental results are in agreement with previous research of compaction/permeability experiments (David and Crawford 1998) but disagree with results of Rhett & Teufel (1992), who showed that permeability can be increased during unaxial compaction of sandstone reservoir. The observation of increased permeability is only matched when two core sample of the Berea Sandstone is at failure point where fissures are generated.

CHAPTER 5: STRESS VARIABILITY AROUND LARGE STRUCTURAL FEATURES AND ITS IMPACT ON PERMEABILITY FOR COUPLED MODELING SIMULATIONS.

5.1 Introduction

Understanding rock mass stress away from the borehole is a major obstacle in the exploration and development of hydrocarbons. It is standard practice in the petroleum industry to use drilling data to determine the orientation and estimate the magnitudes of principal stresses at depth. However, field observations indicate that the orientation of the principal stresses is often locally perturbed by and around discontinuities, such as faults or formation boundaries (Kattenhorn et al. 2000; Maerten et al. 2002). Numerical stress methods have been successfully employed to model the effect of displacing faults on the surrounding rock mass. 3D distinct element code has been used to show how displacing faults generate stress variation in 3D about a fault plane (Camac et al. 2004), verified with field observations. In this work, stress variation mathematic models due to discontinuity and large structure are presented. In addition, consideration is made of this variability and its effect on wellbore's subsidence and compaction due to production. A model was run which incorporate the stress variability expected around an example fault under normal stress field conditions. The models show that the initial stress state conditions associated with a fault give rise to a variation in the stress path during reservoir

production and resultant permeability changes are measured. The extent of the influence of lateral changes around large-scale structural features is thereby assessed and the work demonstrates the importance of incorporating this initial stress variability for production purposes.

5.2 Petroleum geomechanics

This section concerns about geomechanics aspect related to the stress in the crust and *in situ* reservoir condition. Because the surface of the Earth is free, there is no shear stress acting on the surface. As a result, we have the vertical principle stress direction normal to surface (σ_v). Consequently, there are two principle stresses (σ_H and σ_h) remaining in horizontal plane.

According to Anderson (1951), the stress system in the crust can classify into three different stress regimes.

- ✓ Normal fault model: $\sigma_v > \sigma_H > \sigma_h$ ($\sigma_1=\sigma_v$, $\sigma_2=\sigma_H$, $\sigma_3=\sigma_h$)
- ✓ Strike-Slip fault model: $\sigma_H > \sigma_v > \sigma_h$ ($\sigma_1=\sigma_H$, $\sigma_2=\sigma_v$, $\sigma_3=\sigma_h$)
- ✓ Reverse fault model: $\sigma_H > \sigma_h > \sigma_v$ ($\sigma_1=\sigma_H$, $\sigma_2=\sigma_h$, $\sigma_3=\sigma_v$)

These models are shown in Figure 5-1

NOTE:
These figures are included on page 96 of the print copy of the thesis held in the University of Adelaide Library.

Normal Fault Model Strike-Slip Fault Model

Reverse Fault Model

Figure 5-1: Three different stress regimes, after (Hillis 2005)

The vertical stress σ_v increases with depth. In most case, vertical stress is calculated from gravity by multiplying the unit weight of the rock by its depth below the surface. The two remaining of horizontal stresses are usually predicted from elastic rock properties and vertical stress. As a result, variation of elastic rock

properties in different lithologies or geology structure can cause to variation in estimation of horizontal stress as shown in Figure 5-2

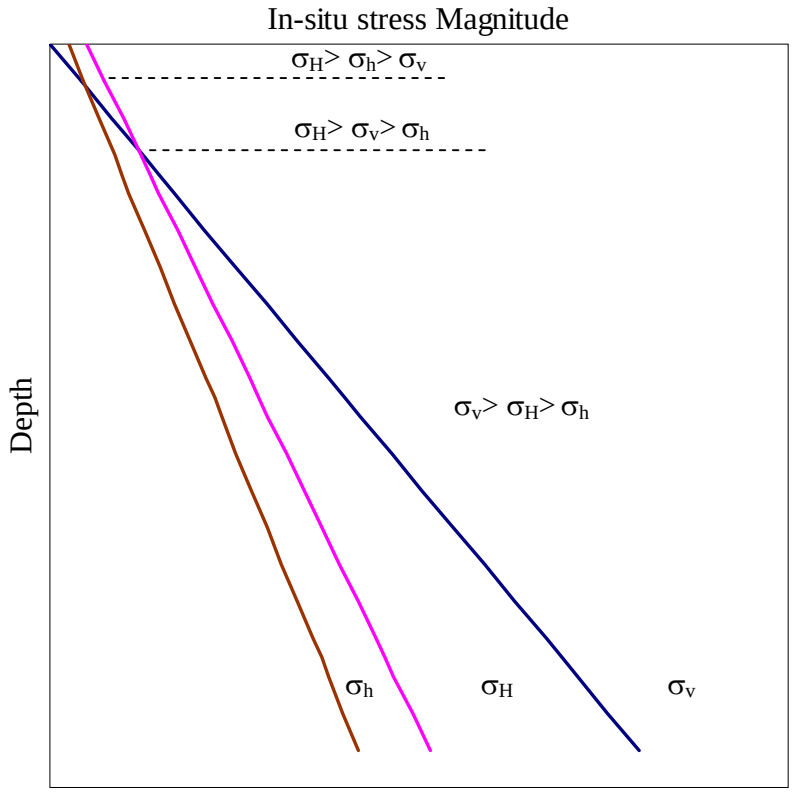

Figure 5-2: Stress variation in field.

In field, rock stress can only be measured at local points in space. Thus, determination of the state of stress in large rock masses is affected by many factors such as heterogeneities, faults, rock density and horizon boundaries. The effect of heterogeneities on stress field has been the subject of some Australian field observations by Hunt et al. (2003). The results presented a relationship for the ratio of maximum to minimum principal stress (k), fault orientation (θ) and friction angle (ϕ)

between faults and the generated stress perturbation in the surrounding rock mass. The results show that faults and horizon boundaries can greatly affect the magnitude and orientation of the rock stress components.

5.3 Theory of stress variation due to a large structure.

Rock fracture and fault are created by rock failure which occurs on the plane as a function of the shear stress and normal stress acting on that plane.

The normal stress and shear stress acting on the plane in a two dimensions stress field can be estimated by:

$$\sigma_n = \frac{1}{2}(\sigma_1 + \sigma_2) + \frac{1}{2}(\sigma_1 - \sigma_2)\cos 2\theta \qquad (5\text{-}1)$$

$$\tau = \frac{1}{2}(\sigma_2 - \sigma_1)\sin 2\theta \qquad (5\text{-}2)$$

Where σ_n is the normal stress, τ is the shear stress, σ_1 and σ_2 are minimum principle stress and maximum principle stress, respectively. θ is the angle between the maximum principle stress and the plane.

Plotting Equation 5-1 and Equation 5-2 we have Mohr's circle of stress with radius: $(\sigma_2 - \sigma_1)/2$ and centre: $(\sigma_2 + \sigma_1)/2$ showing in Figure 5-3.

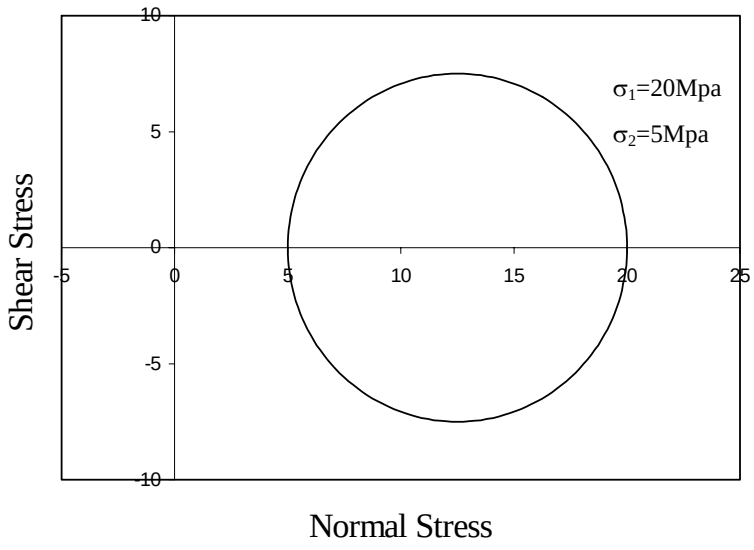

Figure 5-3: Mohr's circle

According to Mohr's hypothesis, rock failure by shear stress occurs when shear stress along some planes in the sample is too large as described by

$$|\tau| = f(\sigma_n) \tag{5-3}$$

By choosing the specific form of the function f, failure criteria are obtained. We have the common form of the Mohr-Coulomb criterion which assumes a liner function f.

$$|\tau| = S_o + \mu\sigma_n \tag{5-4}$$

Here S_o is the inherent shear strength or cohesion of the material, and μ is the coefficient of internal fiction.

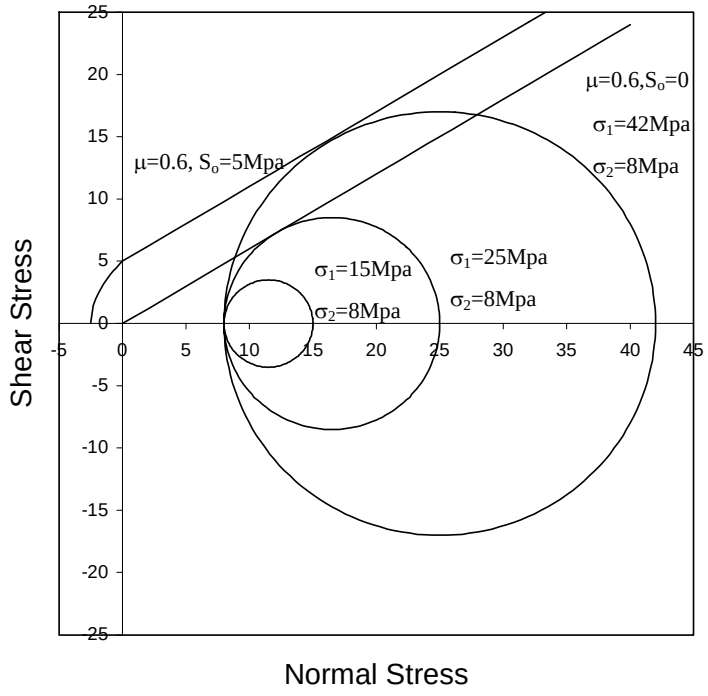

Figure 5-4: Stress state at failure situation

The coefficient of friction calculated for the case non-zero of cohesion strength when the sample failure is

$$\mu = tg\phi' = \frac{\tau - S_0}{\sigma_n} \tag{5-5}$$

The common method to calculate the cohesion strength using the unaxial rock strength C_o in laboratory testing is

$$S_o = \frac{C_o}{\left(2\left(\mu^2 + 1\right)^{1/2} + \mu\right)} \tag{5-6}$$

5.3.1 Effective stress principle

Most physical properties of rock in reservoir are controlled by Terzaghi's law of effective stress where effective stress (σ') equals to total stress (σ) minus pore fluid pressure (P)

$$\sigma' = \sigma - \alpha P \tag{5-7}$$

Where α is Biot's constant

According to Teufel et al. (1991) rock deformation and failure occurs in response to effective stress. In general, this means when the pore fluid change in reservoir, effective stress will vary as Figure 5-5. It can be seen that increasing effective stresses equals to variation of pore pressure in conventional model.

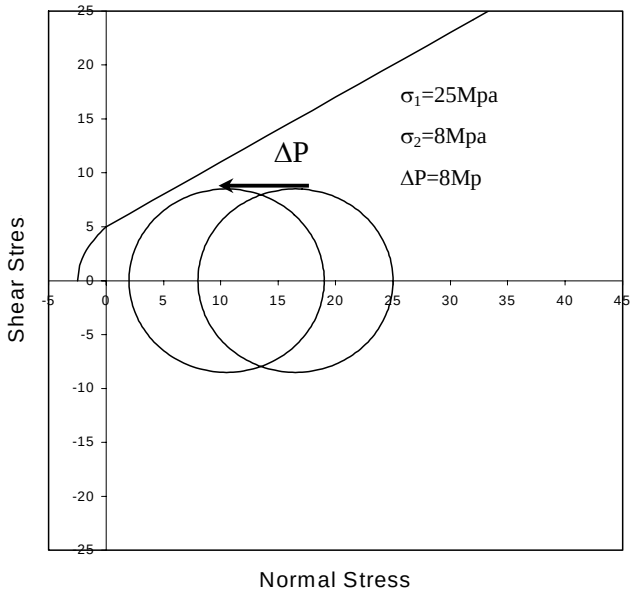

Figure 5-5: Moving of Mohr's circle due to fluid injection

So, effective stress tensor in reservoir can be written as

$$\begin{bmatrix} \sigma_H - \alpha P & 0 & 0 \\ 0 & \sigma_h - \alpha P & 0 \\ 0 & 0 & \sigma_v - \alpha P \end{bmatrix} \quad (5\text{-}8)$$

5.3.2 Influence of pore pressure on stress field

We have so far discussed the principle of effective stress but the changing of horizontal stress due to fluid withdrawing and elastic rock properties have been ignored. This overestimates the value of the stress field. The elastic unaxial strain model, based on passive basin assumption, has been commonly used in estimation of the horizontal stresses. Under conditions of gravitational forces, lateral constrain and no horizontal displacement, horizontal stress in a passive basin without fault is calculated as:

$$\sigma_h = \left(\frac{\nu}{1-\nu}\right)\sigma_v + \alpha P\left(\frac{1-2\nu}{1-\nu}\right) \quad (5\text{-}9)$$

In this case, it is assumed makes that horizontal stresses are equal $\sigma_h = \sigma_H$

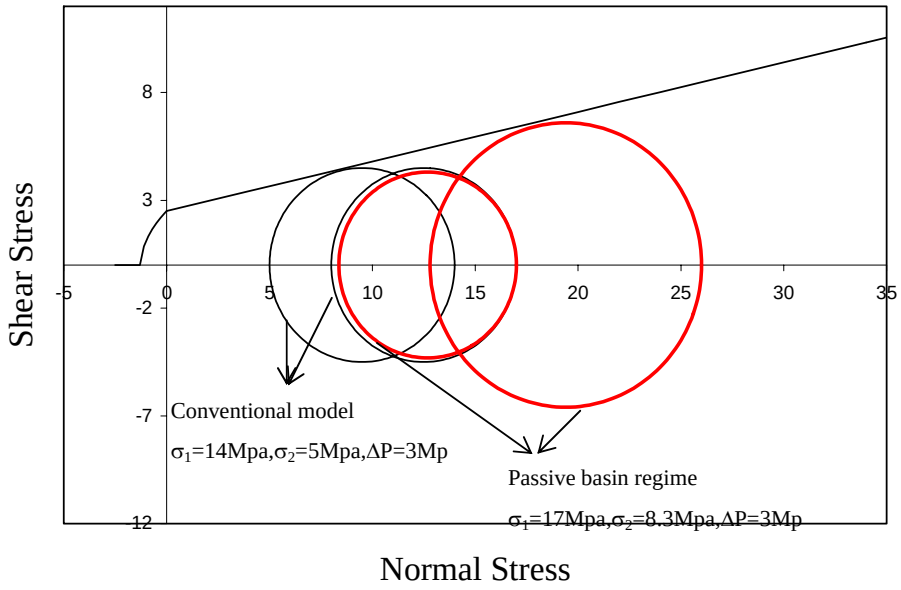

Figure 5-6: Variation of Mohr's circle due to fluid production within a passive basin regime

However, observations in many fields confirm that large structural features can change *in situ* stresses at depth. This means the assumptions of the passive basin model need to be reinvestigated.

5.3.3 Effect of fault or a large structure on stress field.

The normal stress (σ_n) and shear stress (τ) on the fault plane are

$$\sigma_n = \frac{1}{2}(\sigma_1 + \sigma_2) + \frac{1}{2}(\sigma_1 - \sigma_2)\cos 2\theta \qquad (5\text{-}10)$$

$$\tau = \frac{1}{2}(\sigma_2 - \sigma_1)\sin 2\theta \qquad (5\text{-}11)$$

Because only effective stress cause rock deformation and failure, the sliding condition on a pre-existing fault plane also is written as

$$\tau = \mu\sigma_n^{'} = tg\phi'\sigma_n^{'} \tag{5-12}$$

Substituting Equation 5-10 and 5-11 to Equation 5-12, we have

$$\frac{\sigma_3}{\sigma_1} = K_\alpha + (1 - K_\alpha)\frac{\alpha P}{\sigma_1} \tag{5-13}$$

Where

$$K_\alpha = \frac{\sin(2\theta + \phi') - \sin(\phi')}{\sin(2\theta + \phi') + \sin(\phi')} \tag{5-14}$$

Equation 5-14 reaches the maximum value at the fault angle $\theta = 45^0 - \frac{\phi'}{2}$ where the fault is weakest, and stress ratio becomes

$$\frac{\sigma_3}{\sigma_1} = \frac{1 - \sin\phi'}{1 + \sin\phi'} + \frac{2\sin\phi'}{1 + \sin\phi'}\frac{\alpha P}{\sigma_1} \tag{5-15}$$

Applying the Equation 5-15 for a normal fault system, we have

$$\frac{\sigma_h}{\sigma_v} = K_\alpha + (1 - K_\alpha)\frac{\alpha P}{\sigma_v} \tag{5-16}$$

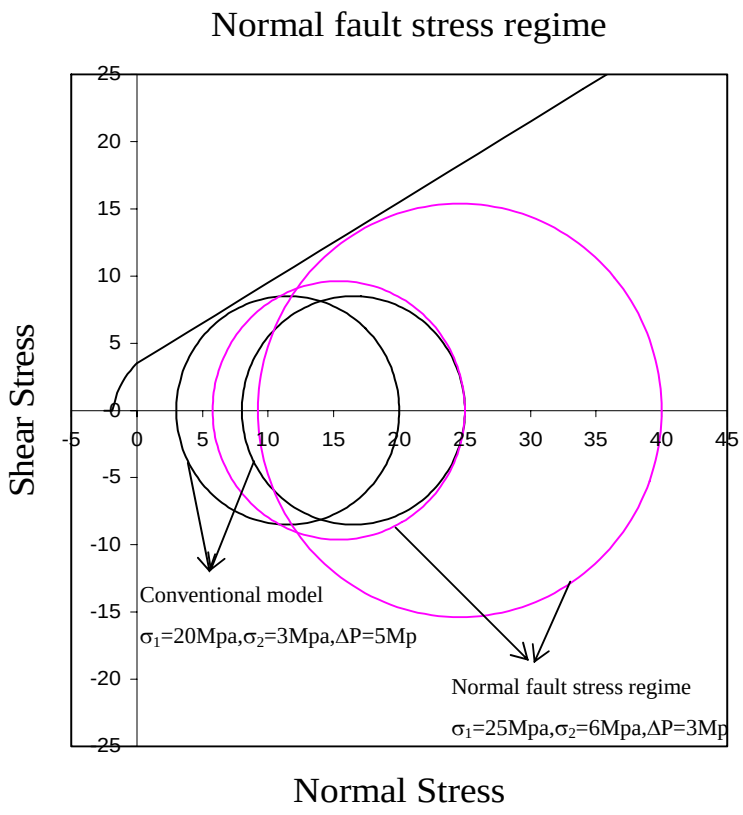

Figure 5-7: Variation of Mohr's circle due to fluid production within normal stress regime.

For reverse fault conditions, where $\sigma_H > \sigma_h > \sigma_v$, the magnitude of the maximum horizontal stress acting on the fault plane can be written as:

$$\frac{\sigma_H}{\sigma_v} = K_\beta + \left(1 - K_\beta\right)\frac{\alpha P}{\sigma_v} \qquad (5\text{-}17)$$

With $K_\beta = \frac{1}{K_\alpha}$

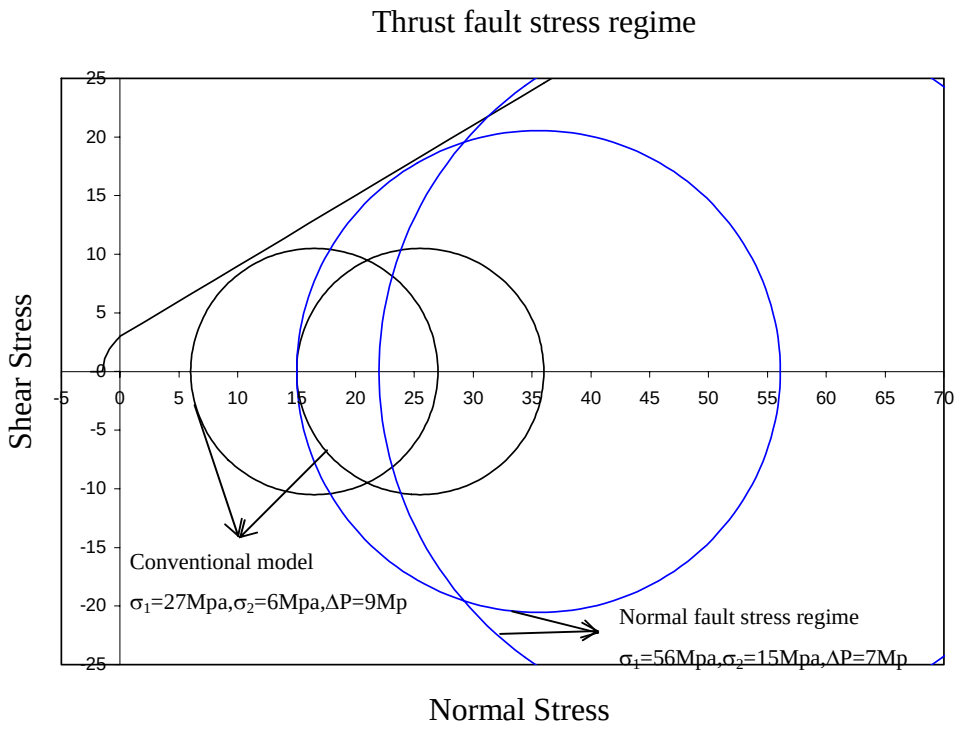

Figure 5-8: Variation of Mohr's circle due to fluid production within thrust stress regime.

Equation 5-17 satisfy the condition of a pure thrust fault if the given fault angle, fault friction and $\nu \geq \frac{1}{(1+K_\beta)}$

Otherwise, the stress regime becomes strike-slip stress system with

$\sigma_H > \sigma_v > \sigma_h$

Finally, we have

$$\frac{\sigma_H}{\sigma_h} = \frac{1}{(\nu(1+K_\beta))}\left(K_\beta - [K_\beta(1-\nu)-\nu]\frac{\alpha P}{\sigma_v}\right) \qquad (5\text{-}18)$$

5.4 Sensitivity of permeability to stress perturbation and influence of a discontinuity on permeability

The previous chapter shows the permeability changes under a depleted reservoir condition. Most researchers reached the conclusion that permeability is reduced from 10% to 30% when confining stress was increased in a range of 1000psi to 8000psi (Holt 1990; Warpinski and Teufel 1992). Further results showed that the reduction of permeability in a low permeability core is greater than reduction of permeability in a high permeability core (Vairogs and Rhoades 1973), implying that only certain rock types demonstrate significant stress sensitive permeability. In most cases, a decrease in permeability occurred with increasing stress. One exception to this is where dilatancy leading to brittle failure occurs under triaxial conditions; in which high shear stresses are acting.

A number of field studies relating to compaction and subsidence in the North Sea have also shown that permeability changes during production significantly influenced the stress path of the reservoir (Rhett and Teufel 1992; Economides, Buchsteiner et al. 1994). Consequently, there is no doubt that the constant permeability values assumed in conventional reservoir simulation may result in considerable errors. The investigation of the influence of the stress path under varying reservoir conditions was further discussed by Mashiur and Teufel (1996). Importantly the results presented, demonstrated that sensitivity of permeability due to stress perturbation was not only dependent on effective stress but also on the size, geometry and other reservoir properties (e.g. reservoir boundary conditions). These experimental results on stress sensitivity demonstrated that the maximum

permeability direction is parallel to the maximum principal stress and the magnitude of permeability anisotropy increases for lower stress paths. The modeled results of other research (Camac, Hunt et al. 2004) showed that the stress regime along the fault strike, are most sensitive to friction angle (ϕ), with the perturbation generated up to 1.4 times the magnitude of the maximum principal regional stress. As a result of increasing stress, permeability and porosity will change as discussed in previous section.

5.5 Case study on the impact of large structure features on permeability

5.5.1 Introduction of case study

To investigate the influence of a discontinuity causing stress perturbation on permeability, the Eromanga-Cooper Basins were used as case example (Figure 5-9). These fields are located in central and eastern Australia. The saucer-shaped Eromanga basin extends over one million square kilometers in Queensland, New South Wales, South Australia, and the southeast of the Northern Territory. The Eromanga-Cooper Basins is overlain by the Lake Eyre Basin, a succession of Tertiary and Quaternary age sediments occurring extensively throughout central Australia.

Figure 5-9: Stratigraphy summary of Eromanga Basin (Boreham and Hill 1998)

These sediments are gently folded in some areas and contain a succession of extensive sandstone formations that serve as oil reservoirs and regional aquifers. The majority of oil producing reservoirs in the Eromanga-Cooper Basins is classified as 'water drive' reservoirs. Oil pools are usually found in formations that also contain considerable quantities of water. As a result of the differing physical properties of oil and water, over time the oil tends to 'float' to the surface and sit above the water. These formations usually exist under pressure so when they are accessed by drilling a borehole the oil will flow to the surface.

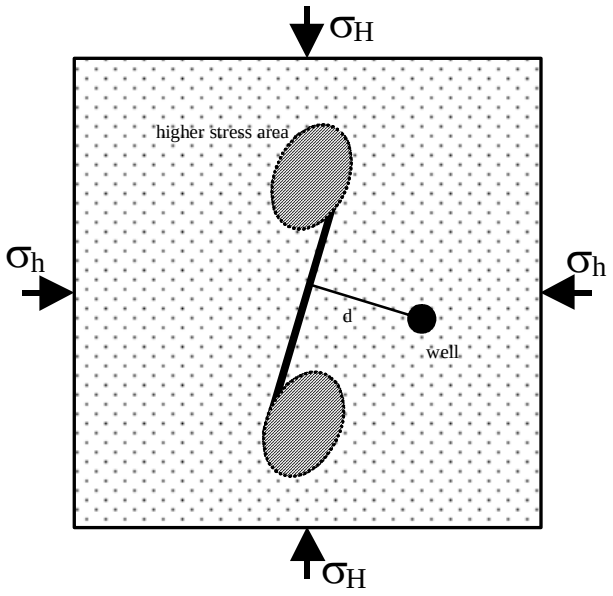

Figure 5-10: Stress perturbation around the tip of fracture

Theoretically, the fault system usually is a consistently parallel S_{Hmax} orientation (Figure 5-10). However, field observed data in Eromanga-Cooper Basin showed that the degree to which the stress field is perturbed relates to the contrast in geomechanical properties at the interface (Camac, Hunt et al. 2004; Reynolds, Mildren et al. 2005). Stress perturbations also occur as a result of slip on preexisting faults in rocks with homogenous elastic properties. In this situation, the stress perturbations are greatest at the tips of the discontinuity and can vary as a result of factors such as the differential stress magnitude, fault models, the friction coefficient on the discontinuity and the strike of the discontinuity relative to the far-field stress.

It is also noted that when fluid is withdrawn from the reservoir, the *in situ* stress will be changed. In turn, due to stress perturbation at the discontinuity, a change in the hydrocarbon production may occur. This situation should be considered seriously at

the point that stress changes associated with depletion are complicated in compaction reservoir under pore fluid pressure reduction (Ta and Hunt, 2005). In this case example, considering the influence of a discontinuity, the minimum stress-depletion response in the far field region of active normal faulting may be expressed (Addis, Last et al. 1996) as following

$$\Delta\sigma_3 = \Delta P\left(2\frac{\sin\phi'}{1+\sin\phi'}\right)$$

This equation is suitably applied for the Eromanga-Cooper basins because the minimum stress acts on the fault plane.

5.5.2 Model description

This study analyses the impact of assigning different initial permeability to a coupled wellbore production model. Table 5-1 shows the values selected for a reservoir simulated using the symmetric well model in the Eromanga-Cooper basins.

Table 5-1: Material properties of reservoir in the simulation

Material properties	Symbol	Values	Field unit
Initial porosity	ϕ	0.15	-
Poisson' ratio	ν	0.25	-
Initial permeability	k	30	mD
Young's modulus	E	5.6 E6	psi
Fluid compressibility	C_f	15.E-06	psi^{-1}
Solid compressibility	C_s	7.0E-06	psi^{-1}
Initial pressure	P_i	5000	psi
Production zone	N/A	1400-1800	ft
Well radius	r_w	0.5	ft
External boundary	R	7932	ft

Depth	z	4798	ft

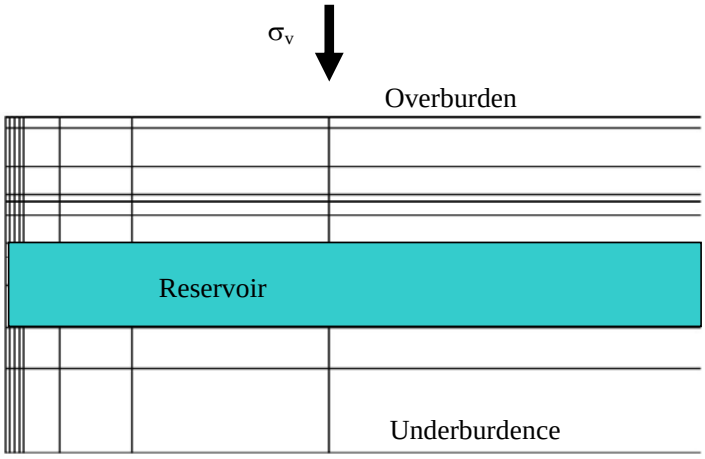

Figure 5-11: Symmetric well model

The importance is to simulate the effect permeability variation due to stress perturbation can have on subsidence and compaction estimates for the oil reservoir within the radial model. The reservoir in this model is assumed to be thin related to the depth, the perforated zone and a field scale example as shown in Figure 5-11. Oil production is simulated over a 200-day period. In this model, the well of radius r_w is producing a single-phase fluid at a constant rate q, from a saturated reservoir. The reservoir is assumed to be homogeneous and isotropic, with a boundary being restrained from any radial displacement at the producing wellbore, but allowing free displacement in the vertical direction. The study looks at the concept of introducing a large structural feature which will laterally give rise to a perturbation in the local stress field that will in turn influence the evolving reservoir permeability and final subsidence. Due to boundary condition that is being restrained from any vertical and

horizontal displacement far from wellbore, the subsidence at the external boundary equals zero. This effect could increase significantly in the area around the wellbore where pore pressure is at a minimum. At a distance far from the wellbore, this influence will decrease and reach the initial value. The coupled model analysis is written using the Matlab programming environment and solves problems involving fluid flow through a saturated elastic porous medium under transient condition. Mechanical properties derived directly from core data were averaged for the purposes of the reservoir simulation.

5.5.3 Results and discussions

Figure 5-12 shows the subsidence of the reservoir during fluid production for the conventional and the stress coupled permeability models with an initial porosity of 15%. The subsidence varied between 0.9ft and 0.95ft for the models run over a 200-day period, respectively. Consequently, it is evident that stress sensitive permeability has an increased effect on the subsidence magnitude.

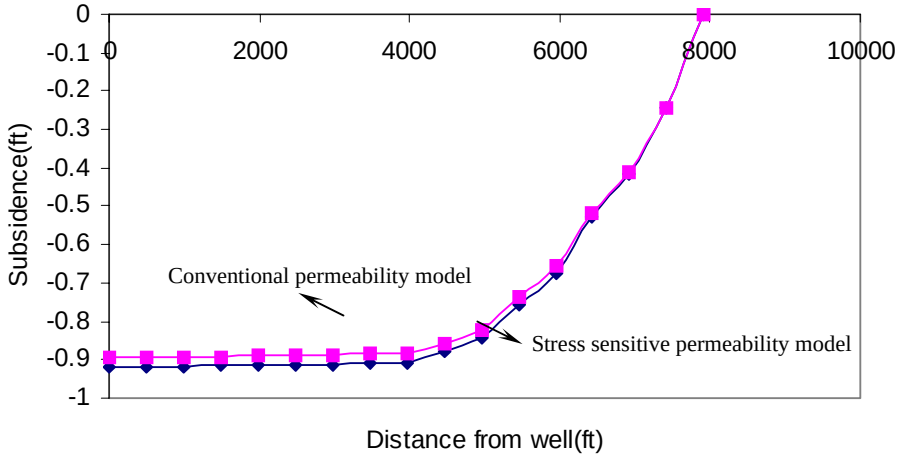

Figure 5-12: Subsidence variation between conventional permeability (permeability fixed throughout model run) and stress sensitive permeability (permeability permitted to vary throughout model run) models after 200 days of production (k_i = 30md, ϕ_i = 0.15).

A simulation of reservoir depletion was also run for different stress sensitive models by applying the same initial conditions for fluid production. Figure 5-13 shows the influence of a discontinuity on possible lateral subsidence variation resulting in three models with different initial stress perturbation at the boundary such as faults or fracture. This is done in order to assess sensitivity for a stress sensitive reservoir to possible variation in stress caused by heterogeneity. It can be seen that the subsidence increases from nearly 0.91ft to 0.95 ft over a 200-day simulation run. The results suggest that an increase in stress due to a large feature could lead to a significant variability in the coupled model runs.

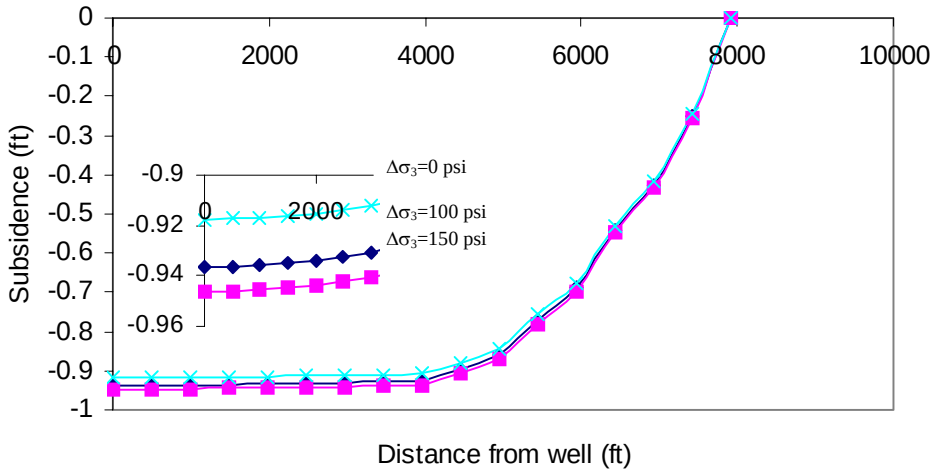

Figure 5-13: Influence of a large structure on subsidence, $\Delta\sigma_3$ is the variation in the predicted applied horizontal stress possible around a discontinuity such as a fault,

(applied in the stress sensitive permeability models after 200days with k_i=30md, ϕ_i=0.15).

Moreover, because the deformation increased in the near wellbore region, rock properties are expected to change inelastically. Consequently, petrophysical parameters, including permeability and porosity, will be further complicated. So detailed, more qualitative calculation investigations are required in future within this plastic regime.

5.6 Conclusions

This chapter presents the impact of a large structure on stress regime. Mathematical models were derived for each fault model so as estimate stress perturbation. All models are based on Mohr–Coulomb's criteria in faulted area. Analysis of different fault stress regimes show that effective stress regimes vary significantly when compared to a conventional model.

Chapter 5 also emphasizes on reservoir engineering applications. Important results described in this chapter illustrate a step forward in understanding in increasing of effective stress that is the main factor controlling permeability in an area surrounding a large structure. The relationship between permeability and the change in effective stress that is perturbed by a large structure is also used in investigation of compaction and subsidence.

CHAPTER 6: DETERMINATION OF NEW RELATIVE PERMEABILITY CURVE DUE TO COMPACTION AND ITS IMPACTS ON RESERVOIR PERFORMANCE

6.1 Introduction

Compaction and subsidence due to oil and gas production can be observed in several fields around the world, in the Gulf of Mexico, the North Sea, and onshore, for example California and Venezuela. In Australia, compaction and subsidence problems were mainly documented for the Gippsland basin.

As a result of compaction, changes in reservoir properties may be observed. Several researches have identified the impact of compaction on reservoir properties. In this chapter the intention is to analyze the variation of water production due to compaction in a field in Venezuela. The produced water appeared to be not associated with any aquifer. So where does the water come from? Analysis by engineers at the time believed the water to be associated with changes in the pore structure, where the produced water is due to volume changes of immobile water and mobile water as the result of compaction. This also means that relative permeability curves would have changed when rock deformed.

The objectives of this chapter may be presented as follows:

- ✓ Overview of methods to predict new irreducible water saturation (S_{wir}) due to compaction;
- ✓ Introduction of methodologies for creating new relative permeability relationships based on new endpoint data;
- ✓ Analysis of water production due to compaction, and critical points of updating relative permeability curves to properly simulate reservoir fluid flow under compaction;
- ✓ Coupled reservoir simulation using updated relative permeability curves applied to an area in the Bachaquero field - Venezuela.

6.2 End-points in relatives permeability curve

6.2.1 Irreducible water saturation

Water saturation is the fraction of water volume in the rock in respect of the total pore volume. Formation water always appears in reservoir formations, even if hydrocarbons are present. It is typically remaining brine (connate water) trapped in geological time in the rock matrix after the migration of oil or gas, displacing some of this water. The distribution of water saturation is dominated by capillary, viscous and gravity forces. The water saturation will be one hundred percent below the free water level (water-wet rock). In the transition zone, water saturation varies, depending on capillary forces. Water saturation becomes irreducible, S_{wir}, higher up in the hydrocarbon column, above the transition zone.

Irreducible water saturation presents the lowest water saturation at the crest of the hydrocarbon accumulation, given by:

$$S_{wir} = \frac{BVWi}{\phi_t} \qquad (6\text{-}1)$$

Where: BVWi is irreducible Bulk Volume Water and ϕ_t is total porosity.

The magnitude of that saturation is governed by fluid densities, wettability, interfacial tension as well as pore size and geometry. As the effect of compaction, pore size and geometry will be changed, affecting the magnitude of irreducible water saturation. Generally, S_{wir} would increase as the pore size decreases; however, that variation of S_{wir} is not a simple linear function. The relationships of porosity and irreducible water saturation, specifically value of $\phi x S_{wir}$, have been studied by several authors.

Weaver (1958) was the first one considering constant value of $\phi x S_{wir}$ in the homogeneous carbonate with the uniform matrix. Later, Buckles (1965) suggests the reciprocal relations between ϕ and S_{wir} to be constant with the idealized system of spherical particles, requiring (1) the linear relationship between surface area and S_{wir} and (2) hyperbolic relations between porosity and surface area. Morrow (1971) correlates irreducible water saturation of wetting phase with the "packing heterogeneity", which depends on the three-dimensional distribution of grains and the consolidating cement. The author suggests that irreducible water saturation would be independent to particle sizes, but have high correlation with packing heterogeneity. Measured irreducible water saturation was then proposed to characterize the packing heterogeneity properties of reservoir rocks.

At the same time, Holmes et al. (1971) comprehensively review effects of rock, fluid properties, and their relations to the fluid distribution of sandstone. The qualitative relations among surface area, average pore entry radius and S_{wir} were established. Some important points relating to the relations of S_{wir} and porosity were generated from their study:

- ✓ The surface area cannot be correlated with porosity as discussed by Buckles (1965); therefore, porosity cannot be combined in any simple form with S_{wir}.
- ✓ The S_{wir} basically has the negative correlation with the surface area and positive correlation with the average pore entry size.
- ✓ The increase in cementation would generally cause the increase in surface area. As S_{wir} increases with the increase in surface area, S_{wir} will consequently increases as the result of the cementation increase.
- ✓ The sandstones with large pore size will have small surface area and high average pore entry radius, hence will have low S_{wir} value. Contrastingly, the smaller-pore-size rock will have higher tortuosities, high surface area, low average pore entry radius, and hence will have high irreducible water saturation.
- ✓ Large scatter of data was observed when plotting porosity-surface area and porosity-Swir, indicating that there is not a simple correlation between porosity and the latter properties not to be simple.

In conclusion, variation in porosity is expected to influence S_{wir} by means of the following: pore volume, surface area, and average pore radius. The relationship between S_{wir} and porosity is, therefore, complicated.

6.2.2 Predicting the variation of S_{wir} according to the variation of porosity

In this section, relationships linking porosity and irreducible water saturation are briefly discussed. Such relationships are derived based on a combination of the modified Carmen-Kozeny's equation and the empirical relationship between permeability, porosity and irreducible water saturation.

A number of correlation equations between permeability, porosity and irreducible water saturation have been suggested by several authors. The general empirical relationship is proposed by Wylie and Rose (1950), is:

$$k = \frac{P\phi^{Q}}{S_{wir}^{R}} \tag{6-2}$$

where P, Q, and R are parameters which are calibrated to fit the core data.

Based on the above general relationship, various relationships are proposed. Among them are the relationship from Timur (1968) based on 155 sandstone core measurements from different field.

Timur's expression is:

$$k = \frac{0.136\phi^{4.4}}{S_{wir}^{2}} \tag{6-3}$$

By comparison, the general form of the modified Carmen-Kozeny's equation gives a correlation of permeability as the function of porosity, specific surface area, tortuosity and pore shape factor, as follows:

$$k = \frac{\phi^3}{F_{ps}\tau^2 S_{vgr}^2 (1-\phi)^2} \tag{6-4}$$

where F_{ps}, τ and S_{vgr} are pore shape factor, tortuosity and specific surface area.

The inverse relationship between tortuosity and porosity is suggested by several authors. Pape et al. (1999) have studied the fractal pore-space geometry and express their relationship as follows:

$$\tau \approx \frac{0.67}{\phi} \tag{6-5}$$

The combination of the (6-3), (6-4) and (6-5) gives:

$$S_{wir} = 0.247 S_{vgr} \sqrt{F_{ps}} \frac{(1-\phi)}{\phi^{0.3}} \tag{6-6}$$

When reservoir fluids are extracted, due to the increment of effective overburden pressure, reservoir formation is compacted. The compaction process can be briefly divided into 2 phases:

- ✓ Re-arrangement: Under overburden pressure, loosed grains are re-arranged to reduce pore volume between them. The tendency of the re-arrangement is to

reduce the exposed grain surface to fluid, hence alters the specific surface area. However, as the definition from Tiab and Donaldson (2004), specific surface area is the total area exposed within the pore space per unit of grain volume, thus would increase if pore volume reduced. As the result, there should be no apparent relationship between specific surface area and porosity. Holmes et al (1971) also support that point when doing the study of lithology, fluid properties and their relationship to fluid saturation. With the assumption of insignificant changes of pore shape factor and specific surface area, the changes of irreducible water saturation from S_{wir1} to S_{wir2} when porosity reduces from ϕ_1 to ϕ_2 should be:

$$S_{wir2} = S_{wi1}\left(\frac{\phi_1}{\phi_2}\right)^{0.3}\left(\frac{1-\phi_2}{1-\phi_1}\right) \qquad (6\text{-}7)$$

As porosity reduces due to compaction, the new irreducible water saturation should become higher.

- ✓ Grain-crushing: This stage may occur with more extreme compaction after no further re-arrangement can be accommodated. The mean grain diameter d_{gr} and grain shape factor K_{gs} significantly change. While the grain diameter decreases, the grain shape factor tends to increase to heighten the level of grain sphericity and roundness. Tiab and Donaldson (2004) suggest that K_{gs} should approaches 6 when grains are perfectly spherical. The general relationship of the mean grain diameter, grain shape factor and specific surface area is suggested as following:

$$S_{vgr} = \frac{K_{gs}}{d_{gr}} \qquad (6\text{-}8)$$

The combination of (6-6) and (6-8) under the reduction of porosity due to grain crushing yields:

$$S_{wir2} = S_{wi1}\left(\frac{\phi_1}{\phi_2}\right)^{0.3}\left(\frac{1-\phi_2}{1-\phi_1}\right)\left(\frac{K_{gs2}}{K_{gs1}}\right)\left(\frac{d_{gr1}}{d_{gr2}}\right) \qquad (6\text{-}9)$$

The slight increment of grain shape factor K_{gs} and especially the reduction of mean grain diameter d_{gr} cause irreducible water saturation to increase much higher in the grain crushing phase to compare with the increment of irreducible water saturation in the re-arrangement phase.

6.2.3 Water production due to compaction

The basic definition of water saturation is:

$$S_w = \frac{V_{water}}{V_{pore}} \qquad (6\text{-}10)$$

Water becomes movable in a reservoir when water saturation is higher than irreducible water saturation. The movable water should be the difference between water saturation and irreducible water saturation timing pore volume.

In reservoir, the bulk volume change due to compaction. The pore volume decreases, causing water saturation to increase.

$$\frac{S_{w1}}{S_{w2}} = \frac{V_{pore2}}{V_{pore1}} = \frac{\phi_2}{\phi_1} \tag{6-11}$$

Therefore, the new water saturation due to porosity change should be:

$$S_{w2} = S_{w1}\frac{\phi_1}{\phi_2} \tag{6-12}$$

The irreducible water saturation, as discussed above, should also increase. However, the increase in water saturation is higher than the irreducible water saturation, which causes the water to be movable. The changes in irreducible water saturation are different depending on stage of compaction, causing the water production to vary. Water production due to compaction can be explained as the following figure:

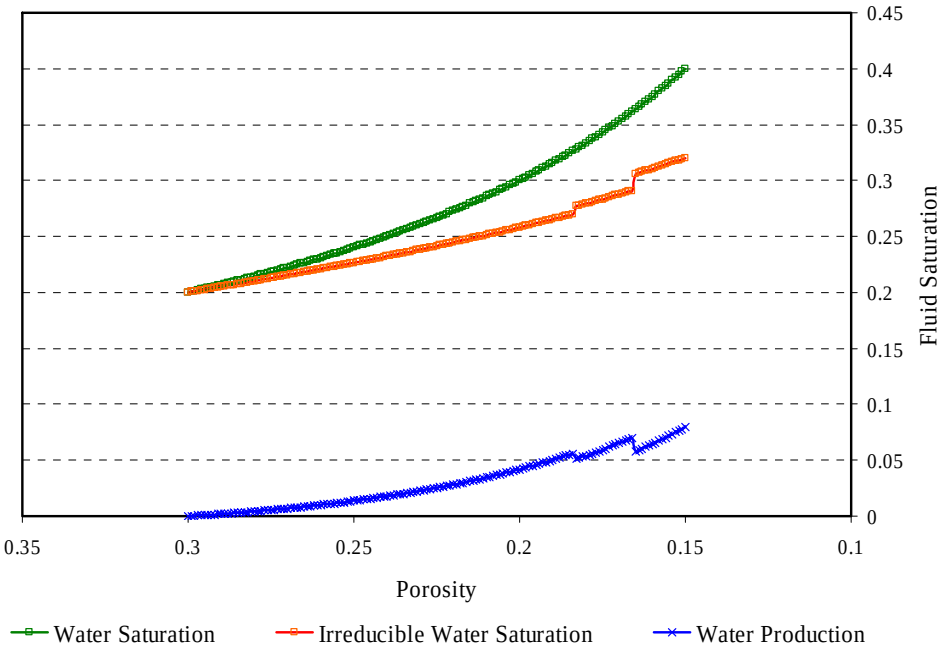

Figure 6-1: Water production due to compaction

As mentioned above, grain crushing phase is the phase that greatly increases the irreducible water saturation. Depending on the level of crushing, water production can be reduced or even halted as described in the Figure 6-1. Due to reservoir heterogeneities, reservoir compaction occurs differently throughout the reservoir, causing water production to be various.

6.2.4 Residual oil saturation

Residual oil saturation is defined as the fraction of volume of oil that cannot be displaced over pore volume. In experimental conditions, both residual oil saturation and irreducible water saturation depend on capillary pressure. However, for the

experiment, the irreducible water saturation is determined from the drainage capillary pressure curve. On the other hand, residual oil saturation is defined by the imbibition capillary curve. Nick et al. (2002) showed that residual oil saturation is also governed by the change in effective permeability which is mainly influenced by capillary pressure. Based on published data from Middle East Fields, they concluded that residual oil saturation is inversely proportional to permeability. It means that if total permeability reduces because of increasing effective stress in compacting reservoir, residual oil saturation will increase.

6.3 Relative permeability models

The permeability of porous media is one important flow parameter associated with reservoir engineering. Permeability depends mainly on the geometry of the porous system. If there are more than two fluids, permeability depends not only on the geometry but also on saturation of each fluid phase, capillary pressure and other factors. There has been research based on both theoretical and empirical considerations to predict relative permeability curves. Some experimental relationships to describe relative permeability may be summarized as follows:

- **Original Brook – Corey relationship**

Corey and Brook (1966) observed under experimental conditions,

$$k_{ro} = (S_e)^{\frac{2+3\lambda}{\lambda}} \qquad (6\text{-}13)$$

$$k_{rw} = (1 - S_e)^2 \left(1 - S_e^{\frac{2+\lambda}{\lambda}}\right) \quad (6\text{-}14)$$

$$S_e = \left(\frac{P_b}{P_c}\right)^{\lambda} \quad (6\text{-}15)$$

Where: λ is a number which characterizes the pore-size distribution. P_b is a minimum capillary pressure at which the non wetting phase starts to displace the wetting phase. P_c is a capillary pressure. k_{ro} is oil relative permeability normalized to absolute plug air permeability and k_{rw} is water relative permeability normalized to absolute plug air permeability

In real situations, relative permeability data are measured on cores cut with a variety of drilling mud, using extracted, restored state and preserved core samples. The relative permeability values were obtained from both centrifuge and waterflood experiments. So, each oil-water relative permeability data set was analyzed and Brook – Corey equations were used to fit the oil and water relative permeability measurements. However, the forms of the Brook-Corey equations used do not always result in a good curve fit of the laboratory results. In addition, due to the difficulty of determining all parameters, the most useful model in petroleum industry used is the modified Brook and Corey model as shown below

- **Modified Brook and Corey relationship**

$$k_{ro} = k'_{ro} \left(\frac{1 - S_w - S_{or}}{1 - S_{wir} - S_{or}}\right)^{n_o} \quad (6\text{-}16)$$

$$k_{rw} = k'_{rw} \left(\frac{S_w - S_{wir}}{1 - S_{wir} - S_{or}}\right)^{n_w} \quad (6\text{-}17)$$

Where

k_{ro}': End point relative permeability normalized to oil absolute plug air permeability

k_{rw}': End point relative permeability normalized to water absolute plug air permeability

S_{or}: Residual oil saturation

S_w: Water saturation

n_o: Corey exponent to oil

n_w: Corey exponent to water

This model can be applied for oil-water and gas-oil systems. The advantage of using this relationship is that the MBC model is smooth and extending an existing relative permeability curve. Normally, low Brook – Corey water exponents are associated with oil wet rock. The oil exponents decline from a value of about 5 at a permeability of 0.1 Darcy to approximately 3 at permeability above 1 Darcy. The exponents range between 1 and 4 with no clear trend based on permeability or reservoir lithology/zonation.

- **Semi-empirical model**

Based on Carmen-Kozeny's equation, Behrenbruch (2006) presented a new semi-empirical model to predict a relative permeability curve as shown by following relationships

$$k_{rw} = \frac{1014 m_w^2 \phi_e^3 S_w}{k} \left[\frac{S_w}{1-\phi_e S_w} - \frac{S_{wir}}{1-\phi_e S_{wir}} \right]^2 \qquad (6\text{-}18)$$

$$k_{ro} = \frac{1014 m_o^2 \phi_e^3 (1 - S_w)}{k} \left[\frac{1 - S_w}{1 - \phi_e (1 - S_w)} - \frac{S_{or}}{1 - \phi_e S_{or}} \right]^2 \quad (6\text{-}19)$$

In the above equation, m_w and m_o are considered as the slope of the linear relationship in Carmen-Kozeny's space. Clearly, effective porosity appears as a main parameter in relative permeability curves. Consequently, these equations are used in estimating the new permeability curve when porosity changes due to compaction.

To investigate the range of n_w and n_o, Behrenbruch and Goda (2006) rearranged the MBC relationship as following

$$\left(\frac{1 - S_w - S_{or}}{1 - S_{wir} - S_{or}} \right)^{n_o - 2} = \frac{(1 - \phi(1 - S_{wir}))^2}{1 - S_{wir}} \frac{1 - S_w}{(1 - \phi(1 - S_w))^2} \quad (6\text{-}20)$$

$$\left(\frac{S_w - S_{wir}}{1 - S_{wir} - S_{or}} \right)^{n_w - 2} = \frac{(1 - \phi(1 - S_{or}))^2}{1 - S_{or}} \frac{S_w}{(1 - \phi S_w)^2} \quad (6\text{-}21)$$

With parametric study, they showed that n_o and n_w varies in the range of 2.6 – 3.5. These ranges have a maximum at 7 when porosity reduces to unity.

This study attempts to revaluate the range of n_o and n_w in MBC relationship. Our model using Monte Carlo Simulation (MCS) was run with all parameters required for the calculation used with normal distribution data as shown in Figure 6-2 and summarized in Table 1. Once the input data was determined, it replaced the input data in equations 6-20 and 6-21. Monte Carlo simulation was performed for 5,000 iterations.

The results show that with the normal distribution for input data (Figure 6-2), the mean of n_o is about 2.7 and maximum and minimum n_o are 3.37 and 2.14,

respectively. In addition, the standard deviation (Std) of n_o is 0.28. So, there is a 90% confidence interval where n_o falls between 2.40 – 2.98. On the other hand, the mean of n_w is 2.61. The maximum and minimum n_w are 3.32 and 2.09, respectively (Table 6-3). In addition, Std of n_w is 0.21. As a result, there is a 90% confidence interval where n_w compaction falls between 2.27 – 2.97. This distribution also indicates that due to the existence of uncertainty in input data, these interesting results would suggest, depending on available data, the ranges of Brooks and Corey exponents may practically be narrower than suggested by Behrenbruch and Goda (2006), and indeed Brooks and Corey, and other researchers.

Table 6-1: Summary Information

Workbook Name	Statistic to determination of no and nw
Number of Simulations	1
Number of Iterations	5000
Number of Inputs	4
Number of Outputs	2
Sampling Type	Monte Carlo
Simulation Start Time	19/07/2007 16:55
Simulation Stop Time	19/07/2007 16:55
Random Seed	1587511621

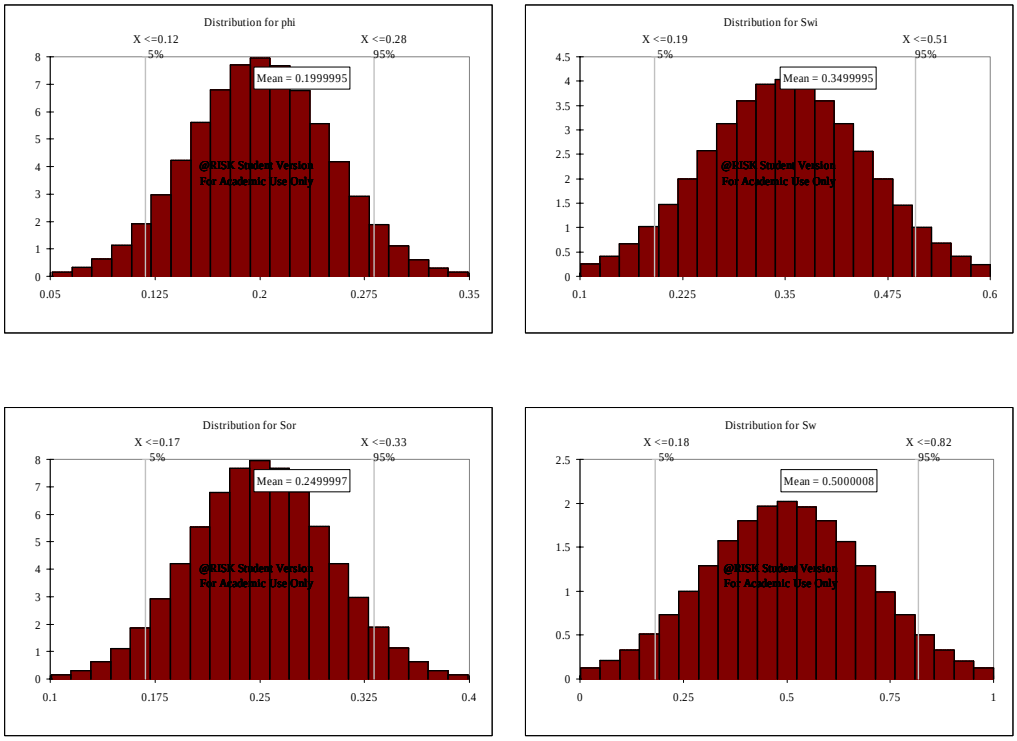

Figure 6-2: Distribution of input data for calculation of n_o and n_w

Table 6-2: Summary of input data for calculation of n_o and n_w

Name	Minimum	Mean	Maximum
Phi (ϕ)	0.05	0.20	0.35
Sw	0.00	0.50	1.00
Sor	0.10	0.25	0.40
Swi	0.10	0.35	0.60

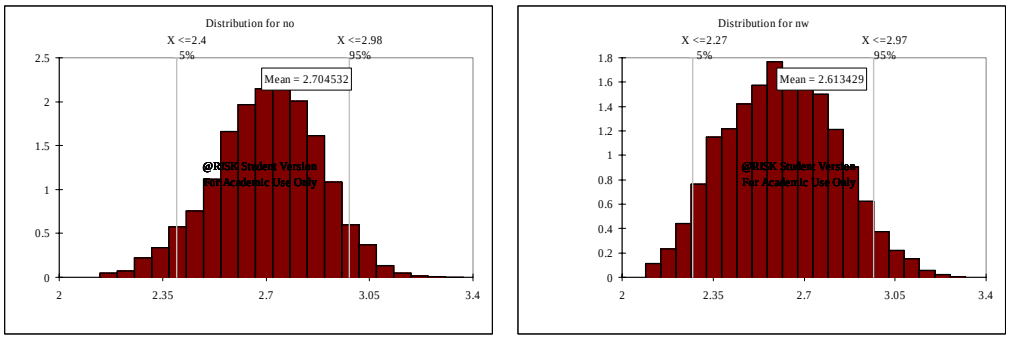

Figure 6-3: Distribution of n_o and n_w

Table 6-3: Summary of n_o and n_w

Name	Minimum	Mean	Maximum	Std
n_w	2.09	2.61	3.32	0.21
n_o	2.14	2.70	3.37	0.18

A sensitivity analysis was conducted for both n_0 and n_w. Figure 6- 4 shows that the impact of all parameters on both n_o and n_w. Simulation results are observed for n_w, with S_{wi} having the biggest impact followed by S_w, porosity and S_{or}. It can be seen that the impact of S_w uncertainty on n_o is larger compared to the impact of S_{or}, S_{wi} and porosity.

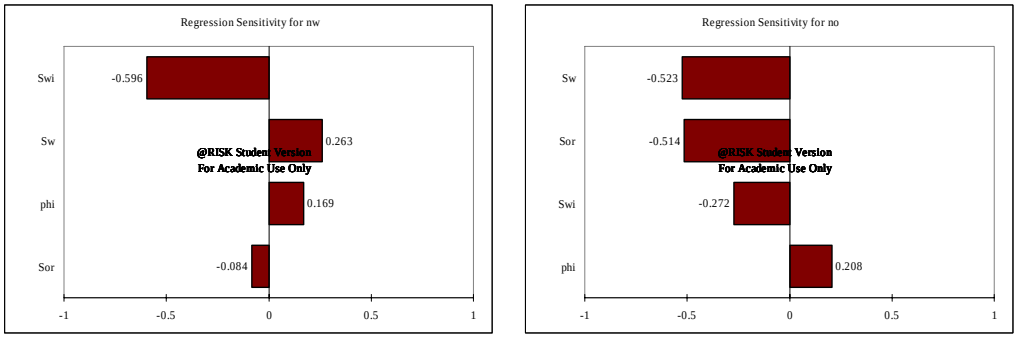

Figure 6-4: Tornado graph to invest the impact of parameters on both n_o and n_w

6.4 Practical implementation

This part gives the results from investigating the compaction problem and the associated problem of taking into account changes in relative permeability as applied to the Lagoven area of the Bachaquero field in Venezuela. The Bachaquero field straddles the shoreline of Lake Maracaibo where part of the field is onshore and part is offshore. The field has produced since the 1930's and subsidence was recorded since 1955. The subsidence prompted the construction of coastal dykes for protection against water flooding of coastal areas. Equipment was installed at certain locations to monitor ground subsidence. In most of the available literature it was cited that compaction is the main drive mechanism in certain parts of this field. In addition, compaction not only changes total porosity and absolute permeability but in general may also affect the wetting properties of the rock. As a result, this phenomenon can dramatically impact reservoir performance, which is not easily modeled by conventional methods.

This case study will only investigate change in relative permeability curves when porosity alters. The study concentrates on a reservoir engineering analysis to evaluate the effect of the change in relative permeability curves on fluid production and interpretation the compaction behavior.

6.4.1 Description of Lagoven

The Lagoven area in the Bachaquero field located in the west coast of Lake Maracaibo has produced heavy oil (varying from 10° - 19° API) from a Post - Eocene reservoir since 1930 (Merle et al. 1976). Field location and a coarse mesh of the investigated area (1/20 of field area) are presented in Figure 6-5 and 6-6. Field data until 1980 showed that there were about 500 wells. The original pressure in the reservoir was about 2258 psi. The main production mechanisms that activates the Lagoven area is compaction drive that is especially significant in the unconsolidated sandstones of Bachaquero field. Compaction is a consequence of fluid pressure reduction in the reservoir during production. This causes all layers to “sink” into the reservoir, which is reflected as subsidence on the ground surface. Average subsidence until 80’s was approximately 6ft. However, compaction is an effective way to maintain the reservoir pressure and reduce water production, therefore, increasing total oil recovery.

Figure 6-5: Structure map of Bachaquero reservoir and reservoir area grid

(Merle, Kentie et al. 1976)

6.4.2 Material properties of reservoir

The properties governing geo-mechanical behavior describe a linearly elastic porous medium. Material properties of the reservoir described are listed in Table 6-4.

Table 6-4: Material properties of reservoir in the simulation

Material properties	Symbol	Values	Field unit
Initial porosity	ϕ	031	-
Poisson' ratio	ν	0.21	-
Initial permeability	k	178	mD
Young's modulus	E	65000	psi
Rock density	ρ_s	128	p/ft^3
Solid compressibility	C_s	25E-6	psi^{-1}
Biot's constant	α	0.95	-

6.4.3 Fluid properties

Physical properties of pore fluids can have a strong influence on the depletion pattern of a reservoir. Generally, the physical properties are a function of the composition of the fluid, the temperature, saturation and pressure. Therefore, the physical properties will vary throughout the reservoir as functions of the spatial location and time as the reservoir conditions change.

Some key properties of the pore-fluid for Lagoven area are given in Table 6-5 and 6-6. The fluid properties used in the simulation are to be taken as mean value and are in no way to be taken as an exact representation of the Lagoven fluid properties.

Table 6-5: Summary of fluid properties

Variables	Symbol	Initial value	Unit
Vertical pressure gradient in oil		0.397	Psi/ft
Temperature at OWC	T	129.6	^{0}F
Water compressibility (gas saturated)	C_w	3.5*10-6	Psi^{-1}
Water compressibility in aquifer	C_{wa}	3*10-6	psi^{-1}
Oil compressibility	C_o	115*10-6	psi^{-1}
Thickness of formation	h_s	637	ft
Average of thickness of oil sand	H	300	ft
Oil viscosity	μ_o	23.00	cp
Initial pressure	P_i	2258	Psi
Initial stress	S	3941.60	Psi

Table 6-6: Critical phase saturation and relative permeability data

Variables	Symbol	Initial value	Unit
Connact water saturation	S_{wc}	0.16	--
Relative oil permeability at 1-S_{wc}	k_{ro}	1	--
Oil residual saturation	S_{ro}	0.2	--
Relative water saturation at S_{ro}	k_{rw}	0.3	--
Initial water saturation	S_w	0.2	--
Initial oil saturation	S_o	0.8	--

The new method, based on an empirical relationship (Behrenbruch and Goda 2006) are used to predict the relative permeability. Figure 6-6 shows the authentic relative permeability curves from experiment measurement before production commenced from the Lagoven area of the Bachaquero field. These curves are believed to be representative because of good agreement between results obtained from MBC and the new method.

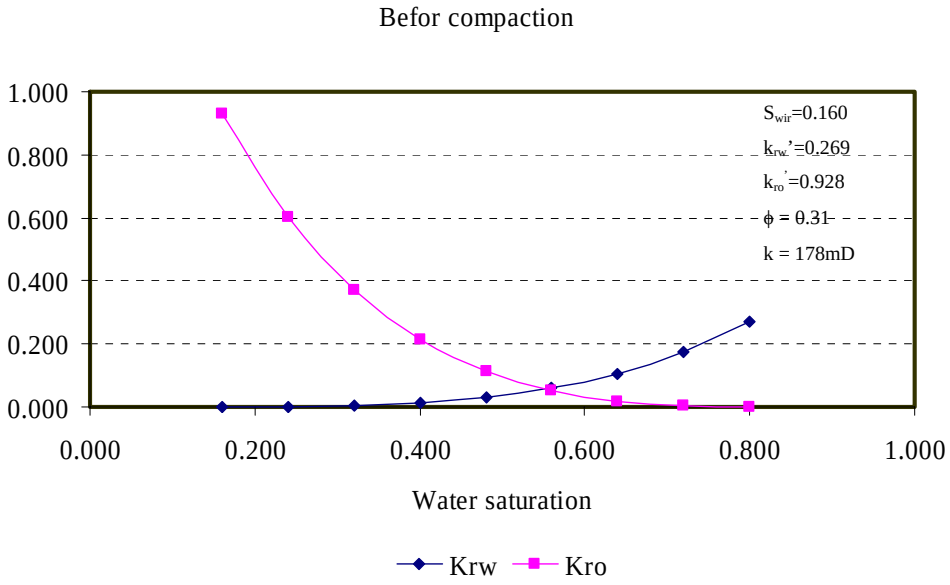

Figure 6-6: Relative permeability curves used in Lagoven area before sand rearrangement

6.4.4 Interpretation of historic data

The primary history data for Lagoven area are presented in Figure 6-7. The first well in the area was drilled in 1944. However, large numbers of wells were developed

after 1953 and reached a level of about 500 wells in 1980. The total oil production rate in Lagoven during the 1955-1980 period varied between 60,000 bbl/d to 160,000 bbl/d. The early peak of almost 160,000 bbl/d was reached in 1957. After that, the number of wells fluctuated due to wells being worked over at the end of 1958 and a drilling campaign in the mid 1960's.

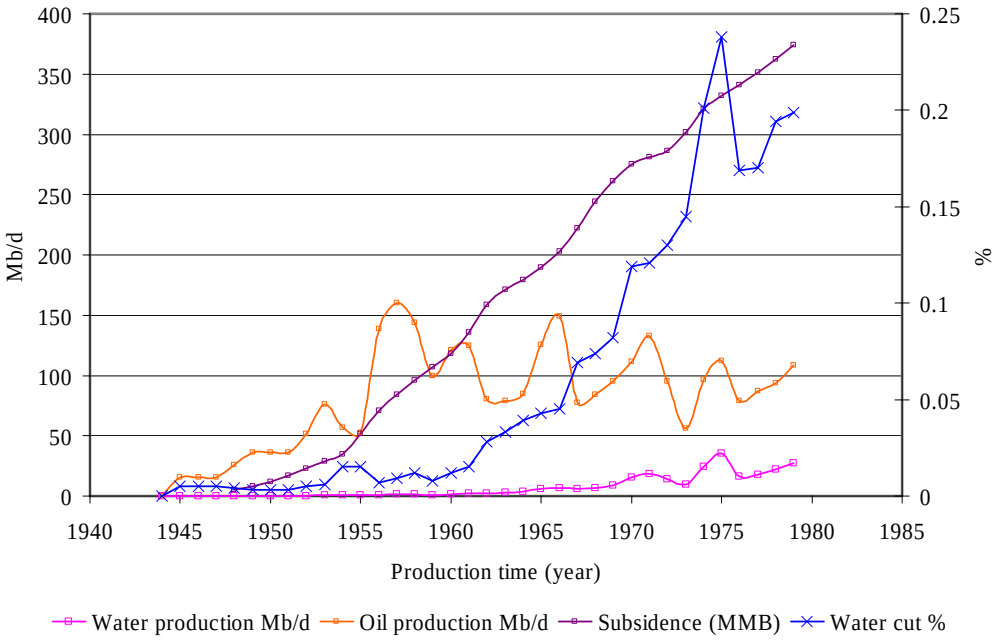

Figure 6-7: Historic data from Lagoven field

The total oil production in Lagoven area during this period amounted to 1.08×10^9 bbl. The total subsidence volume during the same period was about 0.374 $\times10^9$ bbl which corresponds to 35% of the oil production. This indicated that compaction drive was one the main production mechanisms. However, there was no

relationship evidence between subsidence rate and production rate due to lacking of data.

Fortunately, looking at the water cut and subsidence derivative curves, it can be seen that there are 3 main periods when sand particles rearrange in reservoir within subsidence data (Figure 6-8). The first period happened when the large numbers of wells were developed after 1953. In this period, although water cut rate reduces the rate of subsidence increase significantly due to pore structure collapse. The situation recurs every 10 years. As a result, due to compaction or pore collapse, reservoir properties would change every period such as porosity, permeability.

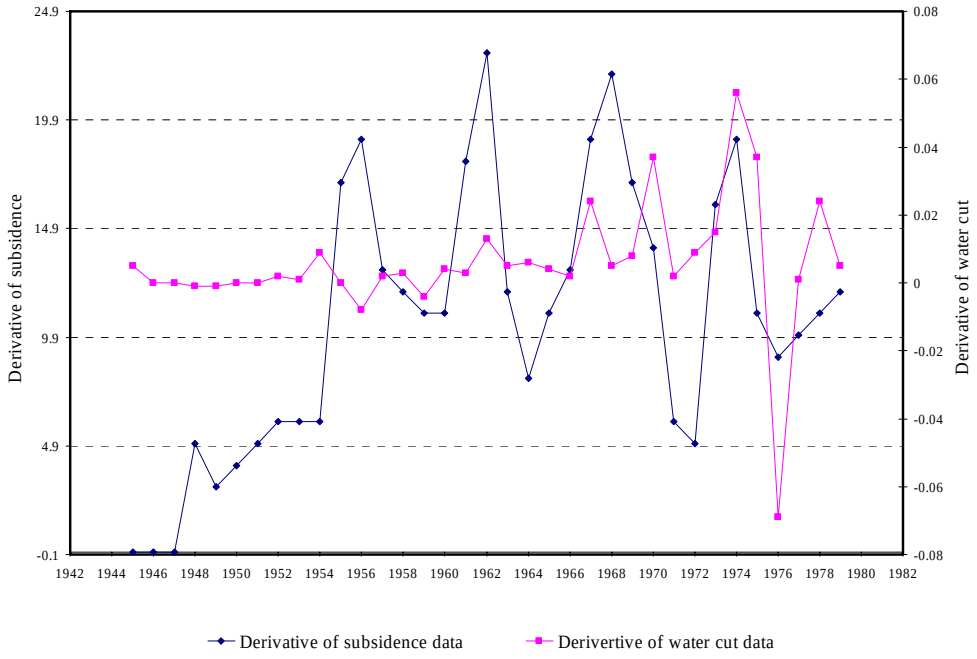

Figure 6-8: Water cut rate and subsidence rate in Lagoven area.

Eclipse Geomechanics (Eclipse 2005) was subsequently used to calculate fluid flow within the reservoir and to look at associated geomechanical processes, including a change of relative permeability curves. For the purposes of reservoir evaluation, it is necessary to identify the rock types to determine the precise rate of porosity and permeability decline with increasing stress for each rock type. Values of porosity and permeability will be predicted on a step-by-step basis for different values of the change in net effective reservoir stress. This allows for prediction of porosity and permeability at different stages of reservoir development.

Knowledge of porosity at different values of *in situ* stress will allow for the determination of new relative permeability curve resulting from the change in wetting surface (equations 6-18 and 6-19). New relative permeability curves are then updated in the coupled reservoir simulator for calculation of both rate of fluid production and compaction prediction. Figure 6-9 shows the new relative permeability curves which are used when reservoir compacts after introducing the large of number of wells in 1953. In this new relative permeability curves, S_{wir} increased from 0.16 to 0.168 according to reduction of porosity from 0.31 to 0.305.

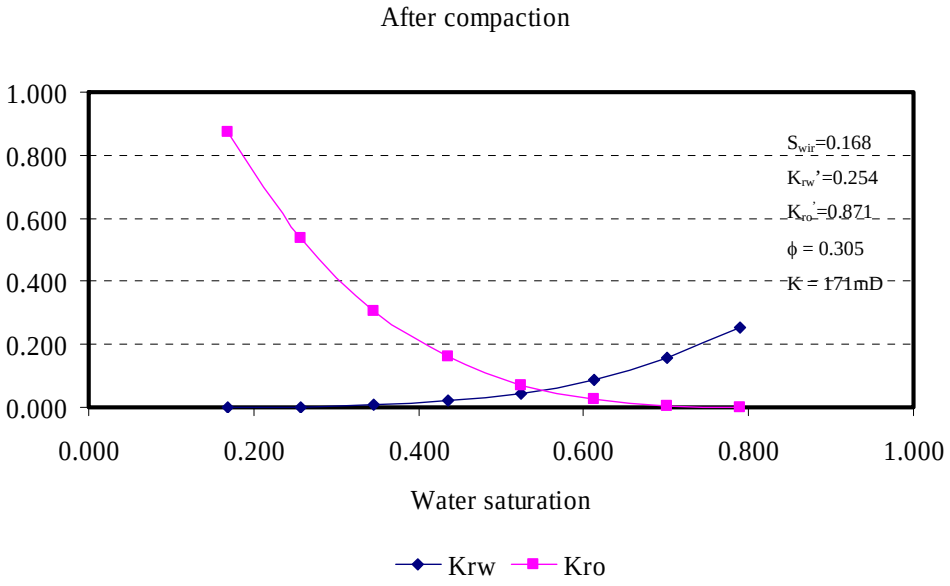

Figure 6-9: Relative permeability curves used in Lagoven area after sand rearrangement

6.4.5 Results and discussions

Water production and water cut - modeling results

Figure 6-10 shows the difference of water production rate between a conventional model and a model with changing relative permeability. The first model that did not take account variation of relative permeability has a higher water production rate. In contrast, the other model which was simulated with the change in relative permeability with higher S_{wir} has, as expected, a lower degree of water production. After 13000 days, the calculated water rate from the second model is approximately 70% lower compared to the result from the first model.

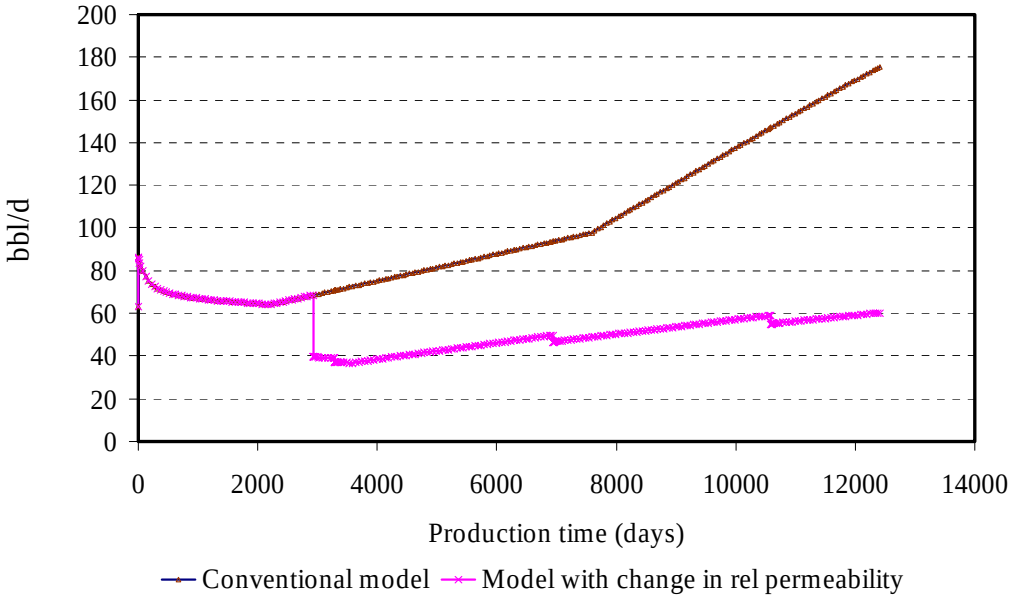

Figure 6-10: Water production rate due to the change in relative permeability.

Figure 6- 11 presented below shows the influence of changes in relative curves on oil and water production in two models. It is obvious that oil production rate peaks when more wells were introduced into reservoir. In contrast, water production rate reduced because of pore collapse when oil production rate increases. It is also note that although the numbers of wells doubled after 10 years of production, water production in the model with new relative permeability curves is still lower than water production without the change in relative permeability curves. The results suggest that due to introducing the new relative permeability with higher S_{wir} and depending on the level of porosity decline, water production may be reduced or stopped completely in a relatively short time, as described in the Figure 6-11.

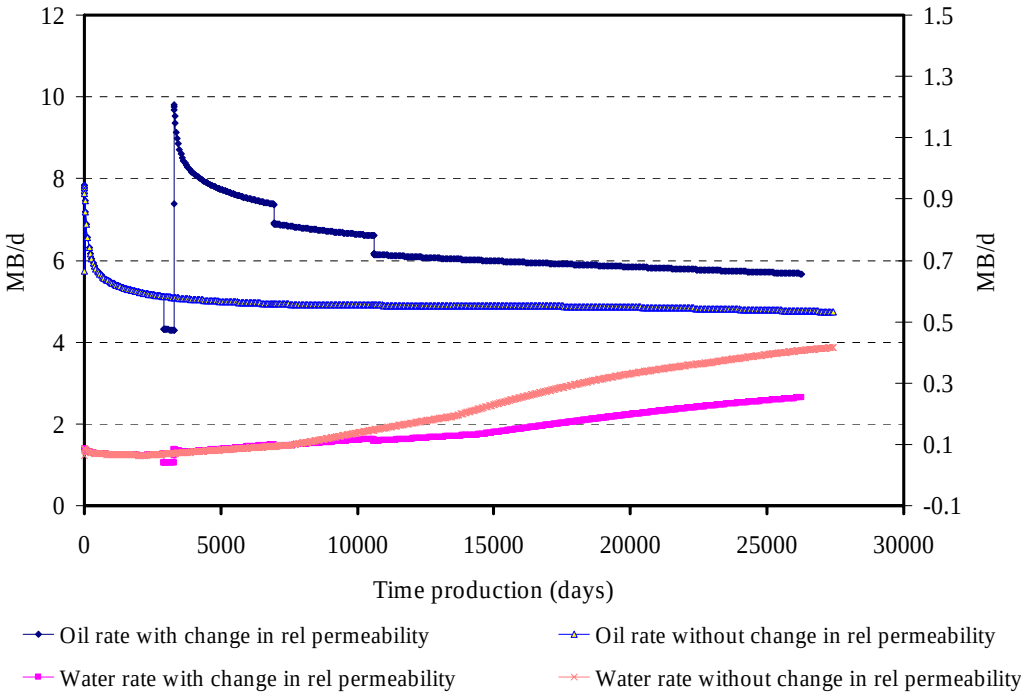

Figure 6-11: Prediction of oil production rate and water production rate

Compaction prediction

Eclipse Geomechanics output of displacement consists of three variables (ROCKDISX, ROCKDISY and ROCKDISZ), describing rock-displacement in x-, y-, and z-directions respectively. The displacements are written to disk at pre-determined dates and times of the reservoir simulation. During the equilibration phase of the model and reduction of pore pressure, massive deformations of the model can occur. The displacement patterns change from a circular bowl to a quasi-elliptical bowl (Figure 6-12a). The introduction of more wells also causes significant pressure

depletion in the reservoir. As a result, the region of compaction mirrors that of well locations (Figure 6-12b).

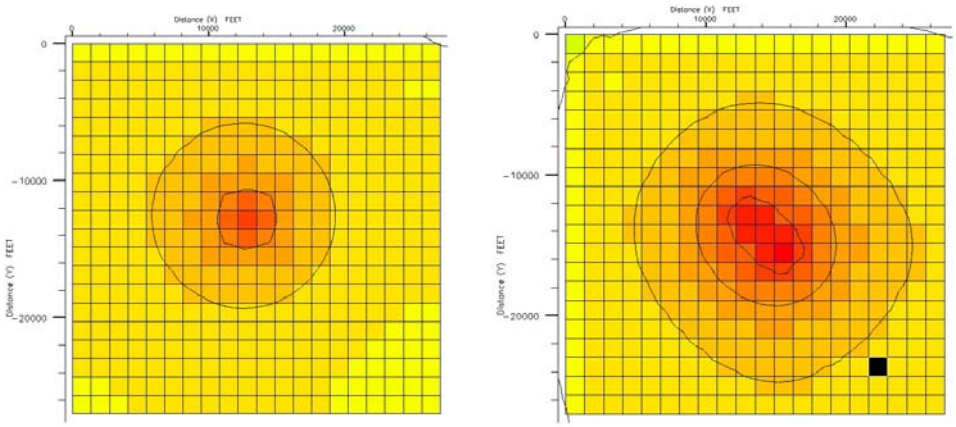

(a) (b)

Figure 6-12: Compaction contour

The compaction profile was also computed. Figure 6-13 presents the comparison between compaction profiles measured in a vertical cross-section that bisects the well location at the end of simulation in both models. The maximum compaction increases from 9.86ft to 10.20ft when compaction takes into account the influence of pore collapse on the change in relative permeability curves. Both the maximum compaction values appear at the centre of bowl, also coinciding with the production well locations.

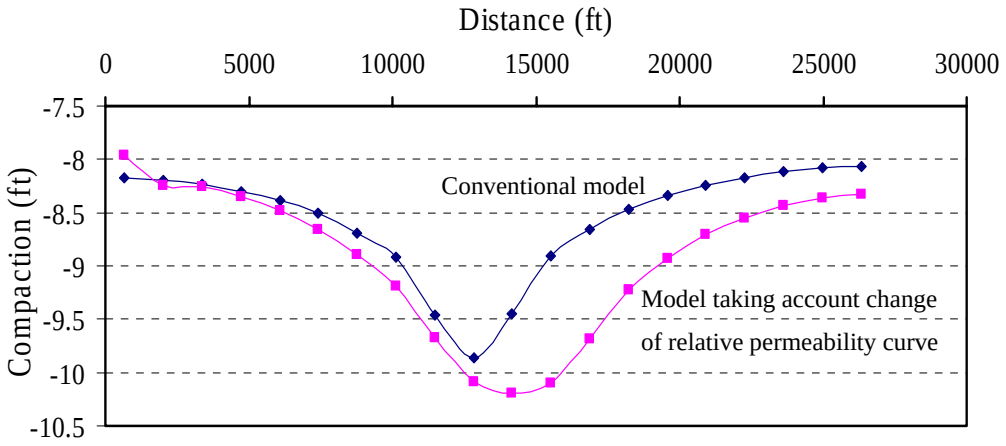

Figure 6-13: Compaction profiles

6.5 Conclusions

The research here suggests that when the reservoir formation is compacted, the compaction process can be briefly divided into 2 stages: rearrangement of sand grains and sand-crushing. Based on the Carmen-Kozeny's equation, a new method has been introduced which is used to determine new values of irreducible water saturation (S_{wir}) due to compaction, calculated at each stage as the reservoir is developed.

The new endpoint value is then applicable for creating new relative permeability curves. Applying this methodology to a case study of a compaction reservoir in a Venezuelan field, it is shown that this method has more accurate applicability for coupled reservoir simulation particularly in investigation of reservoir performance and compaction prediction. Further it is shown that accounting for changes in irreducible water saturation, residual oil saturation, effective porosity, altered

permeability and changes in relative permeability, all as a result of compaction, may be significant. In this way it is possible to better describe overall reservoir performance and petroleum recovery. In addition, the approach can be used to evaluate the extent of formation compaction and reservoir performance resulting from the variation of stress sensitive porosity/permeability. This research also shows that compaction can have an advantage particularly in reducing water production. The theory and practical methodologies developed in this chapter can be extended by applying to other case studies, where compaction and stress sensitivity dominate the drive mechanism.

New distributions of n_o and n_w are determined using Monte Carlo simulation. Values of n_o and n_w are not only a function of S_w but depend on S_{wir}, ϕ as well as S_{or}. The new range of values of n_o and n_w are established. Minimum and maximum of n_o are 2.14 and 3.37. Minimum and maximum of n_w are 2.29 and 3.32. Consequently, the new range resulting from Monte Carlo simulation provides the decision maker with a better range of possible scenarios thus allowing for more accurate decision-making.

CHAPTER 7: DISCUSSIONS

7.1 Introduction

As a comprehensive and broad study that includes many concepts from theory to experiments, from reservoir engineering to rock mechanics, this thesis used some simplifications to achieve the solution to reach the objectives. Advantages and limitations of research are also examined.

7.2 Chapter 2: Model simplifications

The study of motion of a material body using reference configuration is the Lagrangian approach. If the quantities of interest are studied at the current configuration only, the approach is Eulerian. We assume that deformation is infinitesimally small, as in linearised elasticity, the difference between the reference and current configurations vanish. Consequently, Lagrangian and Eulerian approaches become nearly identical. Viscoelastic materials exhibit both elastic properties of a solid and viscous properties of fluids (Sansour 2003).

Particularly, in compaction and subsidence research, there are also three principles of coupled fluid flow – geomechanics model: mass conservation, momentum conservation, and an equation of state. In general, reservoir deformation occurs very slowly compared to fluid flow. Hence, we can apply the fundamental assumptions with the small strain theory in governing partial differential equations for the generalized coupled system in which the solid velocity is much smaller than the fluid velocity.

The Galerkin finite element method is chosen to solve governing equations because of its ability to handle anisotropic and heterogeneous regions with complex boundaries (Young's and Hyochong 1996). However, the impact of chosen grid within the production zone and its effect on compaction and subsidence has not been considered at this stage.

To predict subsidence and compaction, analytical Geertsma's equations are presented. To be applied successfully, Geertsma's equations with some assumptions should be considered in the following situations:

- ✓ The reservoir pressure drop is high and water influx drive is weak.
- ✓ The compressibility of reservoir rock is high. As a result, compaction usually happens in weak and unconsolidated reservoir rock.
- ✓ The reservoir has a considerable thickness which implies that a small rate of compaction over the reservoir interval can cause subsidence at seafloor.
- ✓ The ratio between thickness and breadth of reservoir should be large enough to avoid shielding the overlaying rock on compaction

7.3 Chapter 3: Restrictions when using analytical equations in stochastic – based simulation.

Equation 3-7 and 3-8 in Chapter 3 identifies four parameters influencing reservoir compaction behavior: (1) Poisson's ratio; (2) Young's modulus; (3) reduction of pore fluid pressure; and (4) thickness of reservoir. Results of stochastic – based simulation showed that increases in both Poisson's ratio and Young's modulus reservoir can reduce compaction. However, these parameters were measured at ambient conditions, which can cause some skewness comparing to parameters

measured at *in situ* conditions. So, overburden conditions should take into account when measuring on Young's modulus and Poisson's ratio so as to obtain accurate modelled results. In addition, the reduction in pore fluid pressure is not only dependent on measurement methods but also varies with location, mobility, density, compressibility, reservoir boundary conditions and is the time-dependent. Therefore, reduction of pore fluid pressure could be estimated more accurately if a conventional simulation is performed to predict reservoir pressure.

The stochastic – based simulation also showed that the reduction of pore fluid pressure has a smaller impact on compaction than Young's modulus and Poisson's ratio. In most cases, the drop in pore fluid pressure in a gas field from beginning of the production period to abandonment is small (Geertsma 1973). Therefore, the consideration of reduction of pore fluid pressure may be neglected in gas fields. However, in a case study involving oil and gas fields in the Gulf of Mexico, particularly for fields with solution gas drive (Geertsma 1973), the drop in pore fluid pressure should be considerable so that the effect is greater on compaction investigations, even if the field is a hard rock reservoir where Young's modulus is larger than 140,000psi.

It is noted that compaction and subsidence implementation in the stochastic based simulation involves computer generated distribution of input parameters. Different input distributions chosen could lead to significant difference in distributions of both compaction and subsidence results. To get the best results, it is necessary to collect more data.

7.4 Chapter 4: Finding agreements

From an experiment point of view, the results from the case study in the Cooper-Eromanga basins show that normalized permeability reduces to about 30% for the Namur, Hutton and Murta formations. On the other hand, the normalized permeability for the Poolowanna and Birkhead formations decreases by only 10%. The variation means that the grade of permeability reduction is strongly dependent on the type of formation. This results agree with previous laboratory studies (Vairogs and Rhoades 1973). The variation in the degree of change between differing lithologies is attributed to variation in composition and microstructure between individual samples from various formations. The trend of the data indicates a more or less linear decrease of permeability with increasing effective overburden stress. For fitting a relationship to the overburden pressure and permeability, the empirical and polynomial equation described in (Morton 1989; Jelmert, Torsceter et al. 2000) can be applied to estimate permeability for the Cooper Basin.

7.5 Chapter 5: Advantages of stress models taking into account influence of a large structure.

This chapter is concerned about geomechanical aspect as related to the stress in the crust under *in situ* reservoir conditions. Equations 5-16, 5-17 and 5-18 for a differential stress regime indicate that these stress models are more suitable than conventional model where changes in pore fluid pressure and total stress are independent. The derived equations agree with results conducted by Wu and Addis (1998) where Biot's constant equals to 1.

Stress variation due to a large structure described in Chapter 5 could provide a framework in investigation stress state conditions. Stress regime models associated

with a fault give rise to variation in the stress path during petroleum production. Based on models, we predict that effective stress around a large structure will significantly increase when compared to conventional model. As illustrated in Figure 5-5, 5-6, 5-7 and 5-8, changes in pore fluid pressure are coupled not only with stress change but also with elastic rock properties. Thus, the diameters of Mohr's circle will increase with depletion of pore fluid pressure and reach toward failure envelope (Hillis 2000). When Mohr's circle contacts with failure envelope, pore structure may collapse. As a result, the potential compaction could happen sooner.

7.6 Chapter 6: Limitations in investigation of the impact of pore collapse to fluid production

The effective stress in the reservoir increases as hydrocarbons are produced and pore fluid pressure declines. Under such conditions, certain porous rocks experience a sudden increase in compressibility. This increase coupled with the accompanied irreversible deformation, is often termed as 'pore collapse'. Pore collapse often leads to abrupt compaction of the reservoir rock and thus potentially subsidence of the ground surface. As a result of compaction, surface grain area, pore size and geometry will change. The above change is presented in this chapter where new values of irreducible water saturation are calculated for compaction reservoir. However, change in oil residual saturation has been kept constant to simplify the model. In addition, Chapter 6 limits the modeling to a two-phase fluid flow system. Therefore, the effect of the gas phase is not considered.

CHAPTER 8: CONCLUSIONS AND RECOMMENDATIONS

8.1 Introduction

Chapter 8 covers all the main results in previous chapters including research objectives of Chapter 1 and conclusions from Chapters 2 – 6. The research here presented theoretical and experimental aspects for compacting reservoirs in oil fields. Finally, recommendations are suggested in the area of compacting reservoirs.

8.2 Objectives of Chapter 2: The coupled fluid flow – geomechanics model.

The continuum mechanics theory as applied to a coupled fluid flow – geomechanics simulation has been presented in Chapter 2. This chapter shows the importance of the fully coupled fluid flow – geomechanics model applied in compaction and subsidence calculation. Furthermore, governing equations for a radial model as applied to compaction and subsidence are derived. The finite element method is also used for solving the governing equation of fully coupled fluid flow – geomechanics model. Simplified solutions are also presented that can be employed for quickly estimating compaction and subsidence. These equations will be used in uncertainty evaluation and stochastic simulations in the following chapter.

8.3 Objectives of Chapter 3: Uncertainty in compaction and subsidence estimations.

Chapter 3 has discussed the impact of uncertainty on the calculation of subsidence and compaction. A stochastic model, incorporated within the Monte Carlo simulation program, has been used to investigate the impact of uncertainties in a compacting reservoir. Young's modulus, Poisson's ratio and reduction of pore fluid pressure are considered as uncertain and, therefore input as a distribution. Simulation of compaction and subsidence using stochastic-based distribution input parameters highlighted the following key issues that are not generally mentioned in numerical simulation methods.

- ✓ Young's modulus has a larger impact on compaction than Poisson's ratio. Values of Young's modulus in the case example greater than 140,000psi have an insignificant effect on compaction and subsidence. This value could be used as a quantitative index to predict compaction in reservoirs.
- ✓ The order of importance of Poisson's ratio on subsidence is greater than the effect of Young's modulus. One can thus use Poisson's ratio when estimating subsidence in cases where Young's modulus data is unavailable. Additionally, the reduction of pore fluid pressure has less impact on subsidence and compaction although it is the main reason for increasing effective stress when using the Geertsma' analytical equations in Monte Carlo simulation.
- ✓ Numerical simulation using deterministic parameters is still valid for the purpose of comparison with a stochastic-based simulation. The sensitive analysis shows that compaction estimated from numerical simulation is in the range of 50%

confident interval of results from the stochastic based simulation. Therefore, a stochastic model produces a more comprehensive range of solutions in the evaluation of compaction in petroleum field production project which would otherwise require numerical simulation.

8.4 Objectives of Chapter 4: Investigate stress sensitive permeability and porosity.

Chapter 4 discussed the goals of research related to the change in porosity and permeability when effective stress increases due to fluid production. The chapter presented both theoretical and experimental work in which stress-dependent permeability and porosity relationships are applied in a coupled reservoir simulation. Modified Carmen-Kozeny's equation is then used to generate the relationship between porosity and permeability.

The governing equations have taken into account the relationship between porosity and permeability based on the experimental relations given by the modified Carmen-Kozeny's equation. Numerical simulation using the Galerkin finite element method replicates the subsidence of a simplified reservoir in radial coordinate system. The case study here clearly modeled the influence of changing permeability on subsidence results in a stress sensitive reservoir.

Experimental results in the Eromanga–Cooper basins show that permeability decreased by 5 to 10% of the initial permeability for every 1000 psi decrease in reservoir fluid pressure. Most experimental results are in agreement with previous research of compaction/permeability experiments (David and Crawford 1998) but disagree with results of Rhett and Teufel (1992), who showed that permeability can be increased during unaxial compaction of sandstone reservoir. The observation of

increased permeability is only matched when two core sample of the Berea Sandstone are at failure point where fissures are generated.

The most important result of Chapter 4 shows principles for calculating the reduction of permeability in a pressure depletion scenario. Thus, the methodology can be applicable for determining changes in permeability in both the field and laboratory for a stress sensitive reservoir.

8.5 Objectives of chapter 5: The influence of a large structure on stress regime and its impact on compaction and subsidence predictions.

Chapter 5 has illustrated the impact of a large structure on stress regime. Mathematical models were derived for each fault model so as estimate stress perturbation. All models are based on Mohr–Coulomb's criteria in faulted area. Analysis of different fault stress regimes show that effective stress regimes vary significantly when compared to a conventional model. Subsequently, the selections of fault models, fault friction, friction internal angle and Poisson's ratio are very important to assess the influence of a discontinuity on reservoir compaction and subsidence because it can cause a significant change in stress regime.

Chapter 5 also emphasizes the reservoir engineering applications. Important results described in this chapter illustrate a step forward in understanding for assessing increasing effective stress that is the main factor controlling on permeability in an area surrounding a large structure. The relationship between permeability and the change in effective stress that is perturbed by large structure is also used to investigate compaction and subsidence.

8.6 Objectives of chapter 6: The change in relative permeability curves with compacting reservoir

The research here suggests that when the reservoir formation is compacted, the compaction process can be briefly divided into 2 stages: rearrangement and sand-crushing. Based on the Carmen-Kozeny's equation, the new method using generally analytical equations to calculate the new values of irreducible water saturation (S_{wir}) due to compaction is developed.

The new endpoint value is then applicable for creating new relative permeability curves. Applying these curves for the case study of a compacting reservoir in a Venezuelan field, it is shown that this method is more accurate for coupled reservoir simulation particularly in investigation of reservoir performance and compaction prediction. Subsequently, in the context of a **c**ompacting reservoir, accounting for irreducible water saturation, residual oil saturation, variation of effective porosity, alteration of permeability and the change in relative permeability is important. Furthermore, the approach can be used to evaluate the extent of formation compaction and reservoir performance resulting from the variation of stress sensitive porosity/permeability. This research also shows that compaction can have an advantage particularly in reducing produced water. The theory and practical methodologies developed in this chapter can be extended by applying to other case studies, where compaction and stress sensitivity dominate the drive mechanism. Chapter 6 results represent the most important outcomes of this thesis.

New distributions of n_o and n_w are determined using Monte Carlo simulation. Values of n_o and n_w are not only a function of S_w but depend on S_{wir}, ϕ as well as S_{or}. The new range of values of n_o and n_w are established. Minimum and maximum of n_o

are 2.14 and 3.37. Minimum and maximum of n_w are 2.29 and 3.32. Consequently, the new range resulting from Monte Carlo simulation provides the decision maker with a better range of possible scenarios thus allowing for more accurate decision-making.

8.7 Recommendations for future work

This research recommends the following further research:

- ✓ This thesis deals mainly with elastic rock properties so that further work to take into account extension to plastic and other nonlinear aspects would be a natural progression.
- ✓ The research here focuses on subsidence and compaction problems studies. The theory developed in this research is suggested to investigate other problems such as wellbore stability and sand production.
- ✓ The research covers all aspects of a compacting reservoir. However, the model is still simple and applications are simplified. For example, chapter 6 discusses two-phase fluid flow. It is recommended that future research should be extended to a compositional model.

REFERENCES

Addis, M. A., N. C. Last and N. A. Yassir (1996). "Estimatuon of horizontal stress at the Depth in faulted regions and their relationship to pore pressure variation." SPE Formation Evaluation.

Alcalde, O. R. and L. W. Teufel (2006). Diagnosis of formation damageby rock deformation/compaction through numerical well test simulations. The Internatinal symposium and exhibition on formation damage control, Lafayette, LA, SPE 98053-Society of Petroleum Engineers, Inc.

Al-Harthy, M. H., A. K. Khurana, S. Begg and R. B. Bratvold (2006). "Sequential and system approach for evaluating inverstment decision-influence of functional dependencies and interactions." APPEA journal: 511-522.

Al-Harthy, S. S., J. Dennis, X. D. Jing and J. R. Marsden (1998). Petrophysical Properties Under True-Triaxial Stress For Hydrocarbon Recovery. SPE 39770 paper, presented at Permian Basin Oil and Gas Recovery Conference, Midland, Texas.

Ambastha, A. K. and Y. Z. Meng (1996). "Iterative and numerical solutions for pressure-transient analysis of stress-sensitive reservoirs and aquifers." Computers & Geosciences **Volume 22**(Issue 6): 601-606.

Anderson, E. M. (1951). The dynamics of faulting and Dyke formation with application in Britain. Edinburgh.

Anderson, E. M. (1951). The dynamics of faulting and Dyke formation with application in Britain, Edingburgh.

Bai, M. F., F. Meng, D. Elsworth, Y. Abousleiman and J. C. Roegiers (1999). "Numerical modelling of coupled flow and deformation in fracture rock specimens." Int. Numer. Anal. Meth. Geomech **23**: 141-160.

Behrenbruch, P. and S. Biniwale (2005). "Characterisation of classic depositional environments and rock pore structure using the Carmen_Kozeny equation: Australian sedimentary basins." Journal of Petroleum science and engineering.

Behrenbruch, P. and H. M. Goda (2006). Two-phase relative permeability prediction: a comparision of the modified Brook-Corey methodology with a new Carmen-Kozeny based flow formulation. SPE 101150, SPE Asia Pacific Oil and Gas Conference and Exibition, Adelaide, Australia.

Behrenbruch, P. (2007). Private communication.

Biot, M. A. (1940). "General theory of three Dimenssional consolidation." Journal of applied physics: 155-164.

Boreham, C. J. and A. J. Hill (1998). Source rock distribution and hydrocarbon geochemistry. The petroleum geology of South Australia, Department of Primary Industries and Resources. **4-Cooper Basin**.

Brook, R. H. and A. T. Corey (1966). "Properties of porous media affecting fluid flow." Journal of Irrigation and drainage division **92**(ASCE): 61-88.

Buckles, R. S. (1965). "Correlating and Averaging Connate Water Saturation Data." Journal of Canadian Petroleum Techonology **4**(1): 42-52.

Camac, B., S. P. Hunt and P. Boult (2004). "Fault and top seal integrity at relays and intersections using a 3D distinct element code." APPEA Journal.

Camac, B., S. P. Hunt and P. Boult (2004). Sensitivity analysis for fault and top seal integrity at relays and intersections using a 3D distinct element code: Case study examples given from the Bonaparte Basin, Timor Sea and the Otway Basin, South Australia. APPEA, Canberra.

Chen, H. Y., L. W. Teufel and R. L. Lee (1995). Coupled Fluid Flow and Geomechanics in Reservoir Study-I. Theory and governing Equations. SPE 30752, presented at Annual Technical Conference and Exhibition, Dallas.

Chin, L. Y., R. Raghavan and L. K. Thomas (2000). "Fully Coupled Analysis of Well Responses
in Stress-Sensitive Reservoirs." SPE Reservoir Eval. & Eng. **03**(05): 435-443.

Chin, L. Y., R. Raghavan and L. K. Thomas (2000). "Fully Coupled Geomechanics and Fluid-Flow Analysis of Wells With Stress-Dependent Permeability." SPE Journal **05**(01): 32-45.

Claudia, L. P., H.-Y. Chen and L. W. Teufel (2001). Numerical Well Test Analysis of Stress-Sensitive Reservoirs. SPE 71034 paper - SPE Rocky Mountain Petroleum Technology Conference, Keystone, Colorado, Society of Petroleum Engineers.

Collin, F., C. Schroeder, V. De Gennaro and A. Bolle (2005). "A deterministic/stochastic model to predict the variation in bulk modulus of chalk." Geotechnique **55**(2): 135–141.

Cuisiat, F., M. Gutierrez, R. W. Lewis and I. Masters (1998). Petroleum Reservoir Simulation Coupling Flow and Deformation. SPE 50636 paper, presented at European Petroleum Conference, The Hague, Netherlands.

David, P. Y. and B. Crawford (1998). Plasticity and Permeability in Carbonates: Dependence on Stress Path and Porosity. SPE/ISRM 47582-Eurorock 98', held in Trondheim, Norway, Society of Petroleum Engineers,Inc.

de Waal, J. A. and R. M. M. Smits (1988). "Prediction of Reservoir Compaction and Surface Subsidence: Field Application of a New Model." SPE 14214 paper - SPE Formation Evaluation(June): 347-356.

Diego, G. F., A. M. Marcio and P. Felipe (2004). "Stochastic computational modelling of highly heterogeneous poroelastic media with long-range correlations." International Journal for Numerical and Analytical Methods in Geomechanics **28**: 1-32.

Eclipse (2005). Simulation Software Manuals 2005A, Schlumberger.

Economides, M. J., H. Buchsteiner and N. R. Warpinski (1994). Step-Pressure Test for Stress-Sensitive Permeability Determination. SPE 27380 paper- SPE Formation Damage Control Symposium, Lafayette, Louisiana, Society of Petroleum Engineers.

Ejaer, E., R. M. Holt, P. Horsrud, A. M. Raaen and R. Risnes (1992). Petroleum related rock mechanics, Elsevier Science Publisher B.V.

Fawad, A. C., K. Arild, B. Knut and H. Kaare (2002). "Porosity loss in sand by grain crushing-experimental evidence and relevance to reservoir quaility." Marine and Petroleum Geology **19**: 39-53.

Finol, A. and S. M. Farouq Ali (1975). "Numerical Simulation of Oil Production With Simultaneous Ground Subsidence." Society of Petroleum Engineering Journal.

Fowler, A. C. and C. G. Noon (1996). "Mathematical model of compaction, consolidation and regional ground flow." Geophys. J.Int **136**: 251-260.

Fred, B., M. Badsi and J.-D. van Wees (2000). "Faulting, fracturing and in situ stress prediction in the Ahnetn Basin, Algeria—a finite element approach." Tectonophysics(320): 311–329.

Gambolati, G., F. Massimiliano, T. Pietro, D. Roberto and L. Giuditta (2001). "Finite element analysis of land subsidence above depleted reservoirs with pore pressure gradient and total stress formulations." International Journal for Numerical and Analytical Methods in Geomechanics **25**: 307-327.

Gambolati, G. P. and A. Freeze (1973). " A Mathematical simulation of the subsidence of Venice - I. Theory." Water Resourc Res **9**(721-733).

Gang, H. and B. D. Maurice (2003). "Description of fluid flow around a wellbore with stress-dependent porosity and permeability." Journal of Petroleum Science and Engineering **40**(1-2): 1-16.

Geertsma, J. (1973). "Land subsidence above compaction oil and gas reservoir." Journal of Petroleum Technolgy: 734-744.

Ghaboussi, J. and E. L. Wison (1973). "Flow of compressible fluids in porous elastic media." Int J Numer Methods Eng **5**: 419-442.

Gobran, B. D., W. E. Brigham and J. Ramey (1987). "Absolute Permeability as a Function of Confining Pressure, Pore Pressure, and Temperature." 10156 SPE paper - SPE Formation Evaluation(March): 77-84.

Goda, H. M. and P. Behrenbruch (2004). Using a modified Brook-Corey model to study oil-water relative permeability for diverse pore structure. SPE 88538, SPE Asia Pacific Oil and Gas Conference and Exibition, Perth, Australia.

Gutierrez, M. (1994). Fully Coupled Analysis of Reservoir Compaction and Subsidence. European Petroleum Conference, London, United Kingdom.

Gutierrez, M., R. W. Lewis and I. Masters (2001). "Petroleum Reservoir Simulation Coupling Fluid Flow and Geomechanics." SPE Reservoir Evaluation & Engineering: 164-172.

Hansen, K. S., M. Prats and C. K. Chan (1995). "Modeling of Reservoir Compaction and Surface Subsidence at the South Belridge." 26074 SPE Production and Facilities: 134-143.

Heiland, J. (2003). "Laboratory testing of coupled hydro-mechanical processes during rock deformation." Hydrogeology Journal **11**(1): 122 - 141.

Hillis, R. (2000). "Pore pressure/stress coupling and its implications for seismicity." Exploration Geophysics **31**: 448-454.

Hillis, R.R. and Nelson, E.J., 2005. In situ stresses in the North Sea and their applications: petroleum geomechanics from exploration to development. In: Doré, A.G. and Vining, B. (eds.) Petroleum Geology: North-West Europe and Global Perspectives—Proceedings of the 6th Petroleum Geology Conference. Geological Society, London, 551-564.

Holmes, M., K. D. Dreher and E. A.J. (1971). Lithology and Fluid Properties and Their Relations to the Distribution of Saturating Fluids in Sandstones. 46th Annual Fall Meeting of the Society of Petroleum Engineers of AIME, New Orleans.

Holt, R. M. (1990). "Permeability Reduction Induced by a Nonhydrostatic Stress Field." SPE Formation Evaluation **Volume 5**(Number 4, December): 444-448.

Hunt, S. P., P. Boult and B. Camac (2003). Discrete element stress modelling in the Timor Sea and Otway Basin, Australia. EAGE faults and top seal conference.

James, A. S., S. P. Thomas and U. G. Glenn (2003). "Porosity and permeability of the Tiwi geothermal field, Philippines, based on continuous and spot core measurements." Geothermics **33**(1-2): 87-107.

Jelmert, T. A., O. Torsceter and H. Selseng (2000). "Technique characterises permeability of stress-sensitive reservoir." Oil & Gas Journal(Drilling & Production).

Jim, U., B. Wayne, F.-A. Reem and O. Claus (2006). Offshore Aquifer Update, Onshore Fault Seal Analysis, and Preliminary Numerical Simulation of Coastal Subsidence Risk. Western Australia, CSIRO.

Jin, M., J. Somerville and B. G. D. Smart (2000). Coupled Reservoir Simulation Applied to the Management of Production Induced Stress-Sensitivity. SPE 64790-The SPE International Oil and Gas Conference
and Exhibition., Beijing, China.

John, P. D., K. D. David and A. H. Stephen (1998). "Improved Evaluation and Reservoir Management of Low Permeability, Gulf Coast Reservoirs: Significance of Stress Dependent Permeability." SPE 39873 paper - International Petroleum Conference and Exhibition of Mexico.

Jones, F. O. and W. W. Owens (1980). "A laboratory study of low permeability gas sand." Journal of Petroleum Technolgy: 1631-40.

Kattenhorn, S. A., A. Aydin and D. D. Pollard (2000). "Joints at high angles to normal fault strike: an explanation using 3-D numerical models of fault perturbed stress fields." Journal of Structural Geology **22**: 1-23.

Maerten, L., P. Gilespie and D. P. Pollard (2002). "Effects of local stress perturbations on secondary fault development." Journal of Structural Geology **24**: 145-153.

Mann, R. L. and I. Fatt (1960). "Effect of pore fluid on the elastic propertise of sandstone." Geophysics **Volume 25**: 433-444.

Mashiur, K. and L. W. Teufel (1996). Prediction of Production-Induced Changes in Reservoir Stress State Using Numerical Model. SPE 36697 paper - SPE Annual Technical Conference and Exhibition, Denver, Colorado, Society of Petroleum Engineers.

Massimiliano, F., G. Giuseppe, T. Pietro and B. Domenico (2006). "Stochastic poromechanical modeling of anthropogenic land subsidence." International Journal of Solids and Structures **43**: 3324–3336.

Masud, A. and T. J. R. Hughes (2002). "A stabilized mixed finite element method for Darcy flow." Comput. Method App. Mech. Engrg.191: 4341-4370.

Mattax, C. C., R. M. McKinley and A. T. Clothier (1975). "Core Analysis of Unconsolidated and Friable Sands." 4986 SPE paper - Journal of Petroleum Technology: 1423-1432.

McKinley, J. (1998). "Coupled consolidation of solid, infinite cylinder using a Terzaghi formulation." Computer and Geotechnics **23**: 193-204.

Merle, H. A., C. J. P. Kentie, G. H. C. van Opstal and G. M. G. Schneider (1976). "The Bachaquero Study - A composite analysis of the behaviour of a compaction drive/solution gas drive reservoir." SPE 5529 - Journal of Petroleum Technology: 1107-1115.

Morita, N., D. L. Whitfill, O. Nygaard and A. Bale (1989). "A quick method to detremine subsidence, reservoir compaction and in situ stress induced by reservoir depletion." SPE 17150 - Journal of Petroleum Technolgy.

Morrow, R. N. (1971). "Small-Scale Packing Heterogeneities in Porous Sedimentary Rocks." AAPG Bulletin **55**(3): 514-522.

Morton, J. G. G. (1989). Petrophysics of Cooper Basin reservoir in South Australia. The Cooper and Eromanga Basins, Australia. B. J. O'Neil, Proceedings of Petroleum Exploration Society of Australia, Society of Petroleum Engineers, Australian Society of Exploration Geophysicist (SA branchs), Adelaide.

Murtha, J. (2000). Decisions Involving Uncertainty, A @Risk Tutorial for the Petroleum Industry, Palisade Corporation.

Nathenson, M. (1999). "The dependence of permeability on effective stress from flow tests at hot dry rock reservoirs at Rosemanowes (Cornwall) and Fenton Hill (New Mexico)." Geothermics **Volume 28**(Issue 3): 315-340.

Nguyen, V. K. and M. T. Nguyen (1998). "Subsidence caused by the lowering of ground water at Ho Chi Minh City and its monitoring." Science and technology development journal **1**(6).

Nick, P. V., R. M. Valenti and L. F. Koederitz (2002). A Unified Theory on Residual Oil Saturation and Irreducible Water saturation. SPE 77545 - The SPE Annual technical Conference and Exhibition, San Antonia, Texas.

Noorishad, J., M. S. Ayatollahi and P. A. Witherspoon (1982). "A finite element method for coupled stress and fluid flow analysis of fractured rocks." Int. J. Rock Mech. Min. Sci. & Geomech. Abstr **19**: 185-193.

Osorio, J. G., H.-Y. Chen and L. W. Teufel (1997). Numerical Simulation of Coupled Fluid-Flow/Geomechanical Behavior of Tight Gas Reservoirs with Stress Sensitive Permeability. SPE 39055 paper - Latin American and Caribbean Petroleum Engineering Conference, Rio de Janeiro, Brazil, Society of Petroleum Engineers.

Osorio, J. G., H.-Y. Chen and L. W. Teufel (1999). Numerical Simulation of the Impact of Flow-Induced Geomechanical Response on the Productivity of Stress-Sensitive Reservoirs. SPE 51929 paper - SPE Reservoir Simulation Symposium, Houston, Texas, Society of Petroleum Engineers.

Osorio, J. G., H.-Y. Chen, L. W. Teufel and S. Schaffer (1998). A Two-Domain, 3D, Fully Coupled Fluid-Flow/Geomechanical Simulation Model for Reservoirs With Stress-Sensitive Mechanical and Fluid-Flow Properties. SPE 47397 paper - SPE/ISRM Rock Mechanics in Petroleum Engineering, Trondheim, Norway, Society of Petroleum Engineers.

Ostermeier, R. M. (1995). "Deepwater Gulf of Mexico Turbidites – Compaction Effects on Porosity and Permeability." 26468 - SPE Formation and Valuation: 79-85.

Pape, H., C. Clauser and J. Iffland (1999). "Permeability Presiction based on fractal pore-space geometry." Geophysics **64**(5 (September-October 1999)): 1447-1460.

Patrick, L. C. and I. O. Mohd (2000). 20 Years of Laboratory Oil-Water Relative Permeability Data in the Malay Basin. SPE Asia Pacific Oil and Gas Conference and Exhibition, held in Brisbane, Australia.

Reynolds, S. D., S. D. Mildren, R. R. Hillis, J. J. Meyer and T. Flottmann (2005). "Maximum horizontal stress orientations in the Cooper Basin, Australia: implications for plate-scale tectonics and local stress sources." Geophys. J. Int.(160): 331–343.

Rhett, D. W. and L. W. Teufel (1992). Effect of Reservoir Stress Path on Compressibility and Permeability of Sandstones. SPE Annual Technical Conference and Exhibition, Washington, D.C., SPE 24756 paper - Society of Petroleum Engineers.

Robert, E. and S. Fernand (1994). "Mathematical and Numerical Properties of Control-Volumel Finite-Element Scheme for Reservoir Simulation." SPE Reservoir Engineering **Vol 9, Number 4, November**.

Roegiers, J. C. (2007). Advance in Rock Mechanics - unpublished book. The University of Oklahoma, Norman.

Rozon, B. J. (1989). A generalized finite volume discretization method for reservoir simulation,. SPE 18414 - Reservoir Simulation Symposium, held in Houston, 1989. Texas.

Ruistuen, H., L. W. Teufel and D. Rhett (1996). Influence of Reservoir Stress Path on Deformation and Permeability of Weakly Cemented Sandstone Reservoirs. SPE 36536 paper - SPE Annual Technical Conference and Exhibition, Denver, Colorado.

Sandhu, R. S. and E. L. Wilson (1969). "Finite-element analysis of seepage in elastic media." J Engineering Mech Div **ASCE 95**: 641-652.

Sansour. C, P. Wriggers, J. Sansour (2003), A finite element post-processed Galerkin method for dimensional reduction in the nonlinear dynamics of solids. Applications to shells, Computational Mechanics 32, 104-114.

Schutjens, P. M. T. M., T. L. Blanton, J. W. Martin, B. C. Lehr and M. N. Baaijens (1998). Depletion-induced compaction of an overpressured reservoir sandstone: An experimentsl approach. SPE/lSRM Eurorock 98', held in Trondheim, Norway, SPE/ISRM 47277 paper - Society of Petroleum Engineers.

Schutjens, P. M. T. M., T. H. Hanssen, M. H. H. Hettema, J. Merour, P. d. Bree , J. W. A. Coremans and G. Helliesen (2004). "Compaction-Induced Porosity/Permeability Reduction in Sandstone Reservoirs: Data and Model for Elasticity-Dominated Deformation." SPE Reservoir Evaluation & Engineering: 202-216.

Settari, A. T. and D. A. Walters (1999). Advances in Coupled Geomechanical and Reservoir Modeling With Applications to Reservoir Compaction. SPE 51927 paper, presented at SPE Reservoir Simulation Symposium, Houston, Texas.

Shang, Z. B., H. G. Jeffry, C. Hung-Lung and C. H. Donald (2003). "A Model to Correlate Permeability with Efficient Porosity and Irreducible Water Saturation."

Smits, R. M. M. and J. A. de Waal (1988). "A Comparison Between the Pressure-Lag Model and the Rate-Type Model for the Prediction of Reservoir Compaction and Surface Subsidence." SPE paper 16389 - SPE Formation Evaluation(June): 357-363.

Soares, A. C., J. E. Altoe, P. Bedrikovetsky and F. H. Ferreira (2003). Formation damage due to pore collapse during pressure depletion. SPE European formation damage - SPE 82254, The Hague, Netherlands, Society of Petroleum Engineers.

Sonier, F. (1993). Mathematical and numerical properties of control-volume finite-element scheme for reservoir. 12th SPE Symposium on Reservoir Simulation, paper SPE 25267 held in New Orleans, LA, USA.

Sulak, R. M. and J. Danielson (1989). "Reservoir aspects of Ekofisk subsidence." SPE 17852 - Journal of Petroleum Technolgy: 709-716.

Ta, Q. D., M. Al-Harthy, S. Hunt and J. Sayers (2007). The Impact of Uncertainty on Subsidence and Compaction Prediction. First Sri Lankan Geotechnical Society (SLGS) International Conference on Soil and Rock Engineering, Colombo, Sri Lanka.

Ta, Q. D. and S. P. Hunt (2005). Consideration Of The Permeability And Porosity Relationship In A Fem Coupled Geomechanics And Fluid Flow Model. Intergrated Geoenginering for Sustainable Infracstructure Develpomnet - Hanoi Geoengineering 2005, Ha Noi - Viet Nam, Vietnam National University Publishing House.

Ta, Q. D. and S. P. Hunt (2005). Investigating the relationship between permeability and reservoir stress using a coupled geomechanics and fluid flow model. 9th conference on science and technology, held in Ho Chi Minh City University of Technology, Viet Nam.

Ta, Q. D. and S. P. Hunt (2006). Stress Variability Around Large Structural Features and Its Impact on Permeability for Coupled Modelling Simulations. 4th Asian Rock Mechanics Symposium (ARMS), Singapore.

Ta, Q. D., S. P. Hunt and C. Sansour (2005). Applying fully coupled geomechanics and fluid flow model theory to petroleum wells. The 40th U.S. Symposium on Rock Mechanics-USRMS, Anchorage, Alaska.

Terry, S., B. Garfield, P. Panos and F. John (2000). Fully Coupled Geomechanics in a Commercial Reservoir Simulator. SPE 65107 paper, presented at SPE European Petroleum Conference, Paris, France.

Terzaghi, K. (1925). "Erdbaumechanik auf bodenphysikalischer grundlage." Franz Deutikle, Leipzig und Wien.

Terzaghi, U. (1943). Theoretical Soi Mechnics. New York, Wiley.

Tiab, D. and C. D. Donaldson (2004). Theory and Practice of Measuring Reservoir Rock and Fluid Transport Properties. USA, Petrophysics, Gulf Pub Co.

Timur, A. (1968). "An Investigation of Permeability, Porosity, and Residual Water Saturation Relationship for Sandstone Reservoirs." The Log Analyst.

Trautwein, U. and E. Huenges (2005). "Poroelastic behaviour of physical properties in Rotliegend sandstones under uniaxial strain." International Journal of Rock Mechanics and Mining Sciences **42**(7-8): 924-932.

Trinh, M. T. and G. F. Delwyn (1999). Subsidence in the city of Hanoi, Viet Nam. Proceeding of the Canadian society of Civil Engineering Annual Conference, Regina, Saskatchewan, Canada.

Vairogs, J., C. L. Hearn, D. W. Dareing and V. W. Rhoades (1971). "Effect of Rock Stress on Gas Production From Low-Permeability Reservoirs." Journal of Petroleum Technology: 1161-1167.

Vairogs, J. and V. W. Rhoades (1973). "Pressure Transient Tests in Formations Having Stress-Sensitive Permeability." Journal of Petroleum Technology: 965-970.

Wan, J. (2003). Stabilized finite element methods for coupled geomechanics and multiphase flow. PhD thesis -Petroleum engineering department, Stanford University.

Wang, J. A. and H. D. Park (2002). "Fluid permeability of sedimentary rocks in a complete stress–strain process." Engineering Geology **Volume 63**(Issues 3-4): 291-300.

Warpinski, N. R. and L. W. Teufel (1989). "In-Situ Stresses in Low-Permeability, Nonmarine Rocks." Journal of Petroleum Technology **Volume 41**(Number 4, April): 405-414.

Warpinski, N. R. and L. W. Teufel (1992). "Determination of the Effective-Stress Law for Permeability and Deformation in Low-Permeability Rocks." SPE Formation Evaluation(June): 123-131.

Weaver, A. G. T. (1958). "An Approach to Carbonate Reservoir Evaluation Based on Mercury Injection." Oil in Canada(March 1958): 12-20.

Wu, B. and M. A. Addis (1998). Stress Estimation in Faulted Regimes: the Effect of Residual Friction. SPE/ISRM Eurock '98, Trondheim, Norway, SPE 47210.

Wyble, D. O. (1958). "Effect of applied presssure on the conductivity, porosity and permeability on sandstones." Transactions AIME **213**: 430-32.

Wyllie, M. R. J. and G. H. F. Gardner (1958). "The generalized Kozeny-Carmen equation. Part 2 - a novel approach to problem of fluid flow." World oil: 210-228.

Wyllie, M. R. J. and W. D. Rose (1950). "Some Theoretical Considerations Related to the Quantitative Evaluation of the Physical Characteristics of Reservoir Rock from Electrical Log Data." Journal of Petroleum Technology **189**(1950).

Young's, W. K. and B. Hyochong (1996). The Finite Element Method using Matlab, CRC Press, The United State of America.

Zhou, Y., R. K. N. D. Rajapakse and J. Graham (1998). "Coupled consolidation of a porous medium with a cylindrical or a spherical cavity." International Journal for Numerical and Analytical Methods in Geomechanics **22**(6): 449-475.

APPENDIX

RELATED PUBLICATIONS

ARMA/USRMS 05-769

Applying fully coupled geomechanics and fluid flow model theory to petroleum wells

Ta, Q.D.
Australian School of Petroleum, The University of Adelaide, SA, Australia
Hunt, S. P.
Australian School of Petroleum, The University of Adelaide, SA, Australia
Sansour C.
Australian School of Petroleum, The University of Adelaide, SA, Australia

This paper was prepared for presentation at Alaska Rocks 2005, The 40th U.S. Symposium on Rock Mechanics (USRMS): Rock Mechanics for Energy, Mineral and Infrastructure Development in the Northern Regions, held in Anchorage, Alaska, June 25-29, 2005.

ABSTRACT: In the last century, there has been strong emphasis on numerical formulations related to the interaction between rock deformation and multiphase fluid flow behavior in hydrocarbon reservoirs. The emphasis of this work has been to develop a coupled model for a petroleum well used within a reservoir simulator. The coupled interaction between geo-mechanics and fluid production can significantly influence both the stress state and fluid flow in the reservoir. As a consequence, coupled theory can provide a unique advantage in simulation interaction between porous media and fluid flow. In addition, the coupled well model can be used to model compaction and subsidence problems in the area near wellbore. Applying the advantage of the finite element method, the governing equations will be solved. Initial results show the influences of geomechanical parameters which have been investigated in detail.

INVESTIGATING THE RELATIONSHIP BETWEEN PERMEABILITY AND RESERVOIR STRESS USING A COUPLED GEOMECHANICS AND FLUID FLOW MODEL

Ta Q.D.♣, ♣♣ and Hunt S.P.♣

♣Australian School of Petroleum, The University of Adelaide, SA, Australia
♣♣Ho Chi Minh City University of Technology, Viet Nam

ABSTRACT

In the last two decades, there has been strong emphasis on numerical formulations related to the interaction between rock deformation and multiphase fluid flow behaviour in hydrocarbon reservoirs. This coupled interaction between geo-mechanics and fluid production can significantly influence both the stress state and fluid flow in the reservoir. Many researchers have tried to build a fully coupled model for analysis of the problem. However until now there has been a gap in resolving the full integration of the permeability variable on a coupled model; generally because of the lack of a relationship between permeability and reservoir stress. This study will present a fully coupled model and show how important stress-sensitive permeability is on a radial reservoir, particularly in terms of the final subsidence and consolidation results.

INTERNATIONAL WORKSHOP IN INTEGRATED GEOENGINEERING
HA NOI GEOENGINEERING 2005
Editors
PHAM HUY GIAO, MAI TRONG NHUAN HIROYASU OHTSU, YSHINORI SANADA

INVESTIGATING THE RELATIONSHIP BETWEEN PERMEABILITY AND POROSITY USING IN A COUPLED GEOMECHANICS AND FLUID FLOW MODEL

Ta Q.D
Australian school of petroleum, the university of Adelaide, SA, Australia
Ho Chi Minh City university of technology, Viet Nam
Hunt S
Australian school of petroleum, the university of Adelaide, SA, Australia

ABSTRACT: In the last two decades, there has been strong emphasis on numerical formulations related to the interaction between rock deformation and multiphase fluid flow behavior in hydrocarbon reservoirs. The coupled interaction between geo-mechanics and fluid production can significantly influence both the stress state and fluid flow in the reservoir. Many researchers have attempted to develop fully coupled numerical models for this problem. However, the influence of permeability on the coupled models is still poorly defined due to the lack of a relationship between permeability and reservoir stress and porosity. The emphasis of this work is in describing the mathematical equations for a fully coupled radial model in which the influence of changing of porosity on the permeability parameter is taken into account. As a consequence, this coupled method can be used more rigorously to model compaction and subsidence problems.

INTERNATIONAL SOCIETY FOR ROCK MECHANICS (ISRM)

4th Asian Rock Mechanics Symposium

held in Singapore from
8 to 10 November, 2006.

International Advisory Board

Mojtaba **GHARAVY** ***(Iran)***

Yossef **HATZOR*****(Israel)***

François **HEUZÉ** ***(USA)***

John A **HUDSON** ***(UK)***

Chung-In **LEE** ***(Korea)***

Nielen van der **MERWE** ***(South Africa)***

Yuzo **OHNISHI** ***(Japan)***

Qihu **QIAN*****(China)***

John **ST. GEORGE** ***(New Zealand)***

A **VARADARAJAN** ***(India)***

Kwet Yew **YONG*****(Singapore)***

Jian **ZHAO*****(Singapore)***STRESS VARIABILITY AROUND LARGE STRUCTURAL FEATURES AND ITS IMPACT ON PERMEABILITY FOR COUPLED MODELLING SIMULATIONS

QUOCDUNG TA and SUZANNE HUNT

Australian School of Petroleum, The University of Adelaide, SA, Australia (quocdung.ta@student.adelaide.edu.au)

A clear understanding of rock stress and its effect on permeability is important in a coupled simulation where fluid production causes a significant increase in the effective stress within a reservoir. Changing the in-situ rock stress state can alter the reservoir properties. As a result, porosity and permeability could be affected due to the rearrangement of rock particles and the redistribution of sensitive pore structures.

It is known that permeability is more sensitive to stress changes than porosity. Permeability reduction can range between 10% and 30% as reported in previous publications, this is within the elastic range of the material under investigation. Once the material reaches its yield strength a dramatic increase in permeability can then occur or further reduction depending on the mode of failure of the rock type in question. This study reports on permeability reduction under increasing stress (within the elastic range) for a number of rock types, the samples tested are from the Cooper Basin of South Australia; the standard Berea Sandstone is included for validation purposes. The results are used within a newly developed finite element coupled code in order to estimate permeability sensitivity to stress changes for predicting compaction and subsidence effects for a cylindrical wellbore model.

Furthermore, understanding rock mass stress away from the borehole is a major obstacle in the exploration and development of hydrocarbons. It is standard practice in the petroleum industry to use drilling data to determine the orientation and estimate the magnitudes of principal stresses at depth. However, field observations indicate that the orientation of the principal stresses is often locally perturbed by and around discontinuities, such as faults or formation boundaries (Kattenhorn et al., 2000; Maerten et al., 2002). Numerical stress methods have been successfully employed to model the effect of displacing faults on the surrounding rock mass. 3D distinct element code has been used to show how displacing faults generate stress variation in 3D about a fault plane (Camac et al., 2004), verified with field observations. In this work consideration is made of this variability and its effect on wellbore subsidence and compaction models. A series of models were run which incorporate the stress variability expected around an example fault under normal stress field conditions. The models show that the initial stress state conditions associated with a fault give rise to a variation in the stress path during reservoir production and resultant permeability changes are measured. The extent of the influence of lateral changes around large-scale structural features is thereby assessed and the work demonstrates the importance of incorporating this initial stress variability for production purposes.

Keywords: stress sensitive permeability, fault, subsidence.

THE IMPACT OF UNCERTAINTY ON SUBSIDENCE AND COMPACTION PREDICTION

, Q. D.; Al-Harthy , M.; Hunt , S. and Sayers , J.
Ta1 2 1 1,3
[1] *The University of Adelaide, SA, Australia*
[2] *Sultan Qaboos University, Oman*
[3] *Geoscience Australia, ACT, Australia*

ABSTRACT: This paper presents the stochastic approach using Monte Carlo simulation as applied to compaction and subsidence estimation in an offshore oil and gas deep-water field in the Gulf of Mexico. The results reveal both the impact of using probability distributions to estimate compaction and subsidence for a disk shaped-homogenous reservoir as well as taking into account Young's modulus, Poisson's ratio and the reduction of pore fluid pressure.

The uncertainty reservoir model is also compared with numerical simulation using commercial software – Eclipse 300. The stochastic-based simulation results confirm that the deterministic results obtained from the coupled geomechanical – fluid flow model are in the range of acceptable distribution for stochastic simulation. The sensitive analysis shown that Young's modulus has more impact on compaction than Poisson's ratio. The results also presented that values of Young's modulus in this deep-water field in Gulf of Mexico lying beyond 140, 000psi are insignificant to compaction and subsidence. Based on output results of compaction and subsidence with the stochastic model, potential reservoirs presenting subsidence and compaction are described as an uncertainty range within distribution of Young's modulus, Poisson's ratio and the reduction of pore fluid pressure in large-scale regional model.
Keywords: Risk Analysis, Subsidence, Compaction, Monte Carlo simulation and Uncertainty